PhD degree in Systems Medicine

Curriculum in Human Genetics
European School of Molecular Medicine (SEMM),
University of Milan and University of Naples "Federico II"
Settore disciplinare Bio/18

Large gene delivery to the retina by multiple AAV vectors

Patrizia Tornabene
TIGEM, Naples
Matricola n. R11145

Tutor: *Prof. Alberto Auricchio*

Dept. of Advanced Biomedicine, Federico II University;

TIGEM, Naples, Italy

Internal Supervisor: *Prof. Antonella De Matteis*

Dept. of Mol. Medicine and Medical Biotech., Federico II University;

TIGEM, Naples, Italy

External Supervisor*: Prof. Hélène Dollfus*

Centre de Référence pour les Affections Génétiques Ophtalmologiques;

INSERM 1112, Université de Strasbourg, France

Anno accademico 2017-2018

PUBLICATIONS

1) A. Maddalena, **P. Tornabene***, P. Tiberi, R. Minopoli, A. Manfredi, M. Mutarelli, S. Rossi, F. Simonelli, J.K. Naggert, D. Cacchiarelli, A. Auricchio. **Triple vectors expand AAV transfer capacity in the retina.** *Molecular Therapy, 2018. PMID: 29292161*.
*** co-first author**

2) **P. Tornabene**, I. Trapani, R. Minopoli, M. Centrulo, M. Lupo, S. de Simone, P. Tiberi, F. Dell'Aquila, E. Marrocco, C. Iodice, C. Gesualdo, S. Rossi, L. Giaquinto, S. Albert, C.B. Hoyng, E. Polishchuk, F.P.M. Cremers, E.M. Surace, F. Simonelli, A. De Matteis, R. Polishchuk, A. Auricchio. **Intein-mediated protein *trans*-splicing expands AAV transfer capacity in the retina**. *Science Translational Medicine, 2018, under revision.*

INDEX

LIST OF ABBREVIATION

IRDs: inherited retinal degenerations

ALMS: Alström syndrome type I

LCA: Leber congenital amaurosis

AAV: adeno-associated virus

ITR: inverted terminal repeats

GC: genome copies

m.o.i: multiplicity of infection

CDS: coding sequence

AK: F1 phage recombinogenic region

SD: splicing donor signal

SA: splicing acceptor signal

CMV: cytomegalovirus

GRK1: G protein-coupled receptor kinase 1

IRBP: interphotoreceptor retinoid binding protein

bGHpA: bovine growth hormone polyadenylation signal

WPRE: Woodchuck hepatitis virus Post-transcriptional Regulatory Element

Npu: *Nostoc punctiforme*

Rma: *Rhodothermus marinus*

RPE: retinal pigmented epithelium

PR: photoreceptor

OS: outer segment

ONL: outer nuclear layer

INL: inner outer nuclear layer

GCL: ganglion cell layer

iPSCs: induced pluripotent stem cells

WB: western blot

ELISA: enzyme-linked immunosorbent assay

SD-OCT: spectral domain optical coherence tomography

PLR: Pupillary light responses

ERG: electroretinogram

RT-qPCR: Real-Time quantitative PCR

EM: electron microscopy

IHC: immunohistochemical

FIGURES AND TABLE INDEX

ABSTRACT

Gene therapy with adeno-associated viral (AAV) vectors represents, to date, the most promising approach for the treatment of many inherited retinal diseases (IRDs). However, one of the main obstacles for the use of AAV is their packaging capacity limited to ~5 kb. To overcome this limitation dual AAV vectors were developed, in which a large gene is split into two AAVs and then reconstituted in the nucleus of target cells through inter-genome guided recombination. AAV transfer capacity which is expanded by dual AAV up to 9 kb would still not suffice for treatment of IRDs due to mutations in genes larger than 9 kb, such as Alström syndrome type I (ALMS) due to mutations in *ALMS1* (CDS: 12.5 kb). For this purpose, I have generated triple AAV vectors, with a maximal transfer capacity of about 14 kb, encoding for *ALMS1*. Full-length protein expression occurs both *in vitro* and in the mouse retina where around 4% of photoreceptors are transduced by triple AAV vectors. ALMS1 showed correct localization in the mouse retina and this results in improvement of the retinal phenotype of a mouse model of ALMS, which however is mild and transient likely due to the low-photoreceptor transduction levels achieved by triple AAV vectors.

Thus, I have considered an alternative strategy to reconstitute large proteins in the retina which is protein *trans*-splicing mediated by split-inteins which bypasses some of the rate-limiting steps of dual and triple AAV vectors. Split-inteins are genetic elements contained at the 3' and 5' ends of two different coding sequences. Split-inteins self-ligate and precisely excise from their host proteins resulting in the generation of a larger protein. I explored the possibility of dividing a large protein coding sequence in fragments fused to inteins and independently packaged and expressed by AAV vectors: *trans*-splicing of protein fragments would then reconstitute the large protein. I show that delivery of multiple AAV vectors each encoding for one of the fragments of either EGFP or large therapeutic proteins flanked by short split-inteins results in full-length protein reconstitution in the retina of mice, pigs and in human retinal organoids. Moreover, the levels of large protein reconstitution achieved improves the retinal phenotype in a mouse model of Leber congenital

amaurosis type 10. Overall, split-inteins reconstitute proteins both *in vitro* and in photoreceptors at levels that are significantly higher than those achieved via AAV genome recombination by dual AAV vectors, the gold standard for large protein reconstitution.

These data support the use of split-inteins-mediated protein *trans*-splicing in combination with AAV subretinal delivery for gene therapy of inherited blindness due to mutations in large genes.

INTRODUCTION

1. Inherited retinal degenerations

Inherited retinal degenerations (IRDs) represent a diverse group of progressive, visually debilitating diseases that can lead to blindness. IRDs affect around 1 in 3000 people in Europe and the United States (1). They can be broadly divided into monogenic syndromic and non-syndromic forms (*2*) of which retinitis pigmentosa is the best known (**Fig. 1**). The hallmark of these group of diseases is the genetic and clinical heterogeneity with over 260 disease genes identified to date *(RetNet: https://sph.uth.edu/retnet/home.htm).* Additional mutations can be identified using whole genome sequencing (*3*).

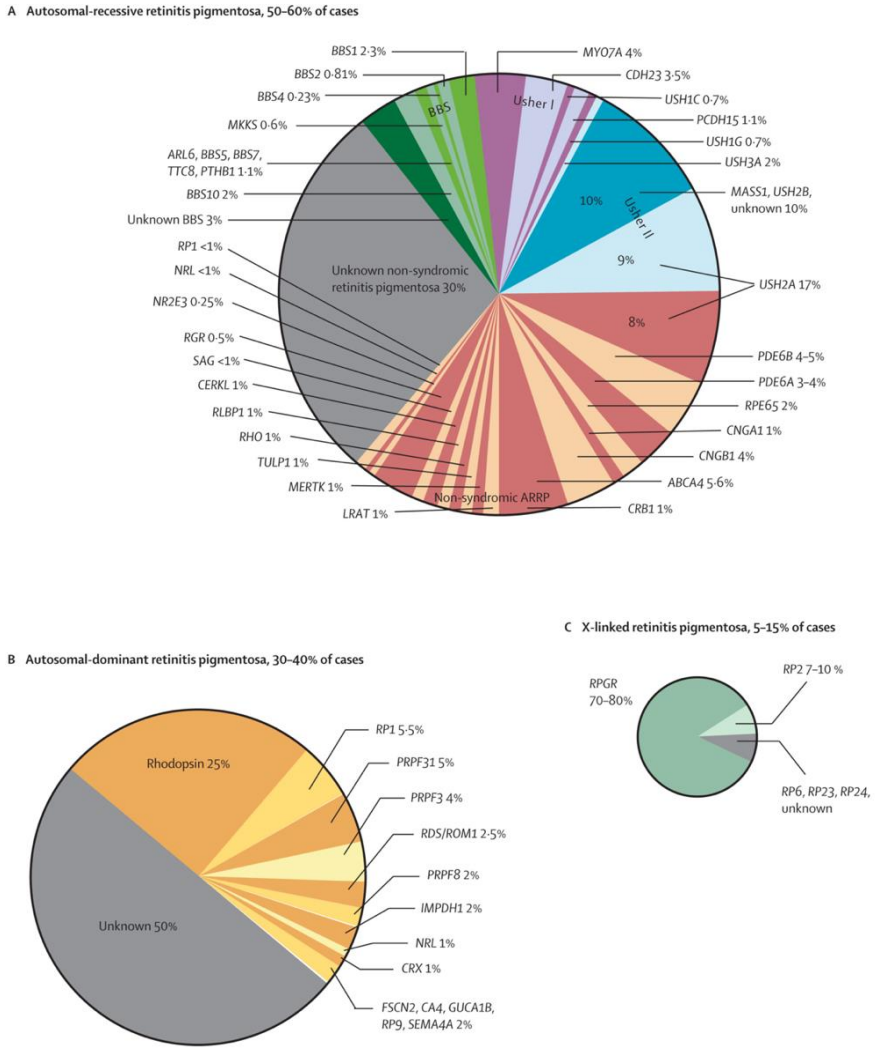

Figure 1. Molecular bases of retinitis pigmentosa

Causal genes and their contributions to (**A**) autosomal-recessive (**B**) autosomal-dominant and (**C**) X-linked retinitis pigmentosa. About 40% of cases are due to genes that are as yet undiscovered. *(Harton et al., 2006).*

Many of the mutations causing retinal dystrophies affect proteins which are specifically expressed either in photoreceptor (PR) cells or in the retinal pigment epithelium (RPE). The main affected cells are the PR, yet, defect in other cell types, such as RPE can lead to reduced photoreceptor function and their subsequent cell death leading to complete vision loss (*4*).

IRDs can be further sub-classified according to the cell type affected, indeed there are two types of PR: rod and cones (**Fig. 2**). Rod dystrophies are caused by disruption of function and/or death primarily of rods which are the cells responsible for peripheral and night vision. Similarly, cone dystrophies affect primarily cones, resulting in impairment of color vision and visual acuity (*5*).

Most of the inherited retinal dystrophies involve a degree of loss of both rods and cones and are therefore called rod-cone or cone-rod dystrophies, depending on which photoreceptor subtype is primarily affected.

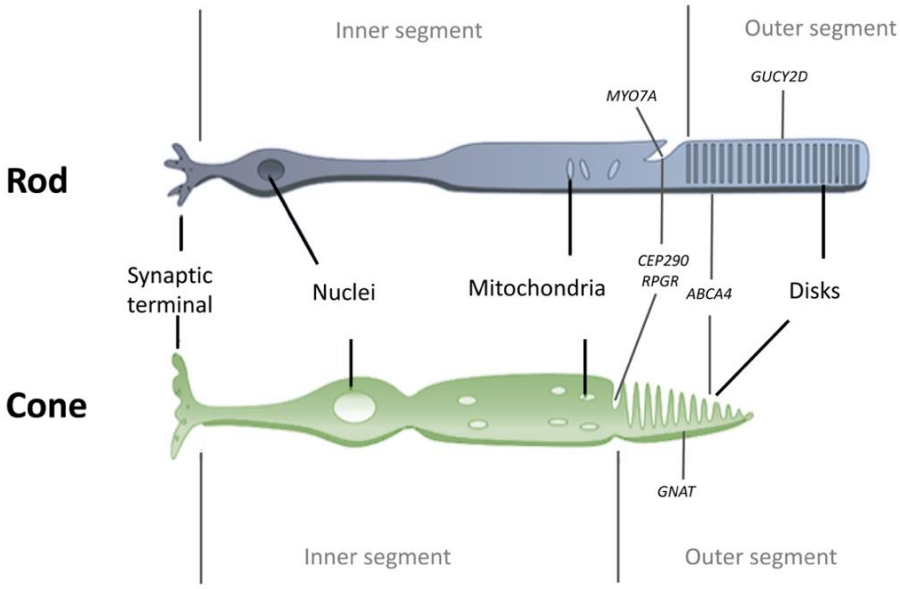

Figure 2. Structure of photoreceptor cell
Difference between rod and cone and localization of proteins encoded by genes commonly mutated in IRDs.

2. Gene therapy with AAV vectors

Gene replacement therapy relies on the delivery of a normal copy of the defective gene to restore function; thus, a vector that targets efficiently and specifically the appropriate cells, is required. Several viral and non-viral vectors have been tested for their ability to transduce PR and RPE cells,

which are the cells mostly affected in retinal degeneration. The vector characteristics for successful transduction of target cells include: the ability to bind to target cell, successful transfer to the nucleus, and the ability to be expressed for a sustained period of time to therapeutic levels and in the absence of toxicity. The main disadvantage of the non-viral vectors is their transient gene expression, contrarily to viral vectors. Among all the viral vectors commonly used for ocular gene transfer, adeno-associated (AAV) vectors have been highly successful in fulfilling all of these criteria (*6*). Moreover, most of the retina's cell types are non-dividing cells which means they are eligible to be transduced by AAV whose genome stays mostly episomal.

2.1 The retina, a good candidate for gene therapy

Additionally, the eye has a combination of unique properties that make it particularly suitable as a model system for gene therapy. Anatomically, the eye is highly compartmentalized thus allowing accurate delivery of vectors suspensions which mostly remain confined to the eye. The eye is also an immune-privileged site given the presence of tight junctions between RPE cells, the blood–retina barrier, local inhibition of immune responses by the unique intraocular microenvironment and systemic induction of immunosuppressive regulatory T cells via eye-specific mechanisms (*7, 8*). Together these advantages reduce the risk of adverse systemic effects (*9*). The transparency of the ocular media and the availability of recently developed *in vivo* imaging techniques allows to non-invasively monitor treatment progress. These include optical coherence tomography (OCT) and fundus autofluorescence used to assess retinal morphology while electroretinograms (ERG), visual evoked potentials (VEPs) and measurements of afferent pupillary light responses (PLR) can be used to assess retinal function. Several of these techniques are available also for small rodents which are the most commonly used animal models of IRDs when testing the safety and efficacy of gene therapy at the pre-clinical level. Additionally, since IRDs typically cause bilateral disease, the untreated contralateral eye offers a valuable control to compare the effects of vector/gene delivery in one eye and disease progression in the contralateral eye, thus limiting inter-individual variability.

The two most common methods of intraocular delivery are intravitreal and subretinal injections. Intravitreal injections consist of the release of the therapeutic agent in the vitreous and result in the exposure of the anterior retina. Although intravitreal vector is technically simpler than subretinal injection, anatomical barriers prevent efficient gene delivery to the outer retina and this route of administration may be more immunogenic than subretinal injection *(10, 11).* Subretinal injections, alternatively, generates a bleb of vector suspension that temporarily separates the neurosensory retina from the underlying RPE, before it is absorbed over a period of hours or days (*11*), however it directly exposes both RPE and PR to the vector-containing solution (**Fig. 3**).

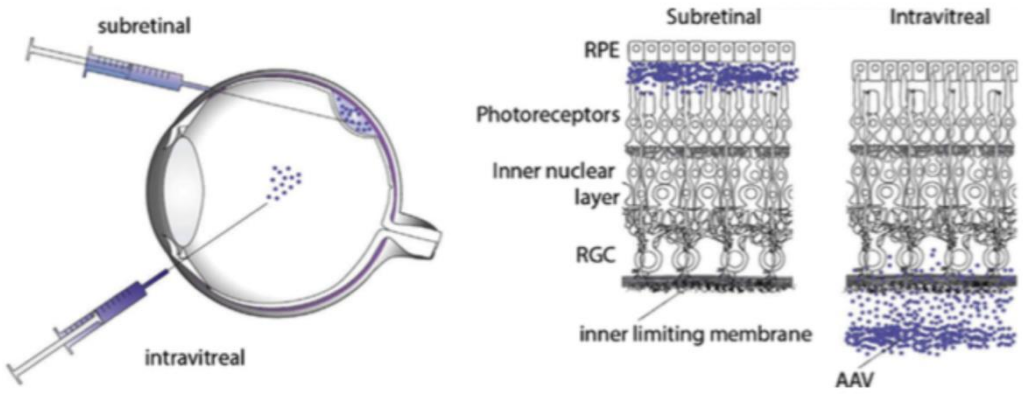

Figure 3. Schematic drawing representing a subretinal and an intravitreal injection of AAV particles *(Dalkara&Sahel, 2014)*

3. AAV biology and recombinant AAV vectors

AAV is a small (25 nm) non enveloped virus with an icosahedral capsid that packages a linear single-stranded DNA genome of about 4.7 kb which is composed of two open reading frames (ORFs), *rep* which encodes for proteins required for DNA replication (Rep 40, Rep 52, Rep 68 and Rep 78) and *cap*, which encodes for structural proteins (VP 1, 2 and 3) that form the icosahedral capsid (*12*). *rep* and *cap* are flanked by two 145 bp inverted terminal repeats (ITRs) which form hairpin-loop secondary structures at the strand termini (*13*). An alternative ORF has been described upstream of

VP 3 that encodes for assembly activating protein (AAP) which has been shown to be involved in the transportation of the native VP proteins into the nuclear region for capsid assembly (*14*) (**Fig. 4**).

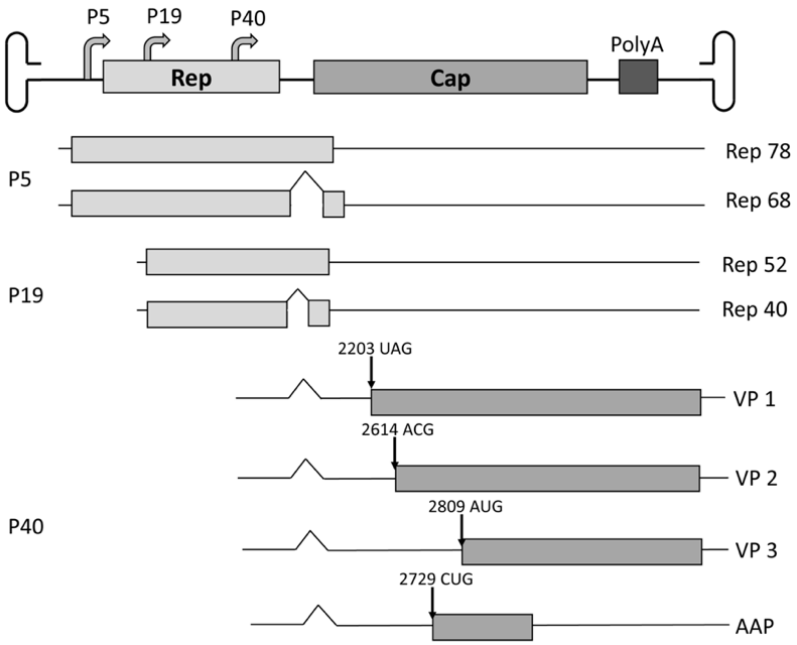

Figure 4. Adeno-associated virus genome

AAV genome is a linear single stranded DNA of 4.7 kb. The genome consists of two open reading frames (ORF) flanked by a 145 bp of inverted terminal repeat sequence. One ORF encodes for the Rep proteins namely Rep 40, Rep 52, Rep68, Rep78 required for viral replication. The second ORF encodes for the capsid proteins namely VP1, VP2 and VP3 that forms the icosahedral capsid. An alternative ORF encodes for a protein called assembly activating protein (AAP).

AAV transduction occurs through a cascade of steps which begins with the interaction of the viral capsid with specific receptors on the surface of the target cell followed by internalization of the virion by endocytosis and intracellular trafficking through the endocytic/proteasomal compartments. AAV particles that escape from there reach the nucleus where they are uncoated allowing the single-stranded genome to serve as a template for second-strand synthesis, ultimately resulting in transcription and expression of the transgene. In the absence of Rep proteins, the recombinant AAV genomes remain episomal and integration occurs at very low efficiency (*15*) (**Fig. 5**).

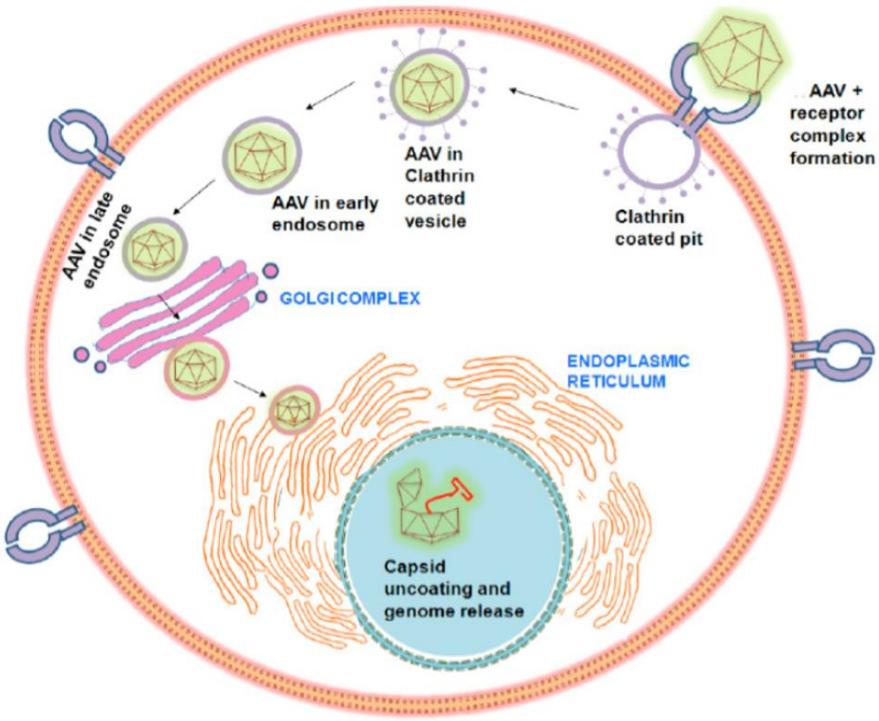

Figure 5. Adeno-associated virus infection

AAV particles bind to the cell surface receptor to form an AAV-receptor complex. This complex is then internalized *via* endocytosis. Intra-cellular trafficking is then initiated with the formation of endosomes. A typically low pH of 6 in early endosome and of 5 in late endosome induces a conformational change in the AAV capsid to expose the N-terminal phospholipase A2 domain and nuclear localization signal. This facilitates AAV endosomal escape and then AAV particles traffic through both the Golgi complex and endoplasmic reticulum *via* the retrograde transport mechanism. Upon translocation into the nucleus, the virus undergoes uncoating of its capsid and the genome is released. The genome might then integrate into the host genome at the AAVS1 site *(Balakrishnan et al., 2014).*

The ITRs are the minimal *cis*-acting elements necessary for viral genome integration, replication and packaging into the capsid and so are the only AAV sequences retained in the AAV vector (*16*). Rep and cap are instead required for the production of AAV vectors and, therefore, they are provided in *trans* to the packaging cells together with the adenoviral helper genes (*14*). The triple-transfection method is the most commonly used for the production of AAV vectors at high yields. It is based on the co-transfection of permissive cells, usually human embryonic kidney 293 cells (HEK293), with three plasmids: one containing the transgene of interest flanked by the ITRs, usually from AAV serotype 2, commonly referred as “transgene expression cassette”, a packaging plasmid containing the *rep* and *cap* genes, and a third plasmid encoding for adenoviral helper genes (*17*). (**Fig. 6**). Column chromatography or CsCl gradient centrifugation are used to purify AAV from both cellular contaminants and empty viral capsids (*17*).

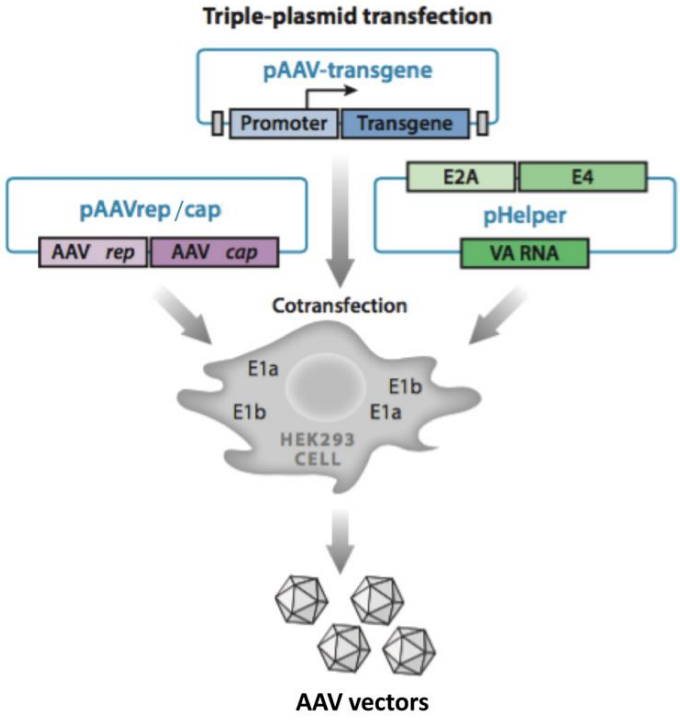

Figure 6. Adeno-associated viral vector production by triple transfection of HEK293 cells
In the triple transfection method, HEK293 cells which endogenously express adenovirus E1a and E1b are cotransfected with: a plasmid containing the remaining adenovirus helper genes (pHelper); a plasmid containing the AAV *rep*/*cap* sequences (pAAVrep/cap); a plasmid carrying the transgene expression cassette between the AAV2 ITRs (pAAV-transgene) *(Modified from Samulski et al.,2014).*

AAV was initially discovered in 1965 as a contaminant of an adenovirus preparation, but was identified as a potentially useful vector for gene transfer in the early 1980s by pioneering work on AAV serotype 2 (*18*). To date, dozens of different AAV variants (serotypes) have been identified and classified (*19*).

3.1 Natural and next-generation AAV serotypes for PR transduction

The versatility of the AAV vectors production system allows the easy exchange of capsids among various AAV variants. This exchange creates hybrid vectors that contain a genome with the ITRs from AAV 2 and the capsid from a different variant (*20*). AAV obtained through this transcapsidation

system are named AAV 2/n, where the first number refers to the ITRs and the second to the capsid (**Fig. 7**)

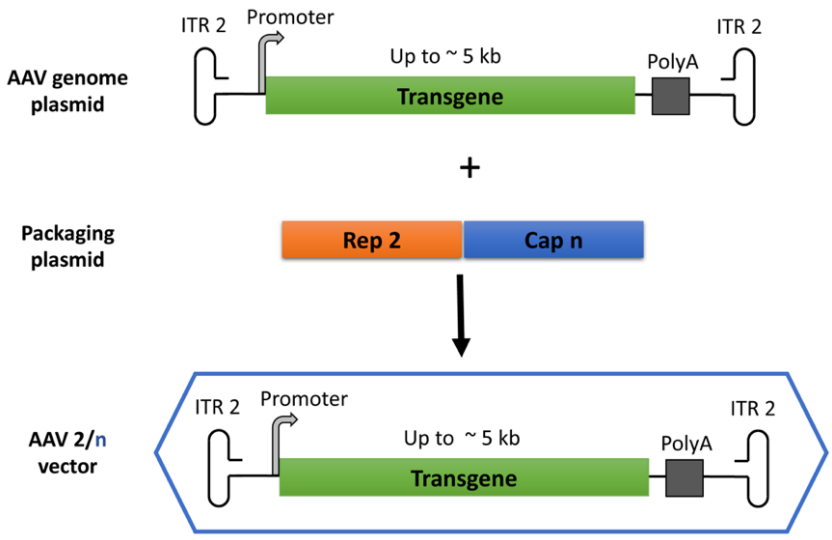

Figure 7. Recombinant vectors based on different AAV serotypes
Recombinant AAV (AAV2/n) consists of the recombinant AAV genome with a transgene expression cassette between the AAV 2 ITRs included in the capsid (encoded by Cap n) of one of the AAV serotypes.

These hybrid vectors generated have the combined advantage of the widely used and safe AAV 2 genome with the improved *in vivo* efficacy of the novel serotypes (*21*).

The capsid is the primary interface between the host and the vector genome. It is presumed to determine cell and tissue tropism, this means that accurate choice of the AAV capsid is required in order to have a selective and efficient transduction of the target cells. In addition to the serotype, cell transduction and targeting is also influenced by the route of vector administration.

Following subretinal injection, most AAV serotypes efficiently transduce RPE cells, with AAV 2/1, AAV 2/4 and AAV 2/6 being the most efficient (*22, 23*). This permissiveness could be due to either the presence of AAV receptors and co-receptors on the cell surface or to the inherent phagocytic property of the RPE that could facilitate entry of AAV particles (*18*).

Conversely, the levels of PR transduction vary significantly among different serotypes. The first evidence that AAV can target PR in addition to the RPE was provided using AAV 2/2 (*24*), however, transduction was relatively inefficient. Since the majority of mutations causing inherited retinal

degeneration occur in genes expressed in PR (*18*), this concern prompted the search for AAV serotypes able to overcome this limitation. AAV 2/5, 2/7, 2/8 and 2/9 have all been demonstrated to efficiently transduce PR, in addition to RPE (*25, 26*) with AAV 2/8 being the most efficient serotype in mice (*25*), pigs (*27*), dogs (*28*) and non-human primates (*29*) (**Fig. 8**).

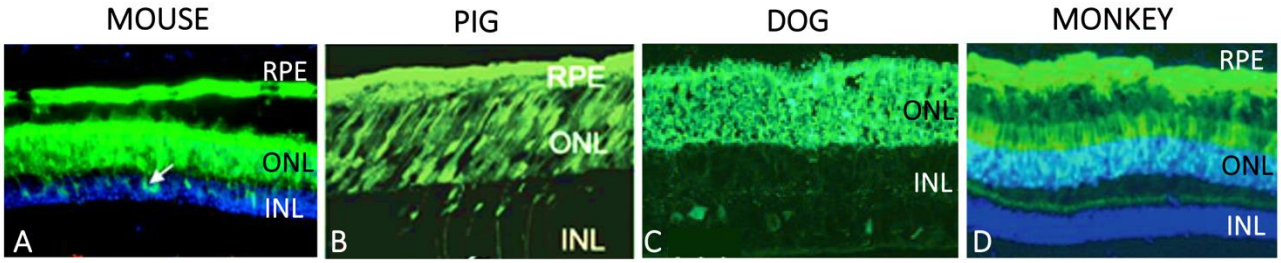

Figure 8. AAV 2/8 transduction in mouse, pig, dog and non-human primates retinas
Subretinal administration of AAV2/8 expressing EGFP in C57BL/6 mice (**A**), pig (**B**), dog (**C**) and non- human primates (**D**). RPE: retinal pigmented epithelium, ONL: outer nuclear layer; INL: inner nuclear layer. White arrows: Müller cell nuclei. [*Modified from* (*Allocca et al, 2007*) (A), *(Mussolino et al, 2011)* (B), *(Stieger et al., 2008)* (C), (*Vandenberghe et al, 2011*) (D)].

In contrast, AAV vectors of any serotype have lower transduction efficiency when delivered intravitreally (*18*) and AAV 2/2 and AAV 2/6 are currently the only serotypes found capable of transducing retinal cells from the vitreous, with a pattern mainly restricted to ganglion and Müller cells (*30, 31*).

Previously, AAV vectors were generated from naturally occurring serotypes (*14, 32*). In recent years, the increasing knowledge of AAV capsid structure and function has allowed the modification of specific amino acid residues by *rational design*, while the development of AAV capsid libraries and high-throughput screening methods enabled the identification of the most efficient capsid variant for the desired cell type through *in vivo* selection (also called *directed evolution*) (*33, 34*) thereby significantly expanded the AAV vector toolkit (*35*). Both strategies have led to the identification of novel AAV variants such as quadruple tyrosine mutants or AAV 2/7m8, which were shown to transduce the outer retina from the vitreous in small animal models (*36, 37*).

Another AAV mutant identified by directed evolution is named ShH10, an AAV6 variant with improved glial tropism after intravitreal administration (*38*).

3.2 Clinical trials of ocular gene therapy with AAV vectors

Currently, clinical trials using AAV represent about 6% of all gene therapy trials (http://www.wiley.co.uk/genmed/clinical) which confirms AAV as the most promising *in vivo* gene delivery tool for the treatment of multiple monogenic diseases, showing outstanding results when immuno-privileged body sites, like the eye, are targeted (*39*) .The first pre-clinical studies that paved the way for clinical trials utilized AAV 2 carrying wild-type isomerase RPE-specific 65 kDa protein (RPE65) to restore vision in a canine model of Leber's congenital amaurosis type 2 (LCA2), a form of childhood blindness due to mutations in *RPE65* (*40, 41*). Based on the success of these animal studies, in 2008, three independent groups initiated gene therapy clinical trials for LCA2 patients (*42-44*). Despite some differences among the various clinical trials (i.e. differences in regulatory sequences included in the vector, in the process of vector production and purification, independent surgical delivery and independent selection and follow up of the patients), all trials have shown similar positive results. In one of them, patients were dosed with a unilateral subretinal injection of a AAV 2-hRPE65 into the contralateral, previously uninjected eyes. This showed prolonged functional improvement in the injected eye from baseline until 3-year follow-up (*45*) which demonstrated for the first time that AAV could be readministered to the human subretinal space in the absence of clinically significant immune responses (*46*). After these encouraging results, a Phase III trial was initiated which showed significant improvement in a newly set-up clinical endpoint, a navigation test. Based on this data, in December 2017 the FDA approved the commercialization of the first gene therapy product (Luxturna) for an inherited disease in the USA (*47*) followed by the EMA in 2018. A number of trials that use AAV have been initiated in various inherited and acquired blinding conditions which so far confirm the safety and efficacy of AAV in the retina (*48*).

4. Strategies to circumvent AAV limited cargo capacity

Despite these important successes in pre-clinical and clinical studies, AAV has still a major drawback: the small packaging capacity, which is considered to be restricted to the size of the parental genome (~ 4.7 kb). As a result, this limits the treatment of several forms of inherited retinal dystrophies caused by mutations in genes whose functional cDNA exceeds 5 kb (**Tab. 1**).

DISEASE	CAUSATIVE GENE	CELL AFFECTED	CDS SIZE (kb)
USH1B	Myosin VIIA (MYO7A)	PR, RPE	6.7
STGD1	ATP-binding cassette, sub-family A, member 4 (ABCA4)	PR	6.8
LCA10	Centrosomal protein 290 (CEP290)	PR	7.5

Table 1. Examples of IRDs caused by mutation in genes with a coding sequence (CDS) larger than 5 kb
USH1B: Usher syndrome type IB; STGD1: Stargardt disease-1; LCA10: Leber congenital amaurosis type 10; RP: retinitis pigmentosa; ar: autosomal recessive.

Several strategies have been used to bypass AAV size limitations, among these oversized AAV and dual AAV vectors are the most commonly used (*49, 50*). Oversize AAV attempt at packaging a sequence larger than 5 kb in a single AAV capsid. Surprisingly, large genes were packaged in single oversized vectors and successfully applied in preclinical gene therapies (*51, 52*). However, these oversized vectors contain predominantly highly heterogeneous genomes that are < 5 kb in size but tend to complement each other thereby restoring the protein reading frame (*50, 53, 54*). It has also been shown that oversize vectors have lower transduction capacity, most likely due to a preferential degradation of vectors encapsidating larger genomes (*49*). Due to this non-homogeneous genomic nature, oversized vectors are of limited value for clinical applications.

4.1 Dual AAV vectors

The inherent ability of AAV genomes to undergo intermolecular recombination at their ITRs and form concatemers (*55*) has been exploited to express large genes *in vivo* by splitting them into two halves (< 5 kb) and packing them into two independent (dual) AAV vectors (*56-58*).

In recent years, several dual AAV approaches, leading to a recombination of the full-length expression cassette within the target cells, have been developed. In the *dual AAV trans-splicing strategy*, the transgene is divided into two parts, at either an endogenous intron or an engineered synthetic intron, and a splice donor (SD) signal is placed at the 3' end of the 5'-half vector and a splice acceptor (SA) signal at the 5' end of the 3'-half vector. Upon co-infection of the same cell by the dual AAV vectors and ITR-mediated tail-to-head concatemerization of the halves, *trans*-splicing results in the production of a mature mRNA that encodes a full-size WT protein (*58*). In the retina, the *trans*-splicing AAV strategy was first reported by Reich et al. (*59*). Conversely, in *the dual AAV overlapping strategy*, the halves of a large transgene expression cassette contain homologous overlapping sequences which drive the reconstitution of a single large genome by homologous recombination in a cell co-infected by both vectors (*56*). The success of this strategy, however, largely depends on the recombinogenic properties of the transgene overlapping sequences. Thus, only if a gene contains a highly recombinogenic region it will be possible to achieve therapeutic levels of expression (*57*). To overcome this problem, a *dual AAV hybrid strategy* was developed by Ghosh et al. This strategy is based on the addition of a highly recombinogenic region from an exogenous gene [i.e. alkaline phosphatase, AP (*57, 60*); or 77 bp sequence from an F1 phage genome, AK (*61*)] to the *trans*-splicing vector to increase recombination between the dual AAV vectors. The exogenous region is placed downstream of the SD signal in the 5'-half vector and upstream of the SA signal in the 3'-half vector (**Fig. 9**).

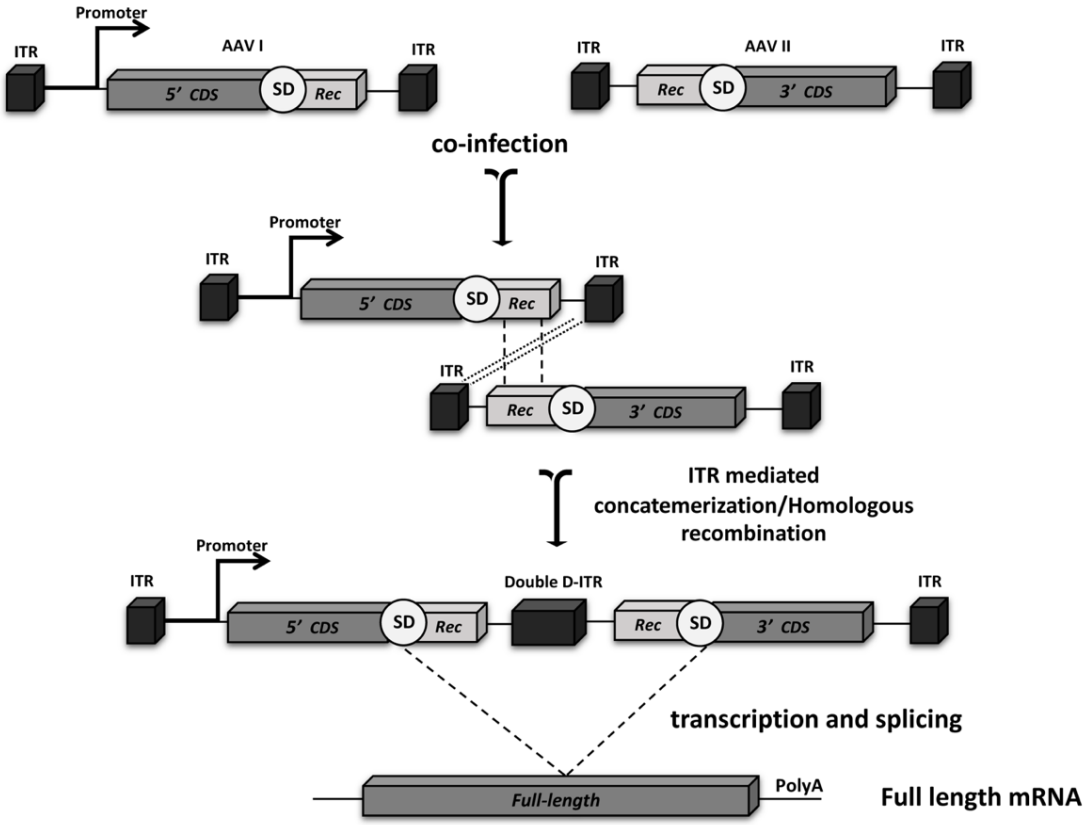

Figure 9. Schematic representation of dual AAV hybrid for large gene transduction

The two halves of a large transgene expression cassette are delivered by two independent AAV hybrid vectors to the same host cell where the full-length gene is reconstituted through ITR-mediated recombination and/or homologous recombination between highly recombinogenic sequences. The splicing donor and acceptor signals allow the subsequent removal of the double D-ITR and the recombinogenic sequences from the full-length transcript. ITR: inverted terminal repeat; CDS: coding sequence; polyA: polyadenylation signal; SD: splicing donor signal; SA: splicing acceptor signal; Rec: recombinogenic region. Dotted lines show overlapping regions for homologous recombination, pointed lines show the splicing occurring between SD and SA.

Different studies have also shown that these dual AAV approaches are efficient at transducing mouse and pig retinas (*61-63*) and results in significant improvement of the retinal phenotype in mouse models of Stargardt disease (STGD1) and Usher syndrome (USH1B), caused by mutation in ABCA4 and MYO7A, respectively (*61, 62*). Furthermore, a Phase I/II clinical trial testing the safety and efficacy of dual AAV in the retina of USHIB patients is being planned (*https://cordis.europa.eu/project/rcn/212674_it.html*). Wu et al, demonstrated that maximum size of the packaged vector DNA never exceeded ~5.2 kb, no matter what AAV serotype was used (*64*). In addition to the cDNA of the therapeutic gene and the ITRs, additional elements need to be included into the genome of AAV encoding a therapeutic protein. At a minimum, these include a

promoter and a polyadenylation signal (*65*), which means that in the best scenery dual AAV vector can be applied only for IRDs due to mutation in genes with a CDS, theoretically, up to 9 kb. A number of IRD genes , some of which are fairly common, are larger than 9 kb, such as CDH23, ALMS1 and Usherin (**Tab. 2**) from which AAV-based therapy are therefore precluded.

DISEASE	CAUSATIVE GENE	CELL AFFECTED	CDS SIZE (kb)
ar RP	Eyes shut homolog (Drosophila) (EYS)	PR, RPE	9.4
USH1D	Cadherin 23 (CDH23)	Neurosensory retina	10.5
ALMS	Alstrom syndrome 1 (ALMS1)	PR	12.5
USH2A	Usherin (USH2A)	Neurosensory retina	15.6
Ad macular dystrophy	Hemicentin 1 (HMCN1)	PR, RPE	17
USH2C	G-coupled receptor 98 (GPR98)	Neurosensory retina	18.9

Table 2. Examples of IRDs caused by mutation in genes with a coding sequence (CDS) larger than 9 kb
USH1D: Usher syndrome type ID; ALMS: Alström syndrome type 1; USH2A: Usher syndrome type IIA; USH2C: Usher syndrome type IIC. ad: autosomal-dominant.

4.2 Protein *trans*-splicing

An alternative method for expressing large proteins relies on protein rather than DNA or RNA trans-splicing, and it is mediated by a group of peptides named inteins (*66*). Inteins are described in analogy to introns in RNA since they are protein insertion sequences that excise themselves from the host protein during post-translational maturation without leaving amino acid modifications in the final protein product. This process called protein splicing occurs spontaneously in unicellular organisms from all domains of life and in the absence of energy supply, exogenous host-specific proteases or co-factors (*67*).

Most inteins are expressed within a single polypeptide chain (*cis*-splicing inteins) but some are split into two polypeptides (*trans*-splicing inteins). Protein *trans*-splicing, i.e. fusion and splicing between

two different proteins, named N and C fragments, is mediated by split-inteins of about 30 to 100 amino acids in length fused at the C- and N-terminal of the N and C fragments, respectively.

The first naturally occurring split-intein was identified in DnaE from cyanobacterium *Synechocystis* sp. strain PPC6803 (*68*). The N- and C-terminal halves of DnaE are encoded by two separate genes: one gene product consists of the N-terminal half of DnaE followed by 123 amino acids (a.a.) intein fragment, the second gene consist of 36 a.a. intein fragment followed by the C-terminal half of DnaE. When co-expressed in *E. coli*, the two protein products associate rapidly to form the intact DnaE protein (*69*). Inteins, including split-inteins, are widely used in biotechnological applications that range from protein purification through self-cleaving tags to protein labeling (*70*) as well as the reconstitution of the widely used CRISPR/Cas9 genome editing nuclease (*71, 72*). In the context of gene therapy, protein *trans*-splicing provides a way to overcome the packaging limit of AAV vectors. A large therapeutic gene can be split into two pieces that fit into vectors with limited packing size. The two pieces are fused with n- and c- intein encoding sequences, respectively. When the two split genes are co-delivered into target cells, their products can be ligated to form the full-length protein through spontaneous *trans*-splicing (*69*) (**Fig. 10**). This strategy has been already used to reconstitute large therapeutic proteins like Factor VIII in liver (*73, 74*) and dystrophin in muscle (*75*).

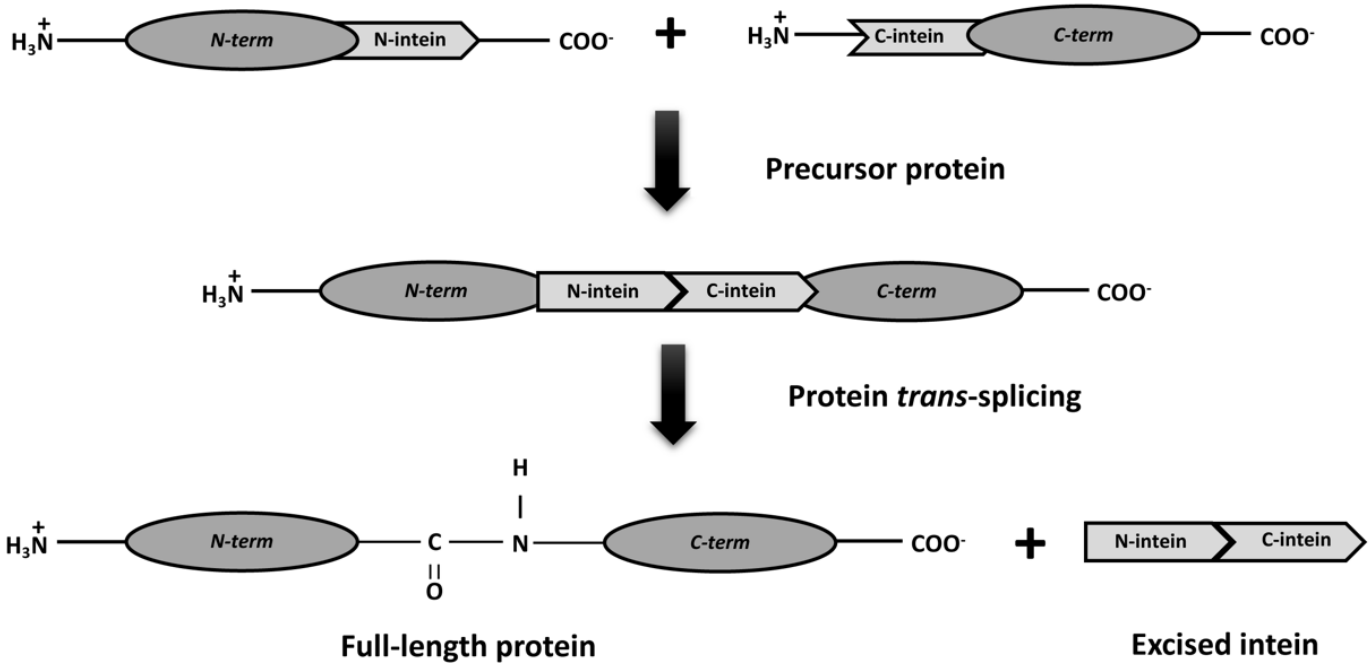

Figure 10. Schematic representation of intein-mediated protein trans-splicing

The N-Intein is fused to the N-terminal of the polypetide. Complementary, C-Intein is located at the C-terminal of the polypetide. After assembly of the two intein fragments, a splicing reaction takes place, where the intein removes itself from the precursor protein and simultaneously ligates the protein via a peptide bond.

AIMS

The overall aim of my PhD project was to circumvent the limited packaging capacity of AAV for treatment of inherited retinal diseases which are due to mutations in large genes (i.e. whose coding sequence exceeds ~ 5 kb). Among the various gene therapy vectors, AAV are the most efficient at targeting PR, the cell type most relevant for gene therapy of inherited retinal degenerations. Importantly, AAV have been demonstrated to be safe and effective in the human retina. To expand AAV transfer capacity, dual AAV vectors have been developed by several groups. Yet, several IRDs are caused by mutations in genes larger than 9 kb, which would not fit even in dual AAV vectors.

The first aim of my project was to further expand AAV transfer capacity beyond dual AAV by including a third vector (triple AAV), thus expanding AAV transfer capacity up to 14 kb, and to test the efficacy of this approach in the retina of a mouse model of Alström syndrome type I (ALMS) due to mutations in *ALMS1* with a CDS of 12.5 kb.

As the efficacy of dual AAV is lower than that of single AAV, **a second, parallel aim of my project was to test** an alternative strategy for large gene expression mediated by AAV, which is based on **protein *trans*-splicing mediated by split-inteins**. To evaluate the efficacy of this strategy I used a mouse model of Leber's congenital amaurosis 10 (LCA10) due to mutations in the large *CEP290* (CDS: 7.5 kb). The mouse model phenocopies human LCA10 which is the most frequent form of LCA (> 25% of total LCA).

The identification of AAV-based strategies that allow the delivery of large genes with high efficiency to the retina would expand the applicability of AAV to these otherwise untreatable diseases.

MATERIALS AND METHODS

Generation of AAV vector

The plasmids used for AAV vector production derived from the pAAV2.1 (*76*) plasmids that contain the ITRs of AAV serotype 2.

For triple AAV vectors:

The triple AAV plasmids were designed as detailed in **Figure 12**. To generate plasmids for triple ALMS-AAV vectors, the three fragments for ALMS1 isoform 1 (NM_015120.4) were obtained by gene synthesis (MWG, now Eurofins Genomics, Ebersberg, Germany). ALMS-AAV I contain the N-terminal CDS (112–4,188 bp); ALMS-AAV II contain the body of the CDS (4,189–8,452 bp); and ALMS-AAV III contain the C-terminal CDS (8,453–12,618 bp) followed by a 3xflag tag and the bovine growth hormone polyadenylation signal (bGHpA).

Note that the ALMS1 CDS was not split at a natural exon-exon junction, due to the exon length. Moreover, fragment I and fragment III were designed in order to generate out-of-frame transcripts in case of undesired concatemerization.

The AK recombinogenic sequence was placed at the 3' of ALMS-AAV I and at the 5' of ALMS- AAV II. Due to size constraint, no recombination signals were placed at the 3' of ALMS-AAV II nor at the 5' of the ALMS-AAV III; full-length gene reconstitution, in this case, relies exclusively on ITR-mediated joining followed by splicing.

The splice donor (SD) and splice acceptor (SA) signals contained in triple AAV vector plasmids are as follows:

5'-GTAAGTATCAAGGTTACAAGACAGGTTTAAGGAGACCAATAGAAACTGGGCTTGT

CGAGACAGAGAAGACTCTTGCGTTTCT-3'(SD);

5'-GATAGG CACCTATTGGTCTTACTGACATCCACTTTGCCTTTCTCTCCACAG-3' (SA).

The ubiquitous cytomegalovirus (CMV) promoter is the one contained in pAAV2.1- CMV-EGFP (*76*); the ubiquitous short CMV promoters are:

-CMV of 260 bp described in (*30*)

-CMV of 173 bp described in (*77*)

-CMV of 268 bp described in (*78*)

the PR-specific human interphotoreceptor retinoid binding protein (IRBP) and the human G protein-coupled receptor kinase 1 (GRK1) promoter have been both described to drive high levels of combined rod and cone PR transduction in various species (*79, 80*).

For AAV intein vectors:

The AAV intein plasmids were designed as detailed in **Figure 21, 33**. The EGFP protein was split at the amino acid (a.a.) Cys.71. All CEP290 splitting points fall in coiled-coil domains (*81*): when CEP290 was split into two polypeptides this occurred at either a.a. Cys.1076 (Set 1) or Ser.1275 (Set 2-3), when it was split into three polypeptides this was at either a.a. Cys.929 and Cys.1474 (Set 4) or a.a. Ser.453 and Cys.1474 (Set 5). Inteins included in the plasmids were either the intein of DnaE from *Nostoc punctiforme (Npu)* (*82, 83*), or an intein composed of mutated N- and C-inteins from DnaE of *Npu* and *Synechocystis sp.* strain PCC6803 (*Ssp*), respectively (*84*), or the intein of DnaB from *Rhodothermus marinus (Rma)* (*75*).

The plasmids used in the study were under the control of either the ubiquitous CMV (*85*) and short CMV 260 (shCMV) (*30*) promoters or the photoreceptor-specific (GRK1) (*79*) promoters. Plasmids encoding for EGFP and CEP290 included the bGHpA.

AAV Vector Production and Characterization

AAV vectors were produced by the TIGEM AAV Vector Core by triple transfection of HEK293 cells followed by two rounds of $CsCl_2$ purification (*86*). For each viral preparation, physical titers (GC/mL) were determined by averaging the titer achieved by dot-blot analysis (*87*) and by PCR quantification using TaqMan (Applied Biosystems, Carlsbad, CA, USA) (*86*).

Transfection and AAV infection of cells

HEK293 cells were maintained in DMEM containing 10% fetal bovine serum (FBS) and 2 mM L-glutamine (Gibco, Thermo Fisher Scientific, Waltham, MA, USA). Depending on the experiment, cells were plated in 6-well plates (1x10^6 cells/well) or 24-well plate (2.5x10^5 cells/well) and transfected 16 hours later with the plasmids encoding for the desired transgene using the calcium phosphate method (1 to 2 µg each plasmid/well); medium was replaced 4 hours later. For the experiments in **Figure 37**, an amount of plasmid encoding for the full-length gene corresponding to the same number of molecules contained in 1 µg of AAV intein plasmids was used. The total amount of DNA transfected in each well was kept equal by addition of a scramble plasmid where needed.

HeLa cells used for experiments in **Figure 38**, were plated in 24-well plates ($5x10^4$ cells/well) and transfected 16 hours later with CEP290 AAV intein plasmids (0.5 µg of each plasmid/well) using Lipofectamine LTX (Invitrogen).

For AAV infection, plated cells were first transfected with 1.5 µg/1x10^6 cells of pDeltaF6 helper plasmid, which contains the Ad helper genes (*88*). After 4 hours, cells were washed once with serum-free DMEM and incubated with AAV 2/2 vectors (m.o.i 5x10^4 GC/ cell of each vector) in a final volume of 700 µL of serum-free DMEM. Two hours later, 1.3 mL of complete DMEM was added to the cells. To increase transgene expression, 7.5 µM Calpain inhibitor I ([PI] A6185; Sigma-Aldrich, St. Louis, MO, USA), which is known to increase AAV-mediated transduction (*89*), was added daily after infection with triple ALMS-AAV.

iPSCs and retinal differentiation culture

Human induced pluripotent stem cells (iPSCs) were derived from fibroblasts which were cultured from skin biopsies using methods described in (*90*). iPSCs were maintained on matrigel (#354277, Corning® Matrigel® hESC-Qualified Matrix; Corning, New York) -coated 6 well plates with mTeSR medium (#85850; Stem cell technologies). Cells were passaged at around 80% confluence using 0.5

mM EDTA (#AM9260G; Ambion) for 2-6 minutes. Retinal differentiation was based on a combination of previously described protocols (*91, 92*). Briefly, iPSCs were plated in V- bottomed 96-well plates (9,000 cells/well) containing RevitaCell Supplement (#A-2644501; Gibco, ThermoFisher) and 1% matrigel to induce aggregates formation. Aggregates were then cultured to generates 3D retinal organoids as reported in (*92*).

RNA extraction, cDNA production, and reverse transcription analysis

Total RNA was extracted using the RT-PCR RNeasy MiniKit (QIAGEN, Milan, Italy) from either HEK293 cells or mouse retina transduced with triple ALMS-AAV vectors. RNA was submitted to DNase I digestion (RNase Free DNase set; QIAGEN) and 20 µl cDNA was generated using the SuperScript III Reverse Transcriptase kit (Thermo Fisher Scientific, Waltham, MA, USA) using oligo dT primers. For each sample, the same amount of RNA did not receive the retrotranscriptase enzyme and was used as a control for genomic DNA contamination. Primers for real-time qPCR were designed using the bioinformatic program "Primer Blast" (https://www.ncbi.nlm.nih.gov/ tools/primer-blast/) and purchased from Eurofins Genomics (Eurofins Genomics, Ebersberg, Germany). Serial dilutions of the cDNAs obtained from infected cells were used to measure the primer efficiency, which was between 1.75 and 2.25. SybrGreen real-time qPCR kit was purchased from Roche (Roche, Monza, Italy) and used following the manufacturer's protocol on the LyghtCycler 96 system (Roche). Five microliters of diluted cDNA (1:25 to 1:50 for *in vitro* experiments and 1:5 for the *in vivo* experiments) and 10 pmol of primers were used for PCR in a total volume of 20 µl. Thermal cycling for all genes initiated with an initial denaturation step at 95°C for 5 min, followed by 45 cycles with denaturation at 95°C for 10 s, annealing at 60°C for 20 s, and extension at 72°C for 20 s. Expression data were then normalized versus the corresponding housekeeping genes [h-β-actin for HEK293 cells and mouse GAPDH (mGAPDH) for retinas].

Western blot analysis and ELISA

Samples (HEK293 cells, retina and retinal organoids) were lysed in radio-immunoprecipitation assay (RIPA) buffer (50 mM Tris-HCl [pH 8.0], 150 mM NaCl, 1% NP40, 0.5% Na-deoxycholate, 1 mM EDTA, 0.1% SDS [pH 8.0]) to extract ALMS1, EGFP, CEP290 proteins. Lysis buffers were supplemented with protease inhibitors (Complete Protease inhibitor cocktail tablets; Roche, Basel, Switzerland) and 1 mM phenylmethylsulfonyl. After lysis, EGFP and CEP290 samples were denatured at 99°C for 5 min in 1X Laemmli sample buffer. ALMS1 samples were denatured at 99°C for 5 minutes, 1X Laemmli sample buffer supplemented with 4 M urea. Lysates were separated by 12% (for EGFP sample), 6% (for CEP290 sample), or gradient (#4561086; Bio-Rad, Hercules, CA, USA) 4%–15% (for ALMS1 sample) SDS-PAGE.

The antibodies and dilutions used for immunoblotting are as follows: anti-ALMS1 (1:1,000, polyclonal; ab4306, Abcam, Cambridge, UK); anti-3xflag (1:1000, A8592; Sigma-Aldrich, Saint Louis, MO, USA); anti-Filamin A (1:1000, #4762; Cell Signaling Technology, Danvers, MA, USA); anti-Dysferlin (1:500, Dysferlin, clone Ham1/7B6, MONX10795; Tebu-bio, Le Perray-en-Yveline, France); anti-β-Actin (1:1000, NB600-501; Novus Biological LLC, Littleton, CO, USA). The quantification of EGFP and CEP290 bands detected by Western blot was performed using ImageJ software (free download is available at http://rsbweb.nih.gov/ij/).

The ELISA was performed either on cells or on mouse and pig retinal lysates using the Max Discovery Green Fluorescent Protein Kit ELISA (Bioo Scientific Corporation, Austin, TX, USA).

Animal Models

Mice were housed at the TIGEM animal facility (Naples, Italy) and maintained under a 12-hours light/dark cycle. C57BL/6J mice were purchased from Envigo (Italy).

-ALMS (referred as *Alms1*$^{-/-}$) mice were imported from The Jackson Laboratory (Bar Harbour, MI, USA). The mice were maintained by crossing heterozygous females with heterozygous males. The

Alms1$^{-/-}$mouse harbors the chemically-induced Alms1 c.1080 + 2T > C splice mutation (exon 6-intron 6 splice junction) predicted to result in a frameshift and truncation of ALMS1 (*93*). The genotype of mice was confirmed by PCR analysis on genomic DNA (extracted from the mouse tail tip) followed by DNA sequencing. The primers used for the PCR amplification are as follows:

Fw: 5'-GGTGCACAGAGTGAAAGAATTGC-3';

Rev: 5'-ACTTACCAGTTAAGCCTTGTAGG-3'

which generate a product of 147 bp that was subsequently sequenced using the Fw primer.

-BXD24/TyJ-Cep290rd16/J (referred as *rd16*) mice were imported from The Jackson Laboratory (JAX stock #000031). The *rd16* mouse carries an in-frame deletion of 897 bp encompassing exons 35-39 (*94*). The mice were maintained by crossing homozygous females with homozygous males.

-The Large White female pigs (Azienda Agricola Pasotti, Imola, Italy) used in this study were registered as purebred in the LWHerd Book of the Italian National Pig Breeders' Association and were housed at the Centro di Biotecnologie A.O.R.N. Antonio Cardarelli (Naples, Italy) and maintained under a 12-hours light/dark cycle.

Subretinal injection of AAV Vectors in mice and pigs

This study was carried out in accordance with the Association for Research in Vision and Ophthalmology Statement for the Use of Animals in Ophthalmic and Vision Research and with the Italian Ministry of Health regulation for animal procedures. All procedures on mice were approved by the Italian Ministry of Health; Department of Public Health, Animal Health, Nutrition and Food Safety on March 6th, 2015. Surgery was performed under general anesthesia, and all efforts were made to minimize animal suffering. Mice were anaesthetized with an intraperitoneal injection of 2 mL/100g body weight of ketamine/xylazine, then AAV 2/8 vectors were delivered subretinally *via* a *trans*-scleral *trans*-choroidal approach, as described by Liang et al. (*95*). Eyes were injected with 1 µL, 0.5 µl (for *rd16* pups) of vector solution. The AAV2/8 doses (GC/eye) varied across different

mouse experiments, as described in the Results section. Calpain inhibitor I A6185; Sigma-Aldrich, St. Louis, MO, USA), at a final concentration of 30 µM, was added to the vector mix in mouse eyes injected with triple *ALMS*-AAV vectors intended for histology and real-time qPCR analysis.

Pig eyes were injected with 2 adjacent subretinal blebs of 100 µl of AAV 2/8 vector solution. The AAV 2/8 dose was 2x10^11 GC of each vector/eye, thus co-injection of two AAV vectors resulted in a total dose of 4x10^11 GC/eye.

Histology, Light and Fluorescence Microscopy

To evaluate transgene expression in histological sections, eyes from C57BL/6J mice or Large White pigs were fixed in 4% paraformaldehyde (PFA) overnight and infiltrated with 30% or a gradient 10-30% (for pig eyes) sucrose; the cornea and the lens were then dissected, and the eyecups were embedded in optimal cutting temperature compound (O.C.T. matrix; Kaltek, Padua, Italy). Ten-micrometer-thick serial retinal cryosections were cut along the horizontal meridian, progressively distributed on slides, and mounted with Vectashield with DAPI (Vector Lab, Peterborough, UK). Then, the cryosections were analyzed under the confocal LSM-700 microscope (Carl Zeiss, Oberkochen, Germany) using appropriate excitation and detection settings.

For assessment of PR transduction in mouse retinal cryosections following subretinal combined delivery of AAV 2/8-CMV-EGFP, AAV 2/8-CMV-DsRed, AAV 2/8-CMV-EBFP2 vectors, a single section/eye within the transduced area was selected and the whole slice was thus acquired at 40X magnification. A minimum of 600 PR, identified by DAPI (Vector Laboratories, CA, USA) staining, were counted for each eye. PR-expressing EGFP, DsRed and EBFP2 were unequivocally identified based on their identical shape on picture micrographs of the same field. Transduced PR where counted using ImageJ software (http://rsbweb.nih.gov/ij/) and the number of PR co-expressing EGFP, DsRed and EBFP2 were divided by the total number of PR.

To evaluate the thickness of the outer nuclear layer in *rd16* mice injected with AAV CEP290 intein vectors, eyes were fixed in 4% PFA overnight followed by dehydration in serial ethanols and then embedded in paraffin blocks. Serial cross-sections from *rd16* mice (10 µm) were stained with hematoxylin and eosin (H&E). Then, the sections were analyzed under the microscope (Leica Microsystems GmbH; DM5000) and acquired at 20x magnification. For each eye, one image from the temporal injected side of a slice in the central region of the eye was used for the analysis. Three measurements of the ONL thickness were taken by an operator masked to the genotype/treatment group, in each image, using the "freehand line" tool of the ImageJ software.

Immunohistochemistry and immunofluorescence analysis

Fluorescent immunohistochemistry staining of retinal section injected with triple ALMS-AAV vectors was performed as follows: sections were washed in PBS for 10 min and were permeabilized and blocked with 0.3% Triton X-100, 5% normal goat serum (NGS), 3% bovine serum albumin (BSA) in PBS for 3 hours, then the sections were pre-treated with Avidin/Biotin (SP-2001, Vector Lab, Peterborough, UK) according to manufacturer's instructions. Sections were then incubated overnight with anti-FLAG antibodies (1:200 F1804 Sigma-Aldrich, St. Louis, MO, USA) to detect ALMS1 proteins. Endogenous peroxidases were blocked with 0.3% hydrogen peroxide (H1009, Sigma-Aldrich, St. Louis, MO, USA). Signal was developed using the Vectastain ABC kit (PK-6200 Vector Laboratories, CA, USA) followed by the SuperBoost Tyramide signal amplification (B40942, Thermo Fisher Scientific, Waltham, MA, USA) according to the manufacturer's instructions.

HeLa cells transfected with CEP290 AAV intein plasmids were fixed 24 hours post-transfection in 4% PFA for 10 minutes. Cells were blocked in blocking buffer (0.05% Saponin, 0.5% BSA, 50mM NH_4Cl, 0.02%NaN_3 in PBS, pH7.2) for 30 minutes and then incubated as follows: overnight with anti-FLAG antibody (F7425 Sigma-Aldrich) to detect CEP290 protein, and with anti-Acetylated tubulin antibody (T6793, Sigma-Aldrich) to stain the microtubules. After washing in PBS, cells were incubated with

secondary antibodies for 1 hour: goat anti-rabbit Alexa Fluor 594 and donkey anti-mouse Alexa Fluor 488, directed against anti-FLAG and -Ac-Tubulin antibody, respectively.

The antibodies used for immunofluorescence of human retinal organoids are as follows: anti-human cone-arrestin (CAR) (48, 49) (1:10000, 'Luminaire founders' hCAR; gift from Dr Cheryl M. Craft, Doheny Eye Institute, Los Angeles, CA, USA); anti-Opsin, Red/Green (1:200, AB5405; Merck Millipore, Darmstadt, Germania); anti-Recoverin (1:500, AB5585; Merck Millipore); anti-CRX (A-9, 1:250, sc377138; Santa Cruz Biotechnology, Dallas, Texas, USA); anti-Rhodopsin (1D4, 1:200, ab5417, Abcam, Cambridge, MA, USA). Alexa Fluor 594 was used as secondary antibody.

Stained sections were mounted with Vectashield with DAPI (Vector Laboratories, CA, USA). Cryosections were analyzed under the confocal LSM-700 microscope (Carl Zeiss, Oberkochen, Germany) and acquired at either 63x (for retinal sections and HeLa cells) or 40x (for organoid sections) magnification.

Ultrastructural microscopy analysis

Retinal organoids were fixed overnight with a mixture of 2% PFA and 1% GA in 0.2 M PHEM buffer pH 7.3. After fixation, the specimens were post-fixed as described in (*96*). Then they were dehydrated, embedded in epoxy resin and polymerized at 60°C for 72 hours. Thin serial 60 nm sections were cut at the Leica EM UC7 microtome. EM images were acquired from thin serial sections using a FEI Tecnai-12 electron microscope equipped with a VELETTA CCD digital camera (FEI, Eindhoven, The Netherlands).

Spectral domain optical coherence tomography

Spectral domain optical coherence tomography (SD-OCT) images were obtained using the Bioptigen Spectral Domain Ophthalmic Imaging System [(SDOIS); Envisu R2200, Bioptigen, Morrisville, NC, USA)]. Mice were anaesthetized and pupils were dilated by applying 1–2 drops of topical 0.5% tropicamide (Visufarma, Rome, Italy). To prevent corneal desiccation during the procedure, topical lubricant eye drops (Recugel; Bausch & Lomb, Rochester, NY, USA) were applied bilaterally with a small brush. Mice were positioned into the animal imaging mount and rodent alignment stage (AIM-RAS; Bioptigen, Morrisville, NC, USA); the laser source was placed in front of the mouse, and images were acquired by the InVivoVue Clinic software (Bioptigen, Morrisville, NC, USA). Three images, one central, one superior, and one inferior to the optic nerve, were taken from each eye. ONL thickness was manually measured three times from each OCT scan image and averaged.

Pupillary light response

Pupillary light responses (PLR) from *rd16* mice were recorded in dark condition using the TRC-50IX retinal camera connected to a charge-coupled device NikonD1H digital camera (Topcon biomedical system, Oakland, NJ). Mice were exposed to 10 lux light-stimuli for approximately 10 seconds and one picture per eye was acquired by the IMAGEnet software (Topcon Biomedical Systems). For each eye, pupil diameter was normalized to the eye diameter (from temporal to nasal side).

Electrophysiological Recordings

For electroretinographic analyses, mice were dark-adapted for 3 hours. Mice were anaesthetized and positioned in a stereotaxic apparatus, under dim red light. Their pupils were dilated with a drop of 0.5% tropicamide (Visufarma, Rome, Italy), and body temperature was maintained at 37.5 °C. Light flashes were generated by a Ganzfeld stimulator (CSO, Costruzione Strumenti Oftalmici, Florence, Italy). The electrophysiological signals were recorded through gold-plate electrodes

inserted under the lower eyelids in contact with the cornea. The electrodes in each eye were referred to a needle electrode inserted subcutaneously at the level of the corresponding frontal region. The different electrodes were connected to a two-channel amplifier. After completion of responses obtained in dark-adapted conditions (scotopic), the recording session continued with the purpose of dissecting the cone pathway mediating the light response (photopic). To minimize the noise, different responses evoked by light were averaged for each luminance step. The maximal scotopic response of rods and cones was measured in dark conditions (scotopic) with two flashes of 0.7 Hz and a light intensity of 20 cd s/m^2, photopic cone responses were isolated in light conditions with a continuous background white light of 50 cd s/m^2, with 10 flashes of 0.7 Hz and a light intensity of 20 cd s/m^2.

Statistical analysis

The statistical analysis of the data in **Figure 17, 18** has been carried out by calculating the Bayes factor. The p-values of statistical analysis of *Alms1*$^{-/-}$ vs *Alms1*$^{-/+}$ are: for OCT: 39.26; for ERG a-wave: 5.972; for ERG b-wave: 2.415.

The Student's t-test was used to compare data depicted in **Figure 20**. The p-values of statistical analysis between *Alms1*$^{-/-}$ treated eye vs *Alms1*$^{-/-}$ are: for OCT: 0.18 at 4+6 months and 0.47 at 8+10 months; for the ERG a-wave: 0.45 at 5+7 months and 0.64 at 9+11 months; for the ERG b-wave: 0.047 at 5+7 months and 0.73 at 9+11 months.

One-way analysis of variance (ANOVA) with *post-hoc* multiple comparison procedure was used to compare data depicted in ELISA assay for EGFP protein quantification *in vitro* (pANOVA = 2.5E-06), in the mouse retina (pANOVA = 0.033), and in the pig retina (pANOVA = 7.7E-05); ERG analysis in **Figure 41B,C** (a-wave pANOVA= 0.97; b-wave pANOVA= 0.998); OCT analysis in **Figure 41A** (pANOVA= 0.15). The statistically significant differences between groups determined with the *post-hoc* multiple comparison procedure are the following in ELISA assay for EGFP protein quantification

in vitro (single AAV *vs* dual AAV = 3.3E-06; AAV intein *vs* dual AAV = 2.4E-05; single AAV *vs* AAV intein = 0.29), in the mouse retina (single AAV *vs* dual AAV = 0.027; AAV intein *vs* dual AAV = 0.27; single AAV *vs* AAV intein = 0.35) and in the pig retina (single AAV *vs* dual AAV = 1.7E-04; AAV intein versus dual AAV = 2.4E-04; single AAV *vs* AAV intein = 0.97). Student's t-test was used to analyze data in **Figure 42B** (p Student's t-test = 0.004) and **Figure 43B** (p Student's t-test = 0.001).

Data are presented as mean ± standard error of the mean (s.e.m.) which has been calculated using the number of independent *in vitro* experiments or eyes (not replicate measurements of the same sample). Statistical p-values ≤ 0.05 were considered significant.

RESULTS

Specific aim 1

Mouse photoreceptors are simultaneously transduced by three independent AAV vectors injected subretinally

The first aim of my project was to expand AAV transfer capacity up to 14 kb by developing triple AAV vectors, i.e. to add a third vector to the previously described dual AAV system. The enclosed and small subretinal space should favor co-infection and transduction of the same cell by three independent AAV vectors. To test this, C57BL/6J mice were injected subretinally (n=6 eyes) with a mixture of AAV 2/8 vectors separately encoding EGFP, DsRed and EBFP2 under the control of the ubiquitous CMV promoter (dose of each vector/eye: 8x10^8 GC), eyes were harvested 4 weeks post-injection and co-transduction was assessed on retinal cryosections (**Fig. 11**). Specifically, 3.5 ± 0.2% of PR were found to be co-transduced by three independent AAV vectors.

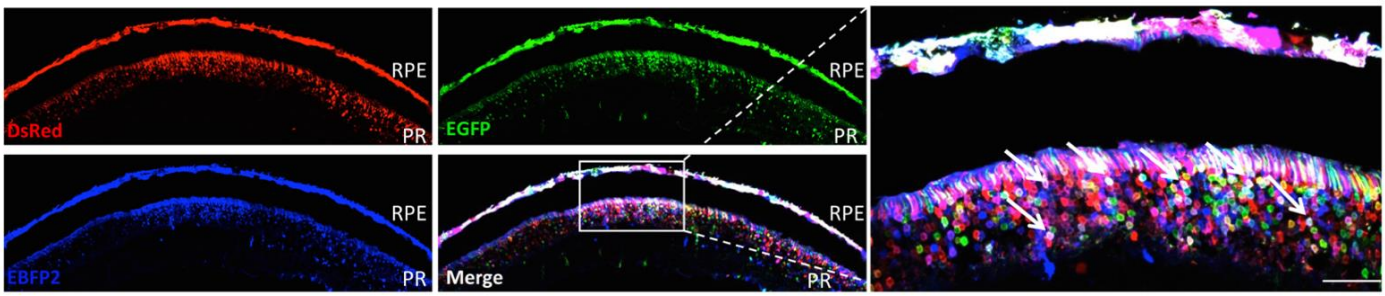

Figure 11. Three independent AAV vectors co-transduce mouse photoreceptors
Fluorescence analysis of retinal cryosections from C57BL/6J mice 4 weeks following subretinal injection of AAV2/8 vectors encoding for either EGFP, DsRed or EBFP2, under the control of the ubiquitous CMV promoter. The pictures, with insets at higher magnification, are representative of n=6 eyes injected with three single AAV vectors. The scale bar (50 µm) is depicted in the figure. EGFP: enhanced green fluorescent protein; DsRed: Discosoma red fluorescent protein; EBFP2: enhanced blue fluorescent protein 2. Merge: overlay of EGFP, DsRed and EBFP2 images; RPE: retinal pigmented epithelium; PR: photoreceptors. Arrows point at white photoreceptors that co-express the three fluorescent reporters.

Generation of triple *ALMS1*-AAV vectors

I then split *ALMS1* into three parts each cloned in a separate AAV vector hereinafter called ALMS-AAV I, ALMS-AAV II, ALMS-AAV III (**Fig. 12**).

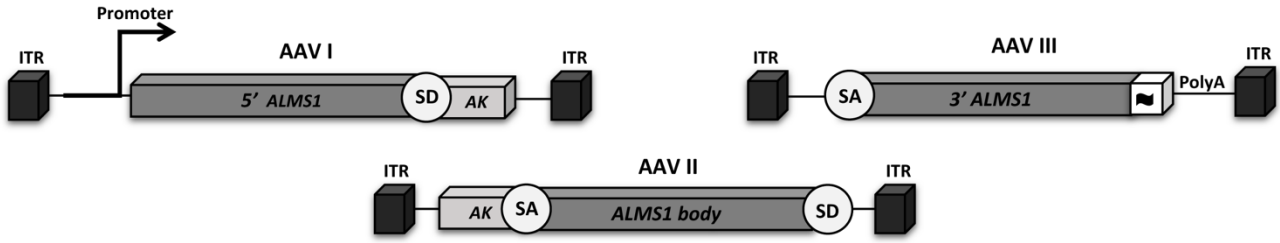

Figure 12. Schematic representation of triple ALMS-AAV vectors
SD: splicing donor signal; SA: splicing acceptor signal; AK: F1 phage recombinogenic region; ⚑ triple flag tag; Promoter: ubiquitous shCMV for the *in vitro* experiments and the human G-protein coupled receptor (GRK1) promoter for the *in vivo* experiments with the exception of western blot analysis where the shCMV was used; PolyA: polyadenylation signal.

Due to the large size of the *ALMS1* CDS (12.5 kb), AAV I requires a small promoter to fit in a normal size AAV. For this reason, several short CMV promoters (*30, 77, 78*) were cloned in an AAV vector expressing EGFP, transfected in HEK293 cells and protein expression evaluated by either fluorescence microscopy or WB analysis (**Fig. 13**). Among these, the short CMV 260 (shCMV) (*30*) was found to drive robust EGFP expression and thus included in the *ALMS*-AAV I vector. In addition, to drive ALMS1 expression specifically in PR, the small human G protein-coupled receptor kinase 1 (GRK1) promoter was included in the second set of *ALMS*-AAV I.

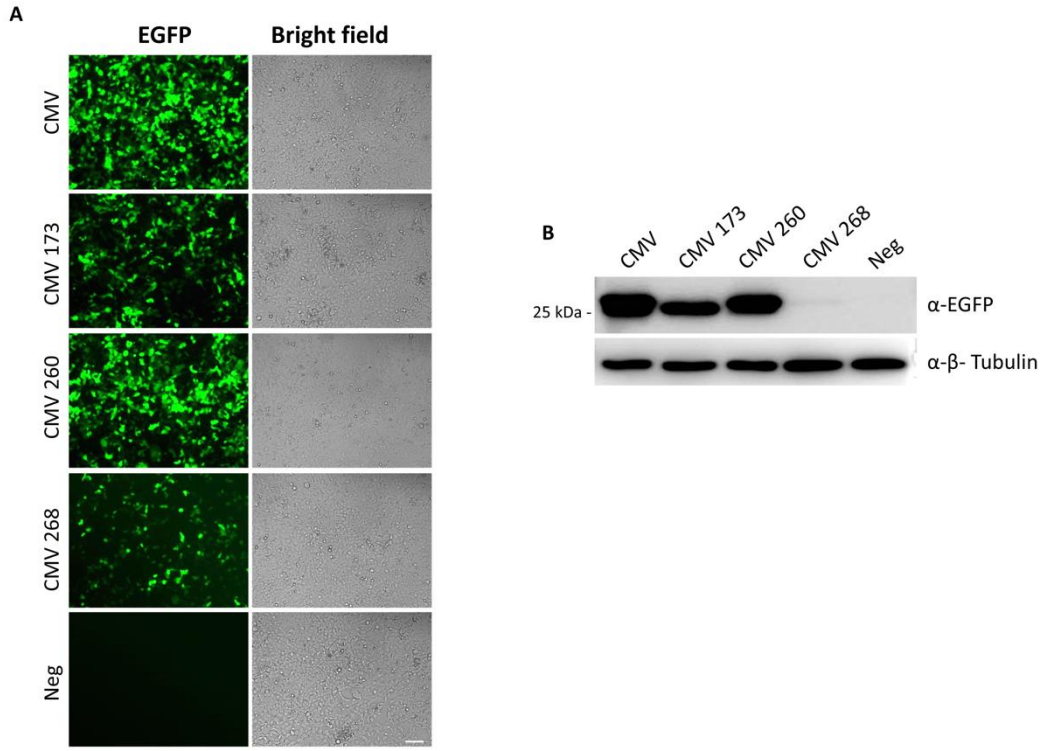

Figure 13. EGFP fluorescence in HEK293 cells transfected with EGFP plasmids with different CMV promoters
Either fluorescence (**A**) or Western blot (WB) analysis (**B**) of HEK293 cells transfected with full-length EGFP plasmids with different CMV promoters. The scale bar (100 µm) is depicted in the figure. pEGFP: cells transfected with a plasmid including the full-length EGFP expression cassette under the control of the: CMV-full-length CMV promoter; CMV 173-short CMV of 173 bp; CMV 260-short CMV of 260 bp; CMV 268-short CMV of 268 bp; Neg: untransfected cells. α-EGFP: WB with anti-EGFP antibodies; α-β-Tubulin: WB with anti-β-Tubulin antibodies, used as loading control.

Triple ALMS-AAV vectors efficiently transduce HEK293 cells

HEK293 cells were infected with the various combinations ALMS-AAV2/2 vectors at an m.o.i of 5x 10^4 GC/cell and analyzed 72 hours post-infection. The expression of full-length and truncated products of ALMS1 was evaluated by WB using either anti-3xflag or anti-ALMS1 antibodies to detect ALMS1. As shown in **Figure 14**, full-length proteins of the expected size (~ 460 kDa) were detected only following co-infection with the three ALMS-AAV vectors. A truncated product of ~270 kDa (B) was detected with anti-3xflag antibodies when ALMS-AAV I+III was included in the infection mix (**Fig. 14A**). The 2 bands of ~171 and ~117 kDa present in all lanes of the WB are presumably due to aspecific antibody binding (**Fig. 14B**).

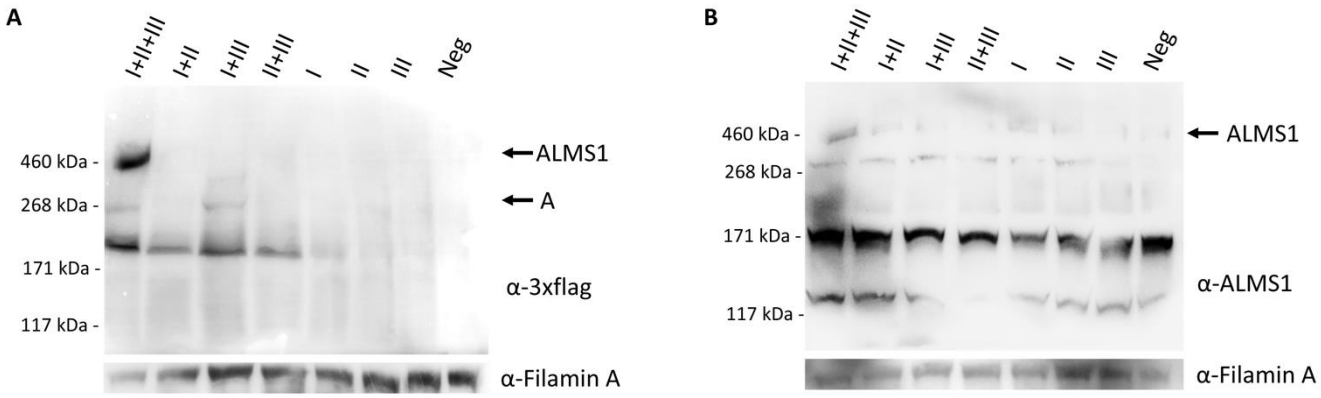

Figure 14. Triple ALMS-AAV vectors efficiently reconstitute ALMS1 in vitro
Western blot (WB) analysis of lysates from HEK293 cells infected with triple AAV 2/2 vectors encoding for ALMS1 under the control of the shCMV promoter and incubated with either anti-3xflag (A) or anti-ALMS1 (B) antibodies. The arrows indicate the full-length ALMS1 protein and A: protein product derived from AAV I+III. α-3xflag: WB with anti-3xflag antibodies; α-ALMS1: WB with anti-ALMS1 antibodies; α-Filamin A: WB with anti-Filamin A antibodies, used as loading control. Neg: cells infected with control AAV 2/2-CMV-*EGFP* vectors. The molecular weight ladder is depicted on the left, 200 µg of proteins were loaded.

Subretinal administration of triple *ALMS*-AAV is safe and results in full-length transgene expression in mouse retina

Then, I tested whether subretinal administration of triple AAV2/8 vectors results in expression of ALMS1 in the mouse retina. To do so, C57BL/6J mice were injected subretinally with triple *ALMS*-AAV vectors (dose of each vector/eye: 2x10^9 GC) under the control of the shCMV promoter. Animals were sacrificed 3 months post-injection and transgene expression was evaluated by WB analysis on eye-cup lysates which revealed full-length ALMS1 expression in 5 out of 8 eyes injected with triple AAV vectors. Moreover, no truncated products were observed in the same injected eyes (**Fig. 15**). I have also evaluated the expression levels of ALMS1 by RT-qPCR and found that transgenic ALMS1 was on average (n=3 eyes) 7 ± 2 % of endogenous (0.22 ± 0.02 % of mGAPDH).

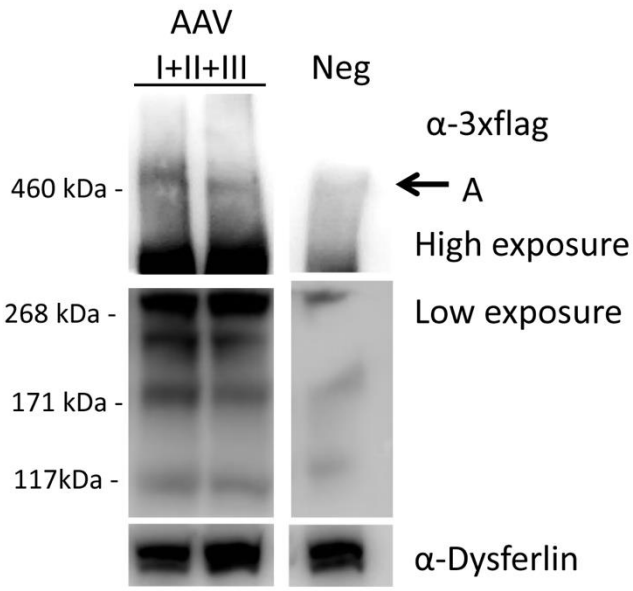

Figure 15. Subretinal administration of triple AAV vectors results in full-length ALMS1 protein expression in the mouse retina

Western blot (WB) analysis of eyecup lysates from C57BL/6J mice 3 months following subretinal injection of triple AAV 2/8 encoding for ALMS1 under the control of the ubiquitous shCMV promoter. The arrow on the right indicate full-length ALMS1. α-3xflag: WB with anti-3xflag antibodies; α-Dysferlin: WB with anti-Dysferlin antibodies, used as loading control. Neg: eyecup lysates following injection with PBS. The molecular weight ladder is depicted on the left, whole eyecup lysates was loaded.

In addition, no evident signs of toxicity were observed by optical coherence tomography (OCT) analysis (**Fig. 16**) in animals injected 2 months before with either triple ALMS or ALMS-AAV I + III, the combination of viruses that produced the highest levels of truncated products *in vitro*.

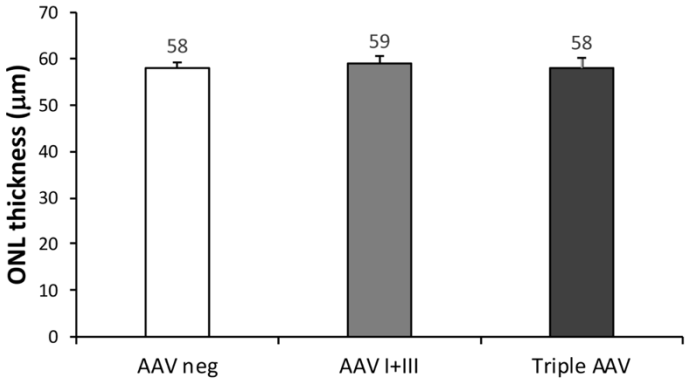

Figure 16. Subretinal delivery of triple AAV vectors is safe in the mouse retina

Spectral domain optical coherence tomogram analysis of C57BL/6J mice injected subretinally with AAV2/8 intein vectors encoding for *ALMS1* under the control of the shCMV promoter. AAV neg: eyes injected with unrelated AAV vectors or PBS; AAV I+III: eyes injected with a combination of AAV I and AAV III vectors; Triple AAV: eyes injected with triple *ALMS*-AAV vectors. Data are represented as mean ± s.e.m. The mean values are indicated above the corresponding bar.

Characterization of the retinal phenotype of a mouse model of ALMS

To test the efficacy of triple *ALMS*-AAV vectors, I used a mouse model kindly provided by the Jackson Laboratory (Bar Harbour, MI, USA) caused by a targeted disruption of the mouse *Alms1* locus (*Alms1*$^{-/-}$). A detailed characterization of the retinal phenotype of the mouse was lacking, thus I have characterized it at different ages. Retinal morphology and visual function of *Alms1*$^{-/-}$ and littermate controls (*Alms1*$^{-/+}$ or wt) mice were analyzed by spectral domain optical coherence tomography (SD-OCT) and electroretinography (ERG). *Alms1*$^{-/-}$ mice displayed a significantly (BF: 39.26) thinner outer nuclear layer (ONL) than those of *Alms1*$^{-/+}$ littermates, which decreased over time (**Fig. 17**).

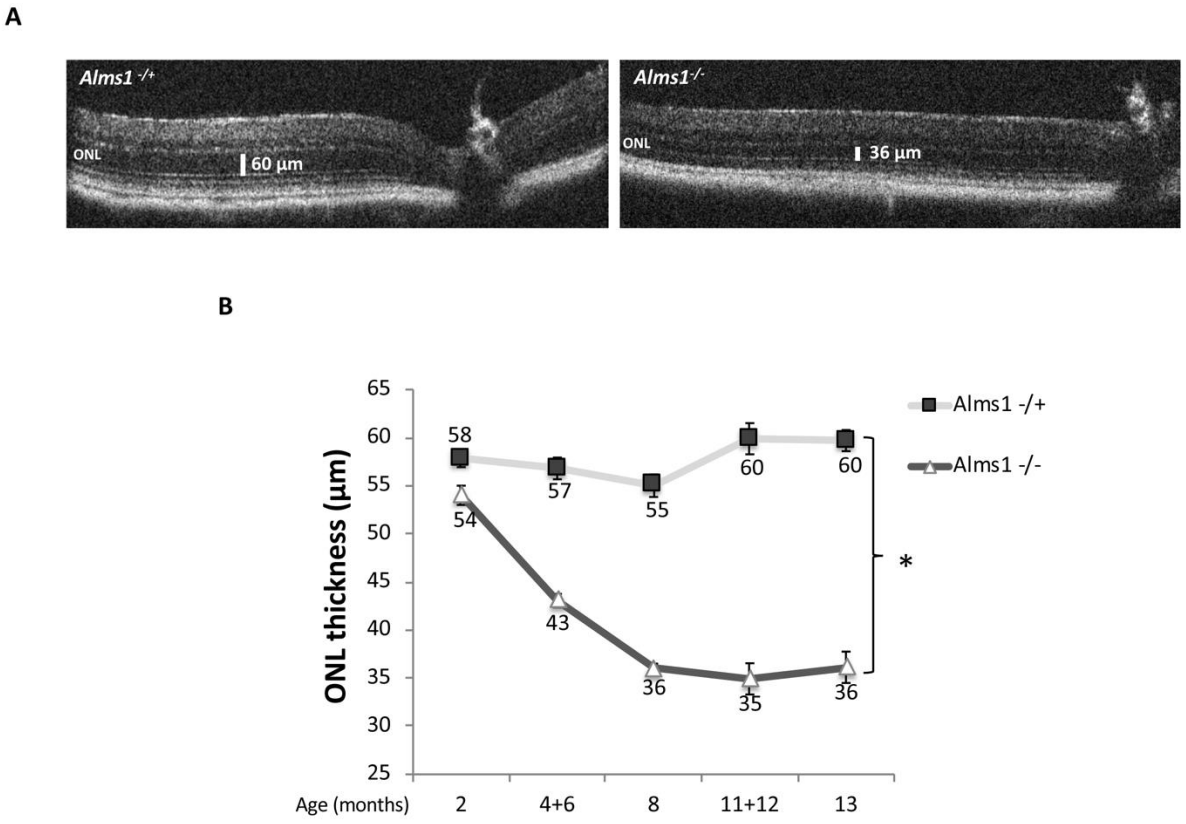

Figure 17. Retinal morphology of Alms1*$^{-/-}$ *mice

(**A**) Spectral Domain Optical Coherence Tomograms (SD-OCT) of 13 month-old *Alms1*$^{-/+}$ and *Alms1*$^{-/-}$ mice. The thickness of the outer nucler layer (ONL) is depicted by a white bar (60 µm for the *Alms1*$^{-/+}$ mouse and 36 µm for the *Alms1*$^{-/-}$ mouse).

(**B**) Measurement of ONL thickness by SD-OCT in *Alms1*$^{-/-}$ (grey line) and *Alms1*$^{-/+}$ (black line) mice over time.

Data are represented as mean ± s.e.m. The mean values are indicated above the corresponding bar.

Consequently, the *Alms1*$^{-/-}$ electroretinographic a-wave and b-wave amplitudes were found to be significantly (BF a-wave: 5.972, b-wave: 2.415) lower than those of *Alms1*$^{-/+}$ or wt control littermates (**Fig. 18**). Both the ONL thickness and the light responses of *Alms1*$^{-/+}$ were similar to those observed in C57BL/6J mice (*data not shown*). In conclusion, the *Alms1*$^{-/-}$ mice display a retinal phenotype at both morphological and functional levels and thus represent a good small pre-preclinical model of ALMS.

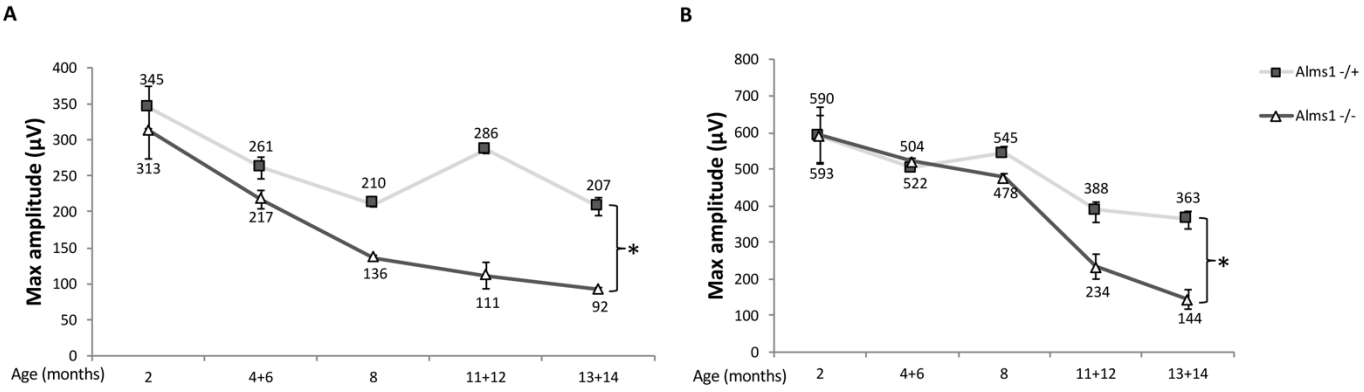

Figure 18. Retinal electrical responses of Alms1$^{-/-}$ mice

Electroretinogram (ERG) analysis of a-wave (A) and b-wave (B) light response in *Alms1* $^{-/-}$ (grey line) and Alms1$^{-/+}$ mice (black line) over time. The asterisks mark significant differences between *Alms1* $^{-/-}$ and *Alms1* $^{-/+}$ mice. The time points of the analysis are depicted below each indicator. Data are represented as mean ± s.e.m. The mean values are indicated above the corresponding bar.

Transient and mild improvement of the ALMS mice retinal phenotype by triple AAV vectors

To test whether the levels of PR transduction obtained with triple AAV vectors are therapeutically relevant, I used a set of triple *ALMS*-AAV vectors which includes an AAV I vector with the GRK1 promoter, which restricts transgene expression to PR, where ALMS1 is known to localize (*97, 98*). Subretinal injection of these vectors (dose of each vector/eye: 2x10^9 GC) in 4-week-old C57BL/6J mice results in ALMS1 proper PR localization 2 months after injection (**Fig. 19**). I can infer that transgenic ALMS1 staining derives from full-length protein, as ALMS1 potential localization signal is

predicted to be at the N terminus of the protein (*99*) while the 3xflag tag at the C-terminus and transcripts from ALMS-AAV I + III would be out of frame.

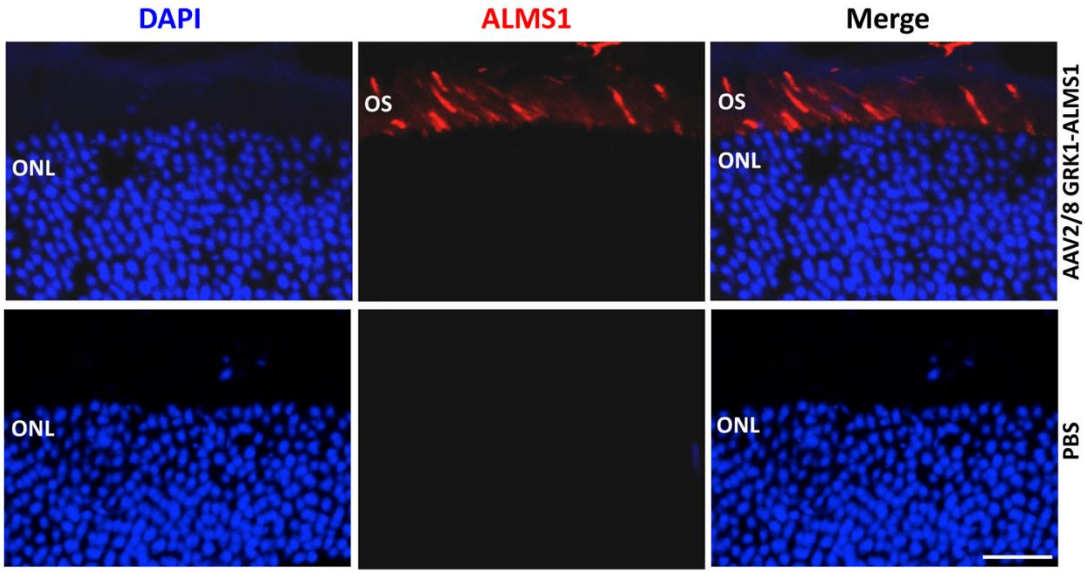

Figure 19. Subretinal administration of triple AAV vectors results in ALMS1 proper localization in mouse PR
Immunohistochemical (IHC) analysis with anti-3xflag antibodies of retinal cryosections from C57BL/6J mice 2 months following subretinal injections of either triple AAV 2/8 encoding for ALMS1 under the control of the PR-specific GRK1 promoter or PBS (indicated on the right of the corresponding images). The pictures are representative of n=4 injected eyes. The scale bar (20 µm) is depicted in the figure. DAPI: 4',6'-diamidino-2-phenylindole staining; Merge: overlay of DAPI and ALMS1; ONL: outer nuclear layer; OS: outer segment.

Triple GRK1-*ALMS*-AAV vectors were then injected subretinally in 4-week-old *Alms1*$^{-/-}$ mice, which received PBS in the contralateral eye. Four months post-injection, I evaluated by real-time qPCR the expression of the transgenic *ALMS1* transcript and found that this was 8.1% ± 6.6% of endogenous. In terms of impact on *Alms1*$^{-/-}$ retinal morphology and function, I observed a modest improvement in the outer nuclear layer (ONL) thickness (**Fig. 20A**), and in the electroretinogram a- (**Fig. 20B**) and b-wave (**Fig. 20C**) amplitudes between 5 and 7 months of age (i.e., 4–6 months after gene delivery), which was lost at 9–11 months of age.

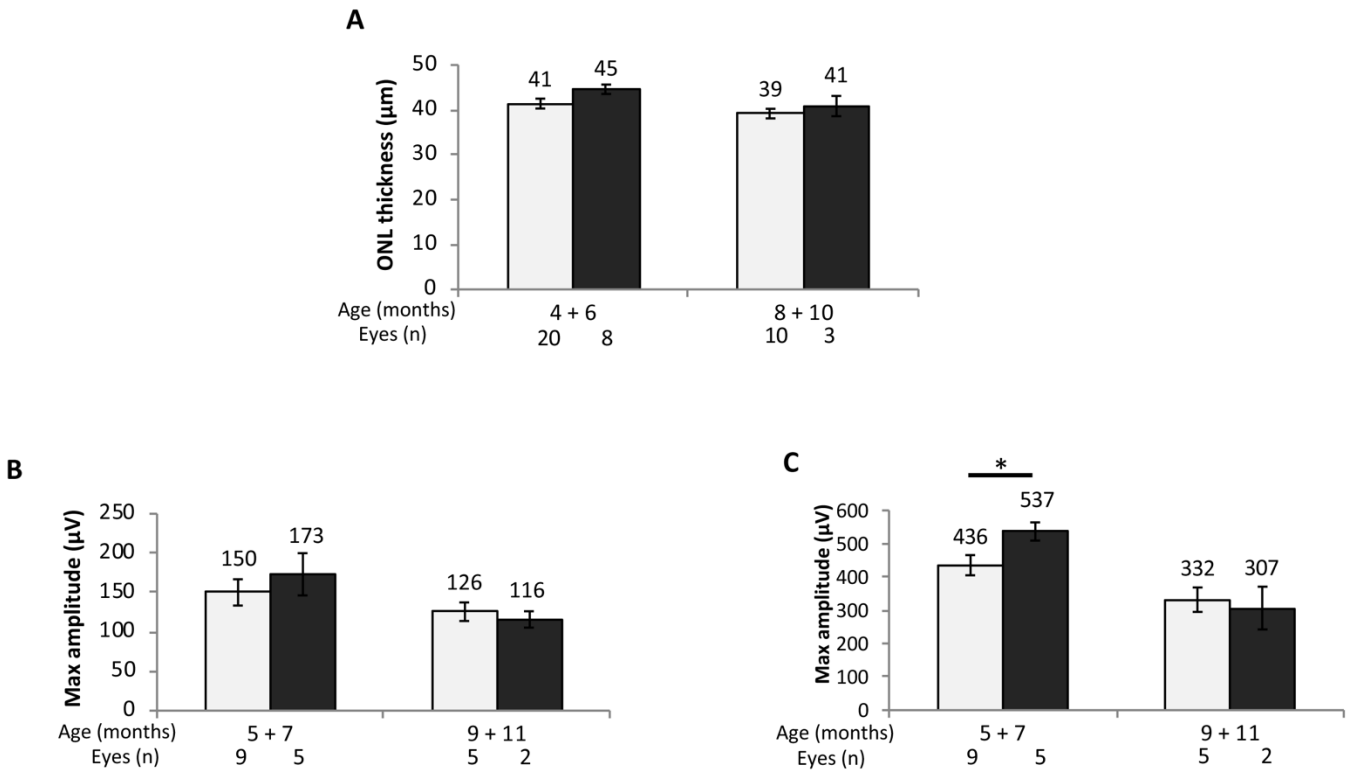

Figure 20. Subretinal administration of triple AAV vectors results in transient improvement of the retinal phenotype of Alms1$^{-/-}$ mice

(**A**) Spectral Domain Optical Coherence Tomograms analysis of *Alms1*$^{-/-}$ mice injected subretinally with either triple *ALMS*-AAV vectors (black bars) in one eye or PBS in the contralateral eye (white bars).

(**B-C**) Electroretinogram analysis of a-wave (B) and b-wave (C) light responses of *Alms1*$^{-/-}$ mice injected subretinally with either triple *ALMS*-AAV vectors (black bars) or PBS in the contralateral eye (white bars).

Data are represented as mean ± s.e.m. The mean values are indicated above the corresponding bar.

Specific aim 2

Generation of AAV-*EGFP* intein vectors

The second aim of my project was to find a strategy for large genes reconstitution in the retina alternative and potentially more effective than dual or triple AAV. To do so, I tested the ability of intein-mediated protein *trans*-splicing in reconstituting large proteins. First, I have generated two AAV vectors each encoding either the N- or the C-terminal halves of the reporter EGFP protein fused to the N- and C- terminal halves of the DnaE split-intein from *Nostoc punctiforme* [Npu, **Fig. 21** (*82, 83*)], respectively. Each AAV vector included appropriate regulatory elements (i.e. a promoter and a polyadenylation signal) and a 3xflag tag to allow detection of both halves as well as of the full-length reconstituted EGFP protein (**Fig. 21**).

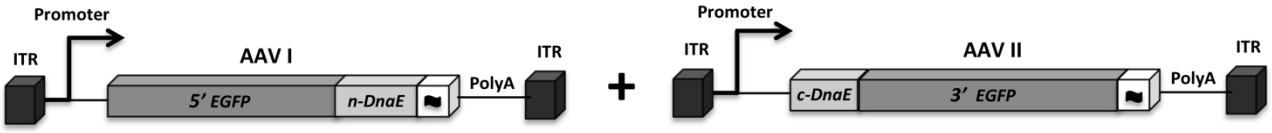

Figure 21. Schematic representation of EGFP-AAV intein
ITR: AAV2 inverted terminal repeats; n-DnaE: n-intein from DnaE of *Npu*; c-DnaE: c-intein from DnaE of *Nostoc punctiforme*; 3xflag tag; PolyA: polyadenylation signal.

AAV-*EGFP* intein plasmids were used to transfect HEK293 cells and evaluate the production of single N- and C-terminal halves as well as of the full-length EGFP protein. EGFP fluorescence, comparable to that observed in cells transfected with a single AAV plasmid that encodes full-length EGFP, was detected in cells co-transfected with the AAV-*EGFP* intein plasmids but not with the single N- and C-terminal AAV-*EGFP* intein plasmids. The presence of *trans*-spliced EGFP protein of the expected size (~28 kDa) along with DnaE intein (~17 kDa) spliced out from the mature protein was confirmed by Western blot (WB) analysis of HEK293 cell lysates only following co-transfection of both AAV-*EGFP* intein plasmids (**Fig. 22**). In addition, quantification of bands' intensity showed that EGFP protein

levels from AAV intein plasmids were 76% ± 37% (n= 3 independent experiments) of those observed from a single AAV plasmid.

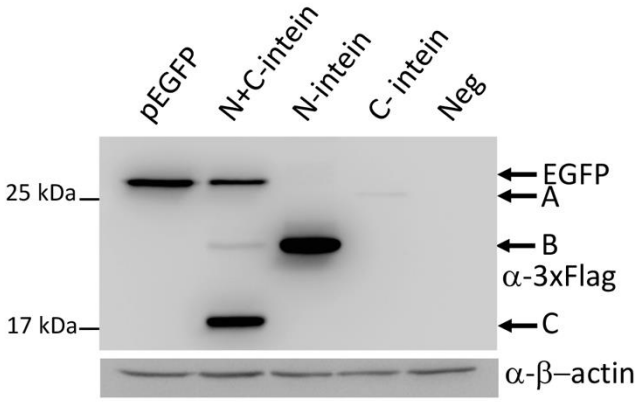

Figure 22. Split-inteins reconstitute EGFP in vitro

Western blot (WB) analysis of lysates from HEK293 transfected with either full-length or AAV intein *EGFP* plasmids with the ubiquitous CMV promoter. pEGFP: cells transfected with a full-length *EGFP* plasmid; N+C-intein: cells co-transfected with pAAV-*EGFP* I+II intein plasmids; N-intein: cells transfected with the single pAAV-*EGFP* I intein plasmid; C-intein: cells transfected with the single pAAV-*EGFP* II intein plasmid; Neg: untransfected cells. The arrows indicate both the full-length EGFP protein (EGFP) and A, B: the C- and N-terminal halves of the EGFP protein, respectively; C: the reconstituted intein excised from the full-length EGFP protein. α-3xflag: WB with α-3xflag antibodies; α-β-actin: WB with α-β-actin antibodies, used as loading control. The molecular weight is depicted on the left. Ten µg of proteins were loaded. The WB are representative of n=5 independent experiments.

AAV-*EGFP* intein reconstitute protein more efficiently than dual AAV vectors *in vitro*

To define the efficiency of AAV intein-mediated protein reconstitution, I compared the levels of EGFP achieved by intein to that of both a single normal size AAV vector and dual AAV vectors, which are considered the gold standard for delivering large genes to PR (*61, 62*). HEK293 cells were infected with either AAV 2/2-CMV-*EGFP* intein or with single and dual AAV vectors that included the same expression cassette (m.o.i 5x10^4 GC)/cell of each vector). Seventy-two hours after infection, cell lysates were harvested and EGFP expression was evaluated by both WB and enzyme-linked immunosorbent assay (ELISA), to quantify precisely EGFP protein levels (**Fig. 23**). Notably, AAV intein reconstituted EGFP protein at levels that were around half of those achieved with a single AAV (single AAV = 0.735 ± 0.2 ng EGFP/µg total lysate, n=5 independent experiments; AAV intein = 0.403 ± 0.04 ng EGFP/µg total lysate, n=5 independent experiments) and 10-times higher than those

obtained with dual AAV vectors (dual AAV=0.046 ± 0.01 ng EGFP/µg total lysate, n=5 independent experiments).

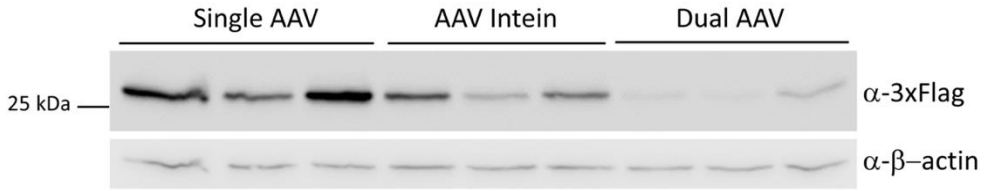

Figure 23. AAV intein reconstitute EGFP expression in vitro at higher levels compared to dual AAV
Western blot (WB) analysis of lysates from HEK293 infected with either single or dual and intein AAV2/2 vectors encoding for *EGFP* under the control of the ubiquitous CMV promoter. α-3xflag; WB with α-3xflag antibodies; α-β-actin: WB with α-β-actin antibodies, used as loading control. The molecular weight is depicted on the left. Ten µg of proteins were loaded. The WB are representative of n=5 independent experiments.

Subretinal administration of AAV-*EGFP* intein vectors results in efficient full-length protein reconstitution in both mouse and pig retina

To investigate whether AAV intein-mediated *trans*-splicing reconstitutes full-length protein expression *in vivo*, C57BL/6J mice were injected subretinally with AAV2/8-CMV-*EGFP* intein vectors (dose of each vector/eye: 5.8x10^9 GC). Eyes were harvested 1 month later and analyzed by microscopy analysis. EGFP fluorescence was detected in all eyes (n=5) in retinal pigment epithelium and, most importantly, in photoreceptors (**Fig. 24**).

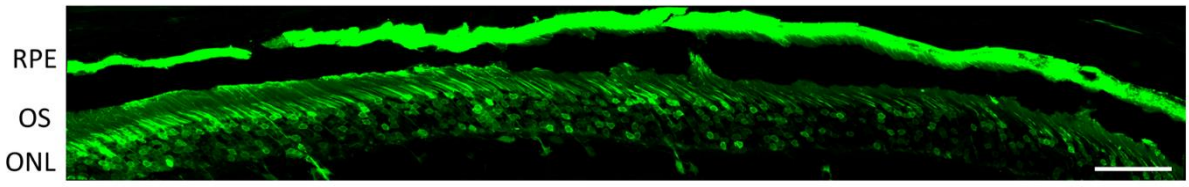

Figure 24. AAV intein-mediated reconstitution of EGFP protein in the murine retina
Retinal cryosections from C57BL/6J mice injected subretinally with AAV 2/8 intein vectors encoding for *EGFP* under the control of the CMV promoter. Scale bar: 50 µm. RPE: retinal pigment epithelium; OS: outer segments; ONL: outer nuclear layer.

To compare AAV intein photoreceptor transduction levels to those of single and dual AAV, mice were injected subretinally with AAV 2/8 vectors (dose of each vector/eye: 5x10^9 GC) that encode EGFP under the control of the GRK1. Eyes were harvested 1 month post-injection and analyzed by either fluorescence microscopy or ELISA. EGFP fluorescence was detected in the photoreceptor cell layer in eyes injected with all set of vectors (**Fig. 25**). Precise quantification of EGFP protein levels by ELISA confirmed that AAV intein reconstituted EGFP protein to levels that were lower compared with a single AAV and about 3-times higher than dual AAV (single AAV = 8.41 ± 2.48 ng EGFP/retina, n=5 eyes; AAV intein = 3.72 ± 0.85 ng EGFP/retina, n=7 eyes; dual AAV =1.38 ± 0.43 ng EGFP/retina, n=7 eyes).

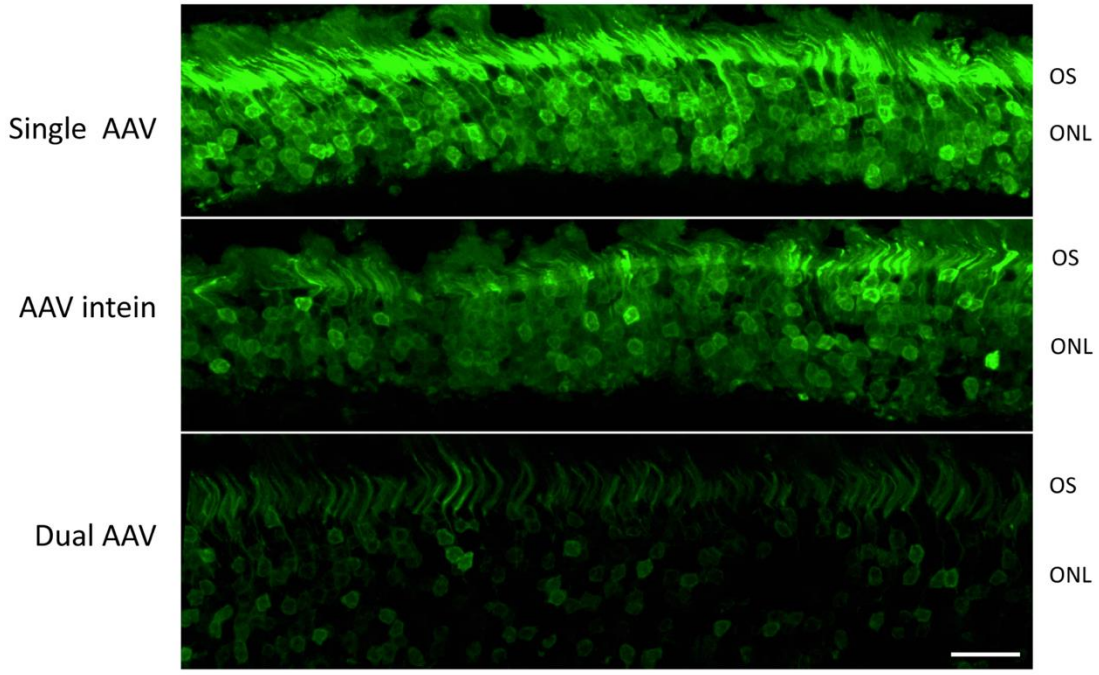

Figure 25. AAV intein reconstitute EGFP expression in the murine retina at higher levels compared to dual AAV
Representative images of retinal cryosections from C57BL/6J mice injected subretinally with either single, intein or dual AAV2/8 vectors enconding for *EGFP* under the control of the PR-specific GRK1 promoter. The scale bar (50 µm) is depicted in the figure. OS: outer segment; ONL: outer nuclear layer.

Then, I have evaluated the efficiency of AAV intein vectors at transducing photoreceptors in the pig retina, which is an excellent pre-clinical model to evaluate viral vector transduction due to its size and architecture (*27*). Thus, Large White pigs were injected subretinally with single, intein and dual AAV2/8-GRK1-*EGFP* vectors (dose of each vector/eye: 2x10^11 GC, delivered through two adjacent subretinal blebs). Eyes were harvested 1 month post-injection and analyzed by either fluorescence microscopy or ELISA. Notably, AAV intein-mediated EGFP protein reconstitution in the photoreceptor cell layer was significantly higher than that mediated by dual AAV and indistinguishable from single AAV vectors, as assessed by EGFP fluorescence (**Fig. 26**). Precise quantification of EGFP protein levels in retinal lysates confirmed that AAV intein reconstitute the protein to levels that are similar to those achieved with a single AAV and about 3-times higher than those obtained with dual AAV vectors (single AAV = 247.5 ± 45.1 ng EGFP/retina, n= 5 eyes; AAV intein = 227.0 ± 15.7 ng EGFP/retina, n=5 eyes; dual AAV = 82.3 ± 9.6 ng EGFP/retina, n=5 eyes).

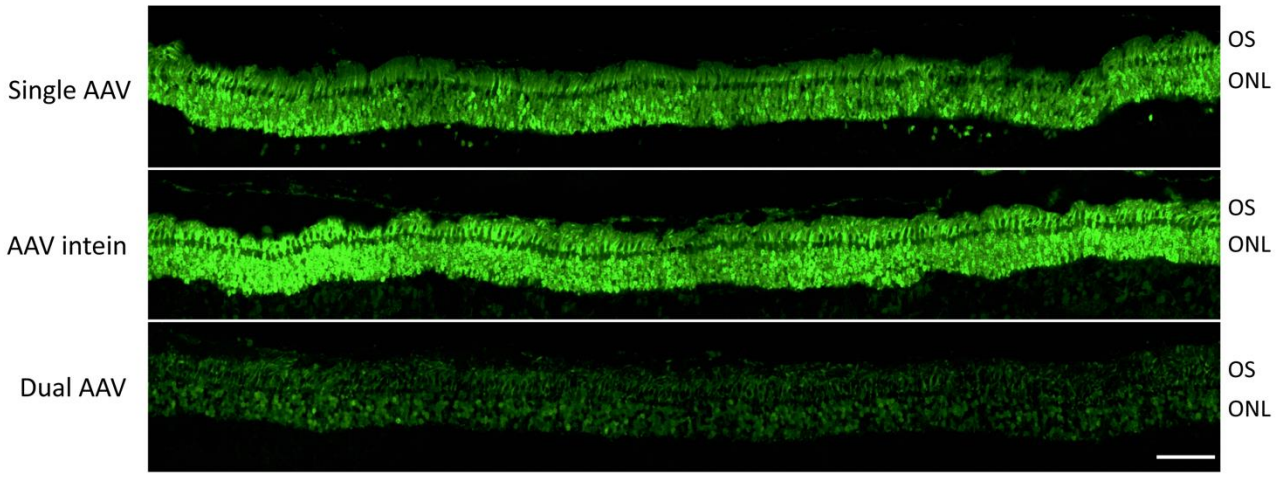

Figure 26. AAV intein reconstitute EGFP expression in pig photoreceptors at levels similar to those of a single AAV
Representative images of retinal cryosections from Large White pig retina injected subretinally with either single, intein or dual AAV2/8 vectors enconding for *EGFP* under the control of the PR-specific GRK1 promoter. The scale bar (200µm) is depicted in the figure. OS: outer segment; ONL: outer nuclear layer.

Development of 3D human retinal organoids to assess AAV intein transduction

Three-D organoids are *in vitro* models that recapitulate, accurately, *in vivo* development. Those derived from human cells are the most relevant because they avoid concerns about interspecies

differences in physiological, pharmacological, and cellular processes (*100*). In addition, 3D retinal organoids from reprogrammed induced pluripotent stem cells (iPSCs) from patients provide unprecedented opportunities for patients-specific disease modeling.

I combined two previously published protocols (*91, 92*), to generate 3D retinal organoids from human iPSCs. As reported in (*92*), the combined protocol recapitulates the main steps of retinal development to form a fully laminated 3D retinal organoid (**Fig. 27**). I further characterized the mature 3D organoid by immunostaining with mature photoreceptor markers (**Fig. 28**).

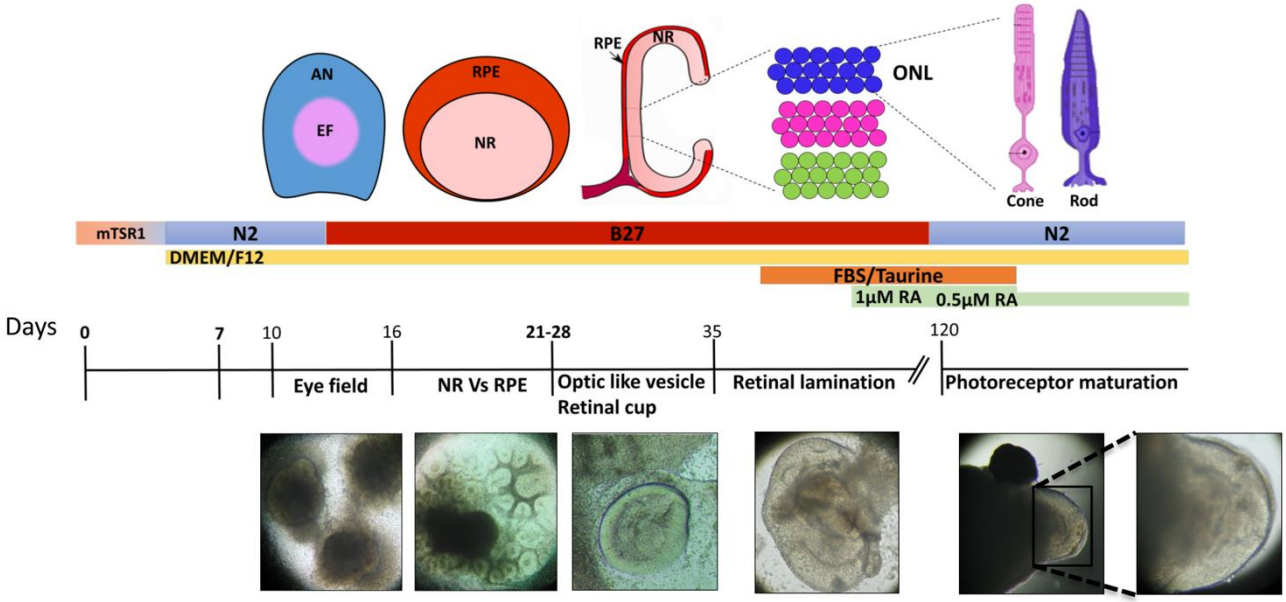

Figure 27. Development of 3D retinal organoids from human iPSCs

Diagram and main steps of 3D retinal organoids development *in vitro.* EF*:* hiPSC differentiated into retinal progenitors that self-organized into eye field-like domains; subsequent differentiation into a central neural retina (NR) domain and a peripheral retinal pigment epithelium (RPE) domain. Retinal cup: the NR domain acquired an optic-cup-like shape and formed a 3D RC when cultured in suspension. Over time, RCs acquired the characteristic retinal lamination, including a well-organized outer nuclear layer.

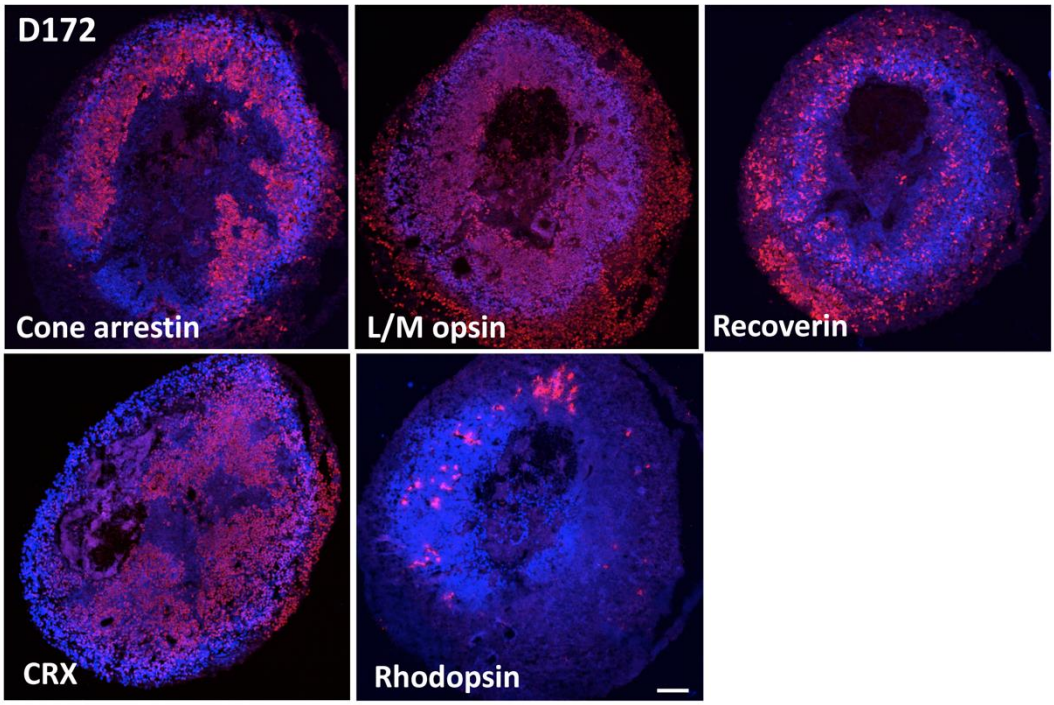

Figure 28. Expression of photoreceptors markers in 3D retinal organoids
Immunofluorescence analysis of retinal organoid at 172 days of culture with antibodies directed to mature photoreceptor markers. Cone arrestin: marker of cones; L/M-opsin: marker of cones; Recoverin: marker of photoreceptors; CRX: marker of photoreceptors; Rhodopsin: marker of rods. The scale bar (100 µm) is depicted in the figure. D: days of culture.

Furthermore, the ultrastructure microscopy analysis revealed the presences of buds of photoreceptor outer segments (**Fig. 29**). In a more advanced stage of culture (at 230 days of culture) I also observed the presence of OS-like structures protruding from the surface of the retinal organoids (**Fig. 30**) as reported in (*101*).

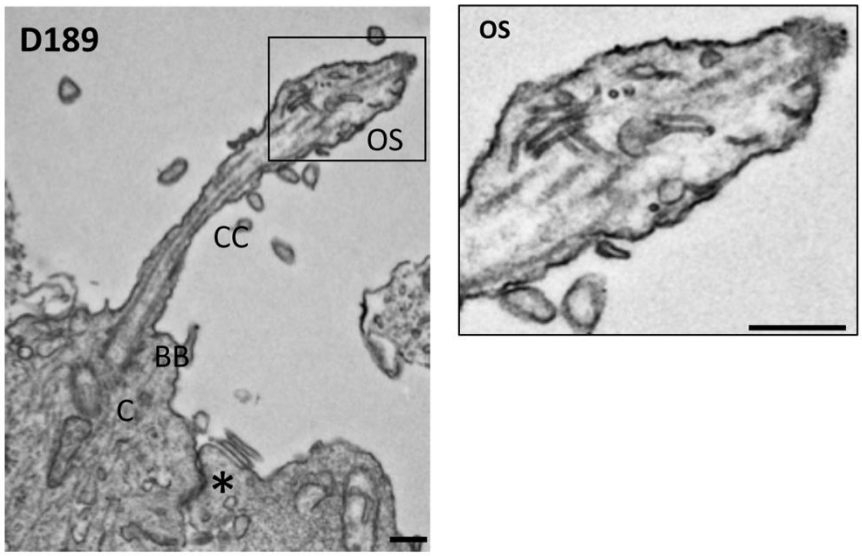

Figure 29. Structural analysis of mature photoreceptors derived from human iPSCs
Electron microscopy analysis reveals the presence of the outer limiting membrane (*), centriole (C), basal bodies (BB), connecting cilia (CC) and sketches of outer segments (OS). The inset shows the presence of disorganized membranous discs in the OS. The scale bar (500nm) is depicted in the figure. D: days of culture.

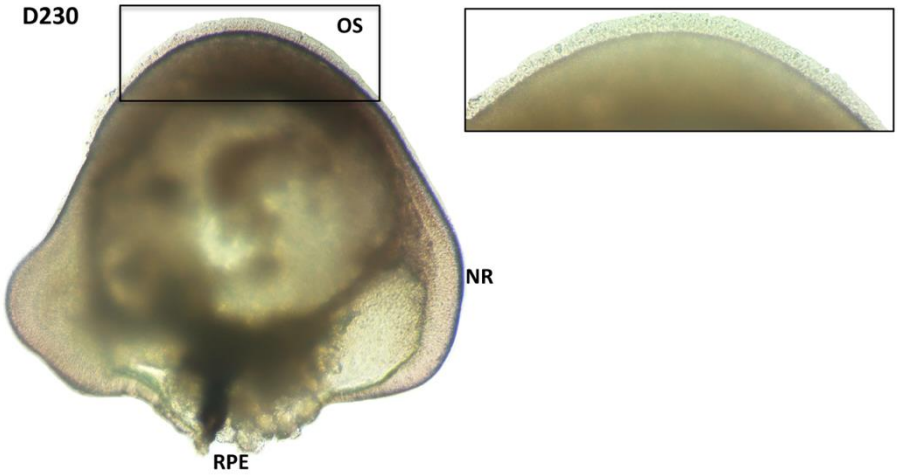

Figure 30. Macroscopic analysis of retinal organoids reveals the presence of diffused photoreceptor's outer segments-like structures
Outer segment-like structures were observed protruding from the surface of retinal organoid at 230 days of culture. The inset shows the presence of segment-like with radial architecture. OS: outer segment; NR: neural retina; RPE: retinal pigment epithelium. D: days of culture.

Using fluorescent reporter proteins, I also assessed the ability of AAV serotype 2 at transducing 3D retinal organoids using either ubiquitous or PR-specific promoters (dose of each vector/organoid: 1x10^12 G) (**Fig. 31**).

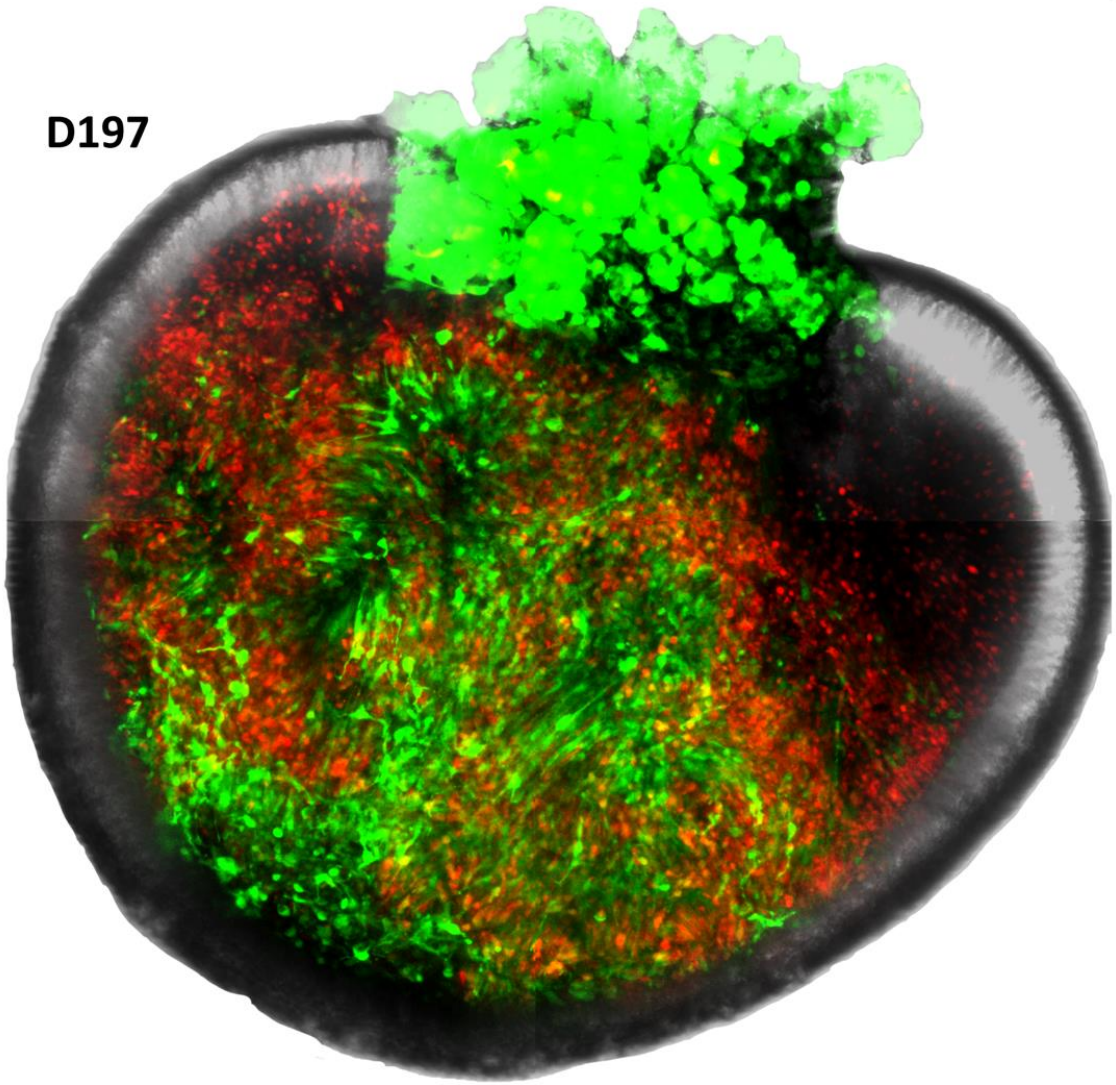

Figure 31. AAV serotype 2 efficiently transduce human 3D retinal organoids
Fluorescence analysis of retinal organoids at 183 days of culture infected with AAV 2/2 encoding for *EGFP* under the control of the ubiquitous CMV promoter and AAV 2/2 encoding for *DsRed* under the control of the PR-specific IRBP promoter. D: days of culture.

The retinal organoid was then infected at 293 days of culture with AAV 2/2 *EGFP* intein vectors under the control of the photoreceptors-specific GRK1 promoter (dose of each vector/organoid: 1x10^12 GC). Thirty days after infection, EGFP fluorescence was detected by microscopy analysis (**Fig. 32A**) proving that protein *trans*-splicing occurs in human photoreceptor-like cells. Then, the organoid lysate was harvested and EGFP protein of the expected size was detected by WB analysis (**Fig. 32B**).

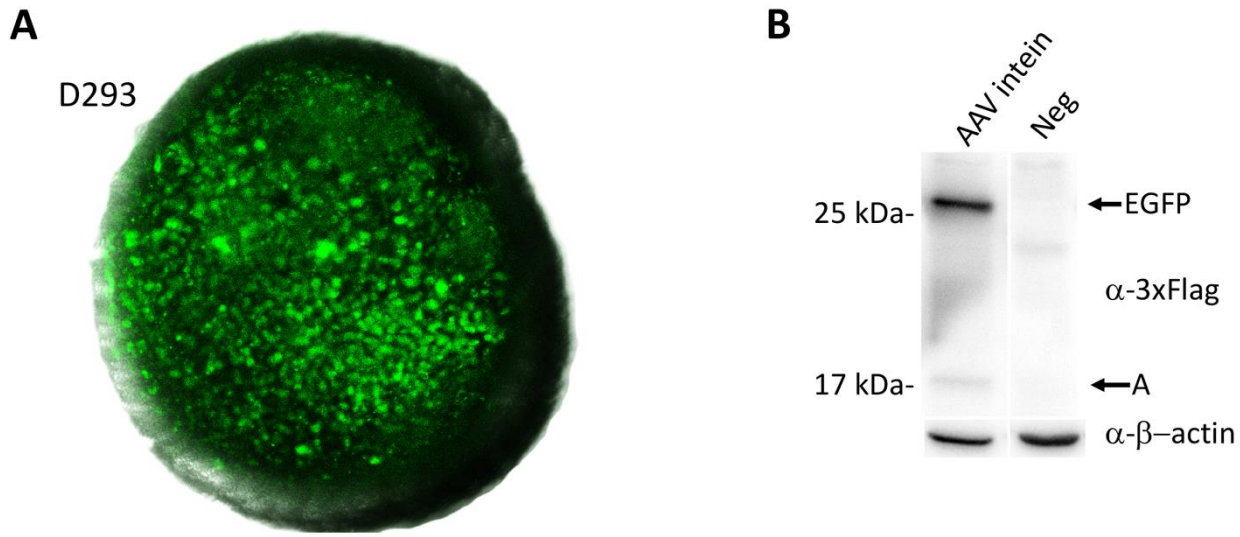

Figure 32. AAV intein reconstitute full-length EGFP protein in human retinal organoid

(**A**) Fluorescence analysis of retinal organoid at 293 days of culture infected with AAV-GRK1-*EGFP*-intein vectors.

(**B**) Western blot (WB) analysis of retinal lysates from human iPSCs-derived 3D retinal organoids infected with AAV2/2-CMV-*EGFP* intein vectors. AAV intein: retinal organoid infected with AAV intein vectors; Neg: not infected retinal organoid. The arrows indicate both full-length EGFP EGFP) and A: the reconstituted intein excised from full-length EGFP protein. α-3xflag: WB with α-3xflag antibodies; α-β-actin: WB with α-β-actin antibodies, used as loading control. The molecular weight is depicted on the left. Whole retinal lysate was loaded.

Generation of AAV-*CEP290* intein vectors

To test whether protein *trans*-splicing can be developed as a mechanism to reconstitute large proteins to levels that are therapeutic, I developed AAV intein vectors to express CEP290, the large protein defective in Leber congenital amaurosis (LCA10). *CEP290* was split into either two (AAV I, AAV II) or three (AAV I, AAV II, AAV III) fragments whose coding sequences were separately cloned in single AAV vectors, fused to the coding sequence of the split-inteins N- and C-termini (**Fig. 33**). The AAV intein vectors included either the ubiquitous short CMV 260 (shCMV) or the GRK1 promoter. Protein splitting points for each sets were selected taking into account both amino acid residue requirements at the junction points for efficient protein *trans*-splicing (*102*), as well as preservation of the integrity of critical protein domains, which should favor proper folding and stability of each independent polypeptide, and thus, of the final reconstituted protein. CEP290 sets in which the protein was split in 3 polypeptides (Set 4 and Set 5, **Fig. 33**) were generated to allow the inclusion of the Woodchuck hepatitis virus Post-transcriptional Regulatory Element [WPRE, (*103*)] to increase transgene expression levels.

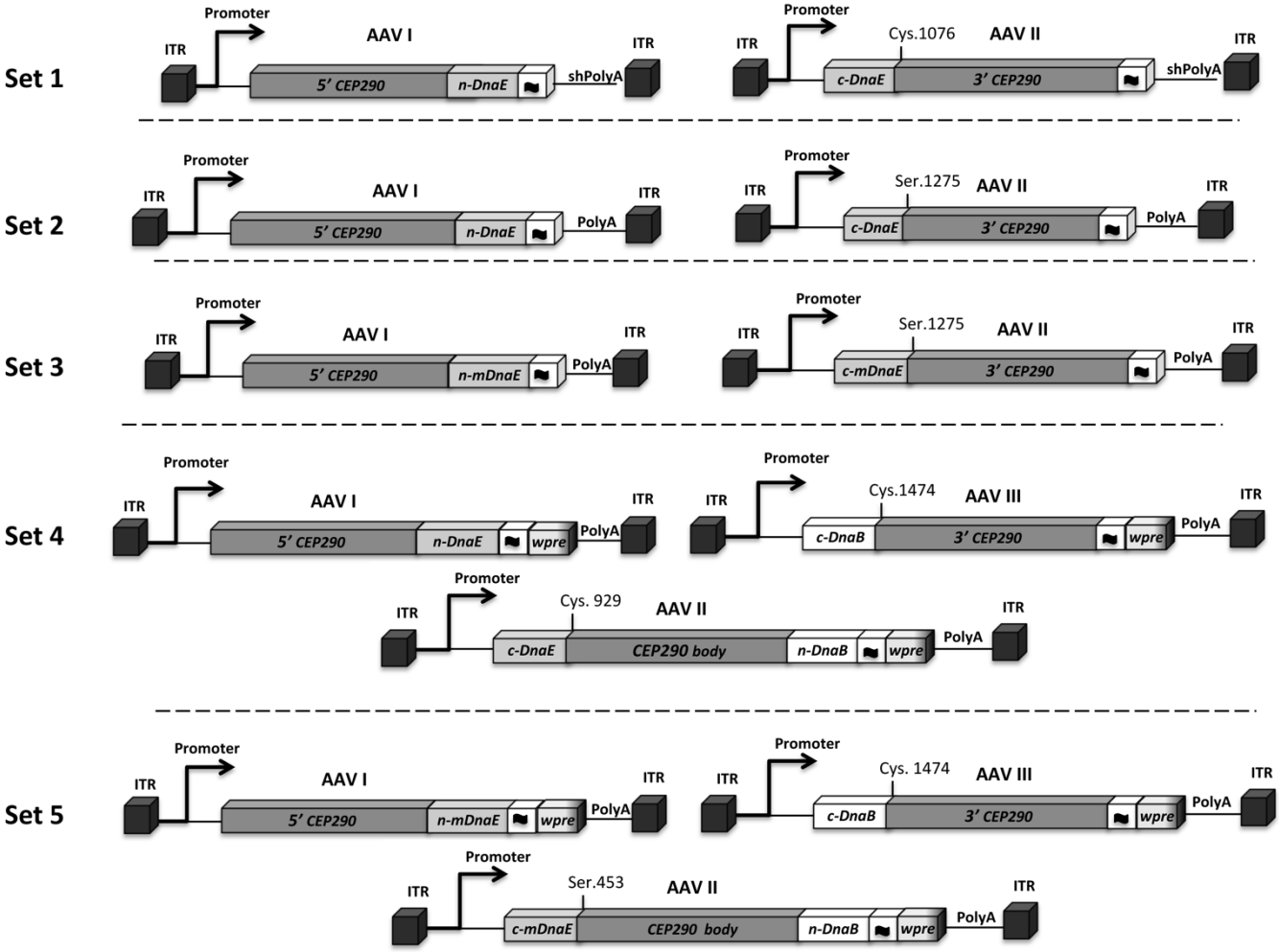

Figure 33. Schematic representation of the various sets of AAV-CEP290 intein

Set 1: n-DnaE: n-intein from DnaE of *Nostoc punctiforme (Npu)*; c-DnaE: c-intein from DnaE of *Npu;* shPolyA: short synthetic polyA;

Set 2: n-DnaE: n-intein from DnaE of *Npu*; c-DnaE: c-intein from DnaE of *Npu;*

Set 3: n-mDnaE: n-intein from mutated DnaE of *Npu (mNpu)*; c-mDnaE: c-intein from DnaE of *mNpu*;

Set 4: n-DnaE: n-intein from DnaE of *Npu*; c-DnaE: c-intein from DnaE of *Npu* between AAV I and AAV II; n-DnaB: N-intein from DnaB of *Rhodothermus marinus* (*Rma*); c-DnaB: c-intein from DnaE of *Rma* between AAV II and AAV III; wpre: Woodchuck hepatitis virus Posttranscriptional Regulatory Element.

Set 5: n-mDnaE: n-intein from DnaE of *mNpu*; c-mDnaE: c-intein from DnaE of *mNpu* between AAV I and AAV II ; n-DnaB: n-intein from DnaB of *Rma*; c-DnaB: c-intein from DnaE of *Rma* between AAV II and AAV III; wpre: Woodchuck hepatitis virus Posttranscriptional Regulatory Element. ITR: AAV II inverted terminal repeats; ≈ : 3xflag tag; Promoter: shCMV for the *in vitro* experiments and the human G-protein coupled receptor (GRK1) promoter for the *in vivo* experiments. Amino acids at the splitting points of each set are depicted in the figure.

To prevent unwanted *trans*-splicing between AAV I and AAV III which could reduce the amount of full-length protein generated, sets 4 and 5 included two different split-inteins at the two splitting junctions, specifically DnaB intein from *Rhodothermus marinus* and either wild-type or a mutated DnaE intein which we show do not cross-react either *in vitro* or in the mouse retina (**Fig. 34, 35**).

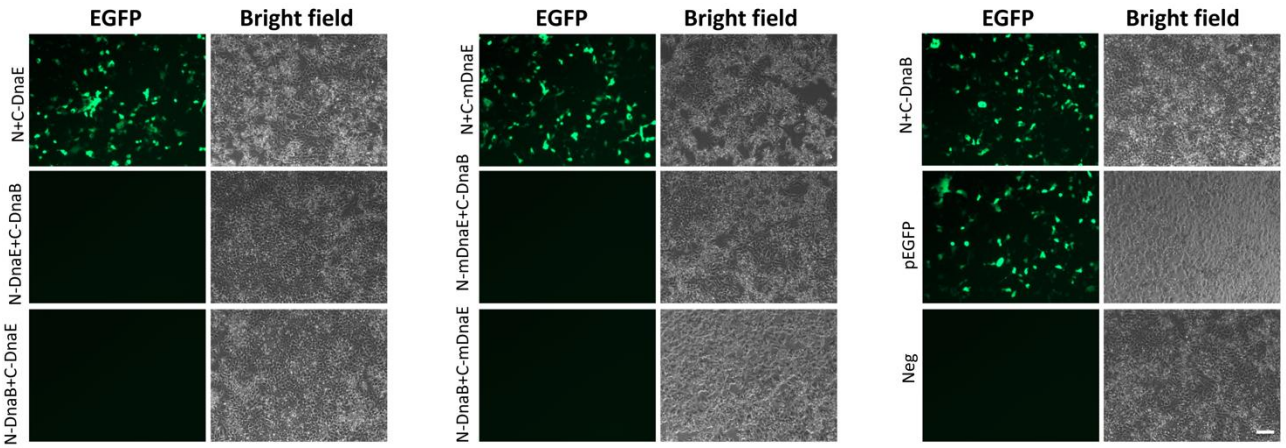

Figure 34. Combination of heterologous N- and C-inteins does not result in detectable EGFP protein reconstitution in vitro

Fluorescence analysis of HEK293 cells transfected with either full-length or AAV intein *EGFP* plasmids under the control of the ubiquitous CMV promoter. The scale bar (100 µm) is depicted in the figure. N+C-DnaE: cells transfected with both *EGFP* pAAV I+II fused to split-inteins from DnaE; N+C-mDnaE: cells transfected with both *EGFP* pAAV I+II fused to split-inteins from mDnaE; N+C-DnaB: cells transfected with both *EGFP* pAAV I+II fused to split-inteins frm DnaB; N-mDnaE+C-DnaB: cells transfected with *EGFP* pAAV I fused to n-intein from mDnaE and *EGFP* pAAV II fused to c-intein from DnaB; N-DnaB+C-mDnaE: cells transfected with *EGFP* pAAV I fused to n-intein from DnaB and *EGFP* pAAV II fused to c-intein from mDnaE; N-DnaE+C-DnaB: cells transfected with *EGFP* pAAV I fused to n-intein from DnaE and *EGFP* pAAV II fused to c-intein from DnaB; N-DnaB+C-DnaE: cells transfected with *EGFP* pAAV I fused to n-intein from DnaB and *EGFP* pAAV II fused to c-intein from DnaE; pEGFP: cells transfected with a plasmid including the full-length *EGFP* expression cassette; Neg: untransfected cells.

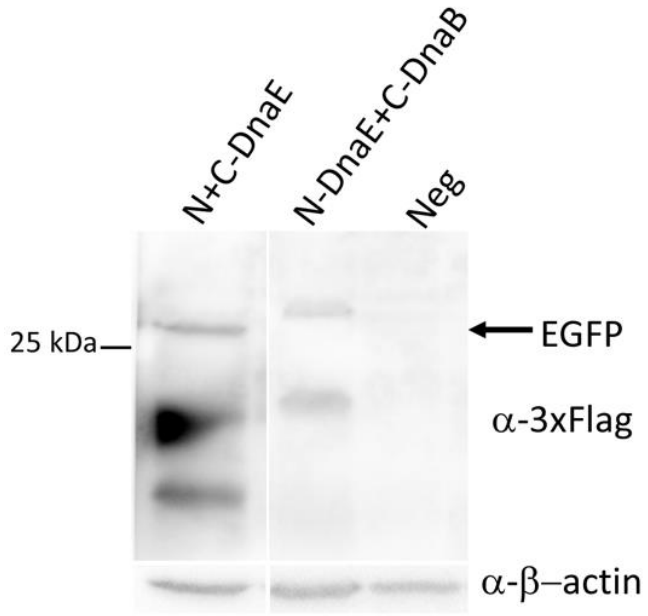

Figure 35. Combination of heterologous N- and C-inteins does not result in EGFP protein reconstitution in vivo

Western blot (WB) analysis of retinal lysates from C57BL/6J injected subretinally with AAV2/8-GRK1-*EGFP* intein vectors. N+C-DnaE: eyes injected with homologous inteins; N-DnaE+C-DnaB: eyes injected with heteterologous inteins; Neg: eyes injected with PBS. The arrows indicate the full-length EGFP protein. α-3xflag: WB with α-3xflag antibodies; α-β-actin: WB with α-β-actin antibodies, used as loading control. The molecular weight is depicted on the left. Whole retinal lysates was loaded.

Identification of optimal CEP90 splitting point is required for efficient AAV intein-mediated protein *trans*-splicing

Then, I compared the ability of each set of AAV intein plasmids to reconstitute the CEP290 protein following transfection of HEK293 cells. WB analysis of cell lysates 72 hours post-transfection showed that full-length CEP290 protein of the expected size was reconstituted from each set of AAV intein plasmids, although with variable efficiency (**Fig. 36**). Set 5 was found to be the most efficient for CEP290 protein reconstitution and thus used in all the subsequent experiments.

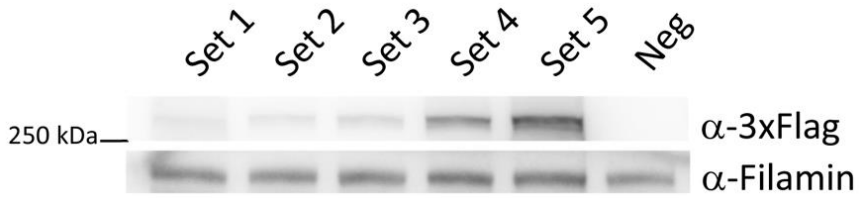

Figure 36. Optimization of intein constructs is required for efficient CEP290 reconstitution in vitro
Western blot (WB) analysis of lysates from HEK293 transfected with different sets of AAV-shCMV-CEP290 intein plasmids. Set 1: cells transfected with CEP290 split (Cys.1076)-intein plasmids; Set 2-3: cells transfected with CEP290 split (Ser.1275)-intein plasmids; Set 4: cells transfected with CEP290 split (Cys.929 and Cys.1474)-intein plasmids; Set 5: cells transfected with CEP290 split (Ser.453 and Cys.1474)-intein plasmids. Seventy µg of proteins were loaded. The WB are representative of n=3 independent experiments.

To better define the efficiency of AAV-*CEP290* intein plasmids, I compared the levels of protein achieved with set 5 (the best set emerged from the comparison above) to those obtained from a single AAV plasmid encoding for the corresponding full-length protein. To this aim, HEK293 cells were transfected with the same equimolar amounts of either the single or the AAV intein plasmids and 72 hours after transfection cell lysates were analyzed by WB (**Fig. 37**). Quantification of bands' intensity showed that the levels of CEP290 protein expression from AAV intein plasmids were 58% ± 4% (n= 3 independent experiments) of those observed with the corresponding single AAV plasmid.

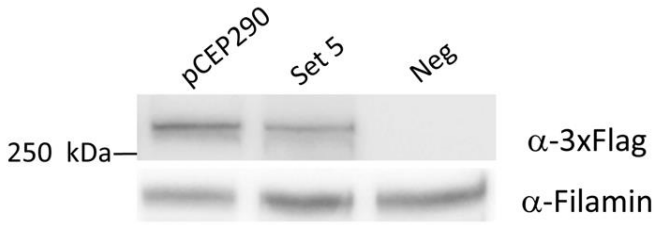

Figure 37. Transfection of AAV intein plasmids reconstitutes CEP290 protein at levels that are ~60% of those from a single plasmid

Western blot (WB) analysis of lysates from HEK293 cells transfected with either full-length or AAV intein plasmids encoding for CEP290 under the control of the ubiquitous shCMV promoter. pCEP290: cells transfected with plasmids including the full-length CEP290 expression cassette; Set 5: cells transfected with CEP290 (Ser.453 and Cys.1474)-intein plasmids. Neg: cells transfected with AAV EGFP plasmids, used as negative control. α-3xflag: WB with α-3xflag antibodies; α-Filamin: WB with α-Filamin antibodies. The molecular weight is depicted on the left. Thirty μg of proteins were loaded. The WB are representative of n=3 independent experiments.

CEP290 aligns along microtubules

Then, I assessed the intracellular localization of the various intein protein products and compared them to that of the full-length protein. Full-length CEP290 has been reported to have a mixed distribution pattern with a predominant puncatate and minor fibrillar pattern. The dissection of the domains responsible for the subcellular targeting of CEP290 showed that the N-terminal domain (a.a. 1-362) targets the protein to vesicular structures thanks to its ability to interact with membranes, while a region near the C-terminus of CEP290 encompassing much of the protein's myosin-tail homology domain mediates microtubule binding (a.a. 580-2479) and when expressed as truncated form has a prominent fibrillar distribution coincident with acetylated tubulin (Ac-Tub) (*81*). In agreement with Drivas et al., immunofluorescence analysis on HeLa cells singularly transfected with either AAV I, II or III intein plasmids or co-transfected with AAV I+II, AAV I+III and AAV II+III showed that products from AAV I and AAV II have a predominant punctate pattern while that from AAV III (encompassing protein's myosin tail homology domain) shows a fibrillar pattern and is the only one to completely colocalize to AC-Tub (**Fig. 38**). Thus, products from AAV I+II have a predominant punctate pattern while those from AAV I+III and AAV II+III have a combined microtubule fibrillar and punctate pattern. Cells co-transfected with the three AAV CEP290 intein plasmids showed a predominant punctate signal partially aligned along microtubules which is

comparable to the signal observed in cells transfected with a plasmid encoding for the full-length CEP290 protein (**Fig. 38**).

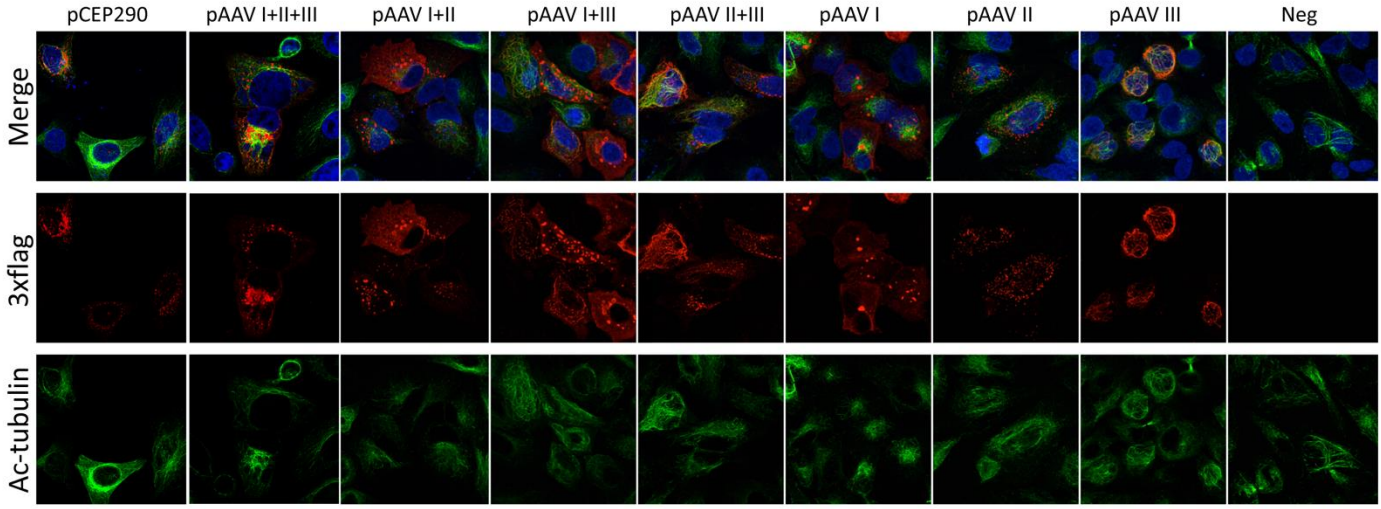

Figure 38. Products from full-length and AAV CEP290 intein plasmids aligns along microtubules
Representative images of immunofluorescence analysis on HeLa cells. pCEP290: cells transfected with a plasmid including the full-length CEP290 expression cassette; pAAV I+II+III: cells co-transfected with both AAV I, AAV II and AAV III; pAAV I+II: cells co-transfected with both AAV I and AAV II; pAAV I+III: cells co-transfected with both AAV I and AAV III; pAAV II+III: cells co-transfected with both AAV II and AAV III; pAAV I: cells transfected with the single AAV I; pAAV II: cells transfected with the single AAV II; pAAV III: cells transfected with the single pAAV III vector; Neg: untransfected cells. Cells were stained for 3xflag and acetylated tubulin (marker of microtubules).

AAV-*CEP290* inteins reconstitute full-length protein more efficiently than dual AAV vectors *in vitro*

Then, I compared the efficiency of AAV intein-mediated large protein reconstitution to that of dual AAV vectors *in vitro*. HEK293 cells were infected with either AAV2/2 dual or intein vectors encoding for *CEP290* (m.o.i: 5x 10^4 GC/cell of each vector) and cell lysates were analyzed 72 hours later by WB. As shown in **Figure 39,** AAV-*CEP290* intein vectors mediated large protein reconstitution at higher levels than dual AAV vectors. As expected, in addition to full-length proteins, shorter polypeptides derived from either the single AAV intein vectors or from *trans*-splicing occurring between AAV II and AAV III were observed (**Fig. 39**) and no polypeptides were generated from AAV I and AAV III due to heterologous inteins (i.e. mDnaE and DnaB).

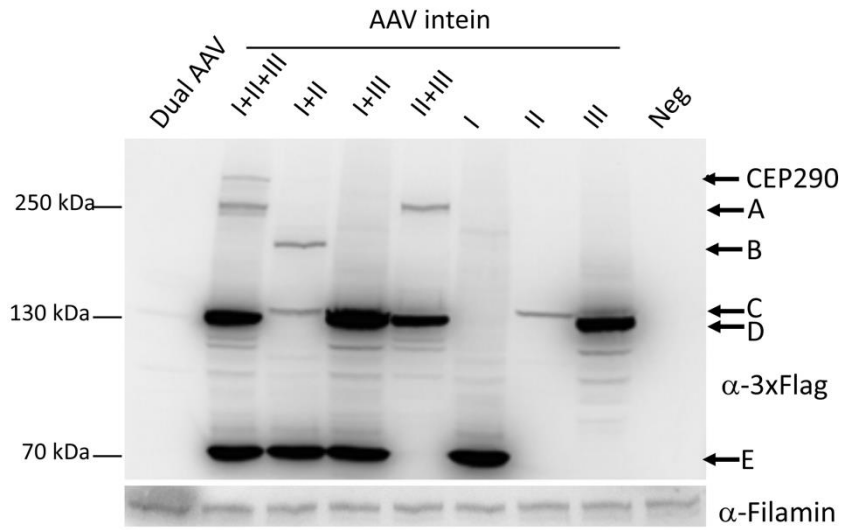

Figure 39. AAV intein reconstitute CEP290 expression more efficiently than dual AAV in vitro
Western blot (WB) analysis of lysates from HEK293 cells infected with AAV 2/2 either dual or intein shCMV-*CEP290* vectors. I+II+III: co-infected with both AAV I, AAV II and AAV III; I+II: cells co-infected with both AAV I and AAV II; I+III: cells co-infected with both AAV I and AAV III; II+III: cells co-infected with both AAV II and AAV III; I: cells infected with the single AAV I; II: cells infected with the single AAV II; III: cells infected with the single AAV III vector; dual AAV: cells infected with dual AAV-*CEP290* vectors; Neg: cells infected with AAV-*EGFP* vectors. The arrows indicate the full-length CEP290 protein and A: protein product derived from AAV II+III; B: protein product derived from AAV I+II; C: protein product derived from AAV II; D: protein product derived from AAV III; E: protein product derived from AAV I. Seventy µg of proteins were loaded.

Subretinal administration of AAV-*CEP290* intein vectors is safe and results in full-length protein reconstitution in the mouse retina

C57BL/6J mice were injected subretinally with AAV-GRK1-*CEP290* intein *vs* dual vectors (dose of each vector/eye: 1.1x10^9 GC). Animals were sacrificed 7 weeks post-injection, and protein expression in retinal lysates was evaluated by WB. Full-length proteins were detected in 50% of AAV CEP290 intein-injected eyes (**Fig. 40**). Conversely, full-length protein expression was evident in 0% of eyes injected with CEP290 dual AAV vectors. Similarly to what observed *in vitro*, we detected polypeptides derived from the single AAV intein vectors and from *trans*-splicing occurring between AAV II and AAV III (**Fig. 40**).

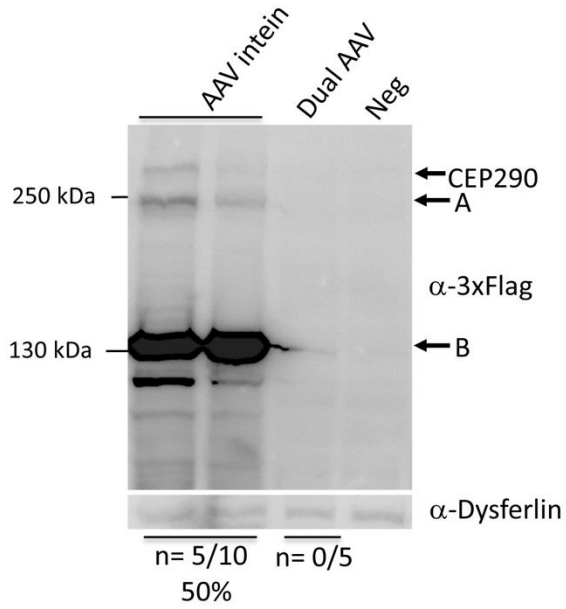

Figure 40. Subretinal delivery of AAV intein vectors results in CEP290 expression in the mouse retina
Western blot (WB) analysis of retinal lysates from C57BL/6J mice injected with either dual or intein AAV2/8 vectors encoding for *CEP290* under the control of the photoreceptor-specific GRK1 promoter. AAV intein: eyes injected with AAV intein vectors; Dual AAV: eyes injected with dual AAV vectors. The arrows indicate the full-length CEP290 protein and A: protein product derived from AAV II+III; B: protein product derived from AAV III. Neg: eyes injected with either AAV-EGFP vectors or PBS. The number and percentage of mouse eyes positive for CEP290 expression for each group is depicted below the corresponding lanes. Whole retinal lysates were loaded.

I additionally investigated the safety of AAV intein vectors in the retina. To this aim, I injected subretinally wild-type C57BL/6J mice with AAV2/8-GRK1-*CEP290* intein vectors (dose of each vector/eye: 1.1x10^9 GC) and retinal morphology and electrical activity were measured at twelve weeks post-injection. The thickness of the ONL measured by optical coherence tomography was not significantly different between AAV intein-, negative control- and PBS-injected eyes (**Fig. 41A**).

Similarly, a- and b-wave amplitudes, measured by Ganzfeld electroretinogram (ERG), were not significantly different between mouse eyes that were injected with AAV intein vectors (n=17) and eyes injected with either negative control AAV vectors (n=10) or PBS (n=10) (**Fig. 41B,C**).

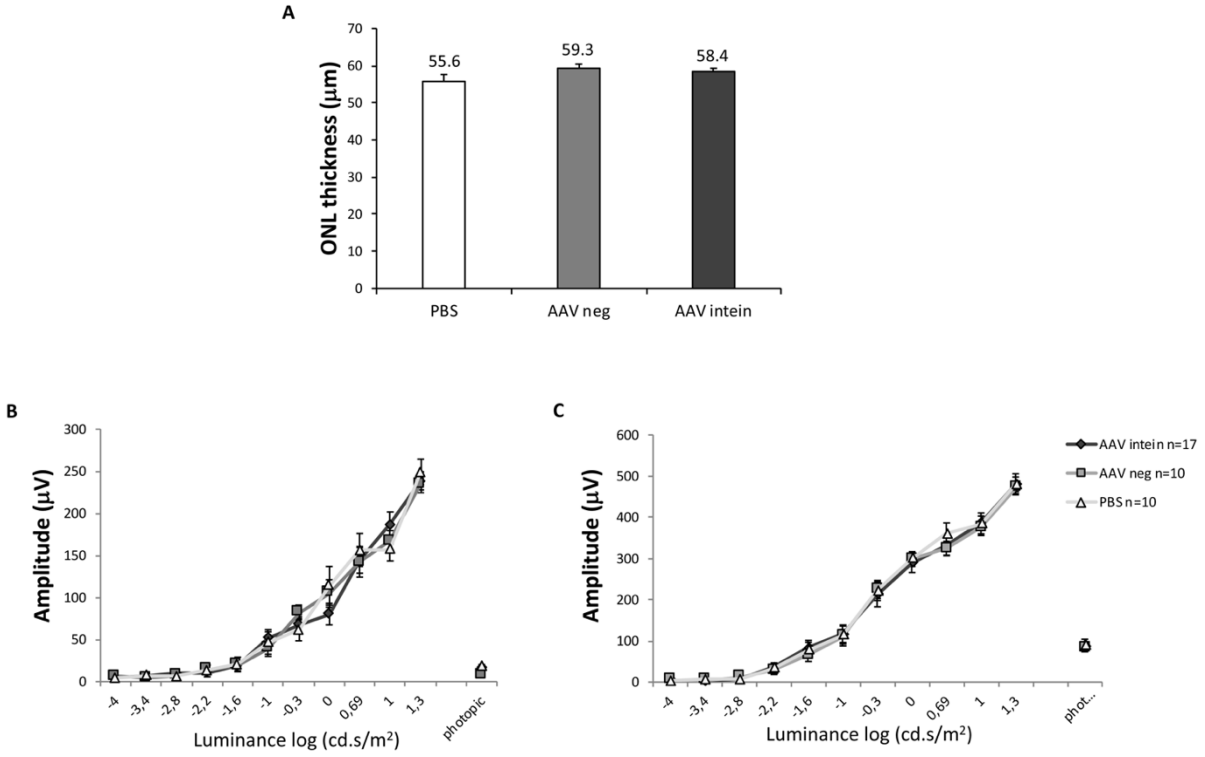

Figure 41. Subretinal delivery of AAV intein vectors is safe in the mouse retina
Spectral domain optical coherence tomogram (A) and electroretinogram analysis of a-wave (B) and b-wave (C) light response of C57BL/6J mice injected subretinally with AAV2/8 intein vectors encoding for *CEP290* under the control of the photoreceptor-specific GRK1 promoter. AAV intein: eyes injected with AAV intein vectors; AAV neg: eyes injected with unrelated AAV vectors or PBS. Data are represented as mean ± s.e.m. The mean values are indicated above the corresponding bar.

Subretinal administration of AAV intein vectors improves the retinal phenotype of an LCA10 mouse model

To determine whether the levels of photoreceptors transduction obtained with AAV intein vectors could be therapeutically-relevant, *rd16* mice, a model of LCA10 which presents with severe retinal degeneration in the first 3-4 weeks of life, were injected subretinally with AAV2/8-GRK1-*CEP290* intein vectors (dose of each vector/eye: 5.5x10^8 GC) at post-natal day 4-6. Microscopy analysis of retinal sections one month after injection showed that the thickness of the ONL, which includes photoreceptors nuclei, was significantly reduced in *rd16* mice compared to wild-type mice, as result of progressive retinal degeneration (**Fig. 42A**). Notably, I found that the ONL thickness in the *rd16*

retinas injected with AAV intein vectors was significantly higher (about 50%) than that of negative control injected *rd16* retinas (**Fig. 42B**; wild-type = 0.63 ± 0.05 µm, n=6).

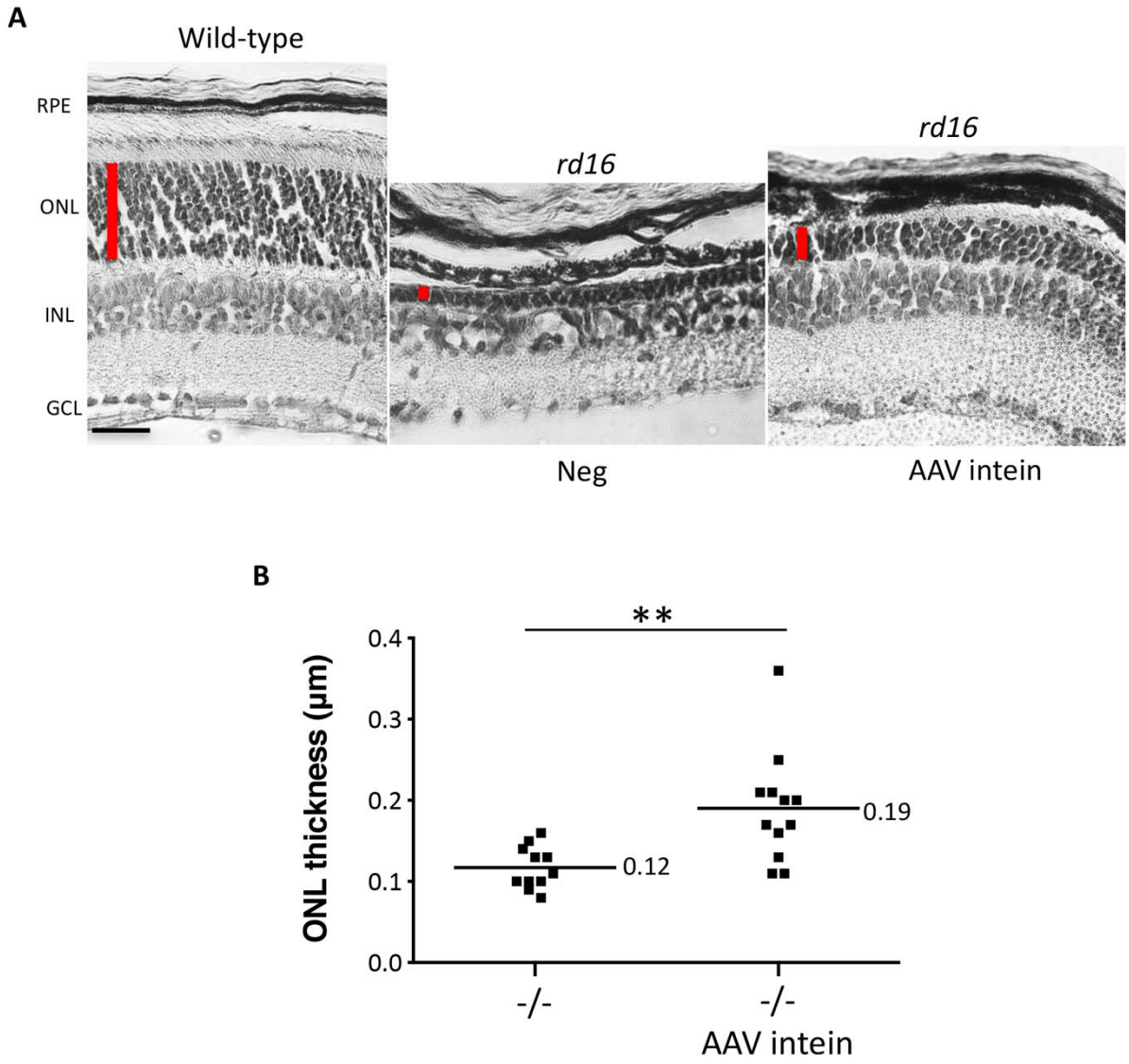

Figure 42. Subretinal administration of AAV intein reconstitutes CEP290 and improves the retinal morphology of rd16 mice.

(**A**) Representative images of retinal sections from wild-type uninjected and *rd16* mice either injected subretinally with AAV 2/8 intein vectors encoding for *CEP290* under the control of the photoreceptor-specific GRK1 promoter or injected with negative controls (Neg). AAV intein: eyes injected with AAV intein vectors; Neg: eyes injected with negative controls. The scale bar (25 µm) is depicted in the figure. The thickness of the ONL measured in each image is indicated by the vertical red line. RPE: retinal pigment epithelium; ONL: outer nuclear layer; INL: inner nuclear layer; GCL: ganglion cell layer.

(**B**) ONL thickness in *rd16* mice following subretinal administration of AAV intein vectors. Each dot represents the mean ONL thickness of one eye. The mean ONL thickness of each group is indicated in the graph. -/-: negative control injected *rd16* mice (AAV I+II-CEP290 or AAV II+III-CEP290 or PBS, n= 11); *-/-* AAV intein: *rd16* eyes injected with AAV intein vectors (n= 12). ** Student's t-test p-value <0.01

Accordingly, retinal functional tests based on pupillary light response (PLR) show a significant higher pupil constriction (about 20%) in *rd16* mice injected with AAV intein vectors than in negative control-injected *rd16* eyes (**Fig. 43B**).

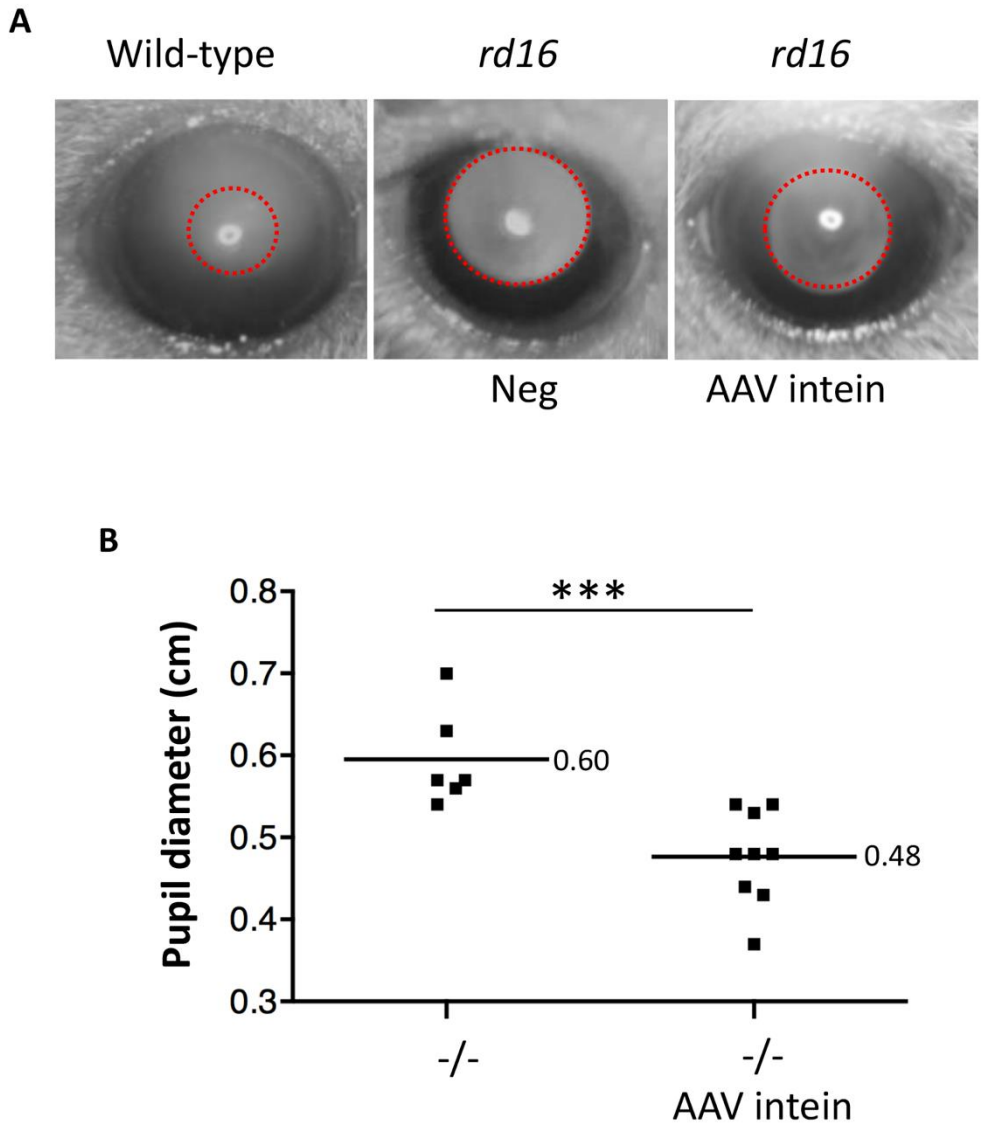

Figure 43. Subretinal administration of AAV CEP290 intein improves pupillary light responses in the rd16 mouse model of LCA10

(**A**) Representative images of eyes from wild-type uninjected and *rd16* mice either injected subretinally with AAV2/8 intein vectors encoding for *CEP290* under the control of the photoreceptor-specific GRK1 promoter or injected with negative controls (Neg). AAV intein: eyes injected with AAV intein vectors; Neg: eyes injected with negative controls. Red circle defines pupils.

(**B**) Pupil diameter in *rd16* mice following subretinal administration of AAV intein vectors. Each dot represents the mean diameter of one eye. The mean diameter of each group is indicated in the graph. -/-: negative control injected *rd16* mice (AAV II+III-CEP290 or PBS, n= 6); *-/-* AAV intein: *rd16* eyes injected with AAV intein vectors (n= 9). *** Student's t-test p-value ≤ 0.001

DISCUSSION

While AAV-mediated gene therapy is effective in animal models and in patients with inherited blinding conditions (*48, 104*) its application to diseases affecting the retina and requiring transfer of sequences larger than 5 kb is limited by the small cargo capacity of AAV. To overcome this, dual AAV vectors, which exploit AAV genome tendency to concatemerize upon infection (*56, 58, 61*) have been developed in order to expand AAV DNA transfer capacity to around 9 kb. In Specific aim 1 of this thesis I demonstrate both *in vitro* and in the mouse retina that similar strategies can be further implemented by including a third vector in the system, thus expanding AAV transfer capacity to approximately 14 kb.

The possibility to further expand the dual AAV vectors to triple in order to express larger genes has been exploited in mouse muscle (*56, 105, 106*) for dystrophin transduction, but with poor efficiency. Although a direct comparison between the triple AAV vectors used in that study and our triple AAV vectors is difficult, the levels of full-length transgene expression we achieve in the retina with triple AAV vectors appear to be higher, as we are able to detect full-length protein reconstitution by WB, in addition to fluorescence analysis on histological sections that were used for dystrophin detection in Lostal et al. (*106*) and Koo et al. (*105*). To understand whether the transduction levels from triple AAV vectors may be therapeutically relevant, we have treated *Alms1* $^{-/-}$ mice with subretinal injections of triple GRK1-*ALMS*-AAV vectors, but, besides a transient improvement, we did not observe a remarkable amelioration of the phenotype. After confirming that transgenic ALMS1 is properly expressed in PRs at levels around 8% of endogenous, there could be several reasons that justify this lack of therapeutic efficacy: (1) as we have transferred the human ALMS1 transgene in *Alms1* $^{-/-}$ mice, we cannot exclude that interspecies differences might be responsible for low therapeutic efficacy; (2) the non-cell-autonomous PR degeneration described in retinitis pigmentosa (*107*) may as well account for the lack of therapeutic effect; and (3) only 3.5% of PR are transduced as assessed in Figure 11, and such fraction might not be sufficient to detect a significant

rescue. It is possible that higher levels of transduction may improve the efficacy of triple AAV vector. This could be obtained (1) with higher vectors doses, (2) with more efficient AAV serotypes than those used here (i.e., AAV Y444, 500, 730F with mutated tyrosine residues) (*37, 108*) (3) by enlarging the transduced area with a different injection technique (i.e., double injection) or by intravitreal injection of highly penetrating serotypes such as AAV7m8 (*36*) (4) by using a more potent expression cassette than the one used in this work, or (5) by co-injection of AAV transduction enhancers (i.e., proteasome inhibitors) (*89*). The low efficiency in PR transduction with triple AAV is similar to what previously observed with dual AAV vectors (*9*). Yet the levels of transduction of both systems in the pig retina are extremely encouraging, as shown in Maddalena, Tornabene et al. (*109*). Briefly, while in mouse PR, transgene expression observed with triple AAV vectors represented only 2% of that obtained with single AAV, in pig retina this increased to 39%. This is consistent with previous work where the relative PR-EGFP expression obtained upon subretinal delivery of dual AAV vectors is 6% in mice (*61*) and 40% in pigs of that obtained with single AAV, which was explained by the higher PR co-transduction rate of two independent AAV observed in pigs (73%) than in mice (24%) (*63*).This could be due to thicker physical barriers in the pig than in the mouse retina that might limit vector diffusion, thus concentrating the vector in a smaller area and maximizing co-infection of the same cells by multiple vectors. Also, species-specific differences in the efficiency of both AAV2/8 transduction and/or vector intermolecular recombination cannot be excluded. This result is particularly important, considering that the pig retina is an excellent pre-clinical model with a size and architecture more similar to the human than the mouse retina.

In agreement with the low levels of unexpected protein products in the mouse retinas, no evident signs of toxicity were observed by optical coherence tomography analysis in animals injected 2 months before with ALMS-AAV I + III, the combination of viruses that produced the highest levels of truncated products *in vitro*. Nevertheless, before considering the system for a therapeutic use in humans, more efforts should be focused to evaluate potential toxicity of truncated products, as well

as strategies to eliminate them, such as the inclusion of degradation signals strategically placed in the vectors, which Trapani et al. (*61*) have recently demonstrated to be effective at abolishing selectively truncated proteins from dual AAV vectors.

Overall, these data demonstrate that triple AAV vectors drive large gene reconstitution both *in vitro* and in mouse retina and leads to the reconstitution of the large therapeutic *ALMS1* mutated in Alström syndrome, thus extending AAV transfer capacity up to 14 kb in the retina. Yet, these levels are lower than those by single AAV (*61, 109*) and are not sufficient for specific applications (*109*) like ALMS1.

So, I have investigated as alternative strategy for effective AAV-mediated large gene in the retina via intein-mediated protein *trans*-splicing, which has been already used to reconstitute large therapeutic proteins like Factor VIII in liver (*73, 74*) and dystrophin in muscle (*75*) or the L-type calcium channel in cardiomyocytes (*110*). I show that inteins reconstitute large proteins in the retina of small and large animal models and in human retinal organoids to levels that are therapeutically-relevant. These levels are significantly higher than those achieved via AAV genome recombination by dual AAV vectors, both *in vitro* and in photoreceptors. Notably, in the large pig retina, we found that the levels of the reconstituted EGFP protein were comparable to those achieved by single AAV vectors. This is similar to what observed with dual AAV where the efficiency of multiple AAV transduction is higher in the pig than in the mouse retina (*61, 109*).

When applying *trans*-splicing to large proteins, construct design needs to take into account: i. preservation at the junction points of amino acid residues needed for efficient protein *trans*-splicing; ii. splitting of the proteins outside of structural domains to avoid incorrect polypeptide folding. Indeed, I have generated several sets of AAV intein constructs for CEP290, and found that their efficiency varied in terms of levels of protein reconstitution. In some cases, one of the polypeptides was less stable than the other which presumably impacted the levels of full-length protein produced. According to my experience, construct design is more critical for AAV intein than for triple

AAV where the use of exogenous recombinogenic sequences as well as splicing signals allows to split a large coding sequence independently of the native protein structure and organization.

Additionally, when using intein-mediated protein *trans*-splicing each polypeptide is expressed from an independent expression cassette that needs to carry the required transcriptional elements which will be included in each of the AAV intein vectors. This is different from triple AAV where the single large expression cassette is split into three fragments with the promoter element present only in the 5' vector and the polyA signal in the 3' vector, no regulatory elements were present in the middle of the CDS. Therefore, when using AAV intein vectors part of the cloning capacity will be taken up by regulatory elements that need to be replicated within each vector. This might be limiting in terms of size constraint, thus to accommodate in two AAV intein vectors the coding sequence of large proteins, as CEP290, short regulatory elements are required. However, these shorter elements are often weak in terms of transcriptional activity. Indeed, here we show that splitting CEP290 into three polypeptides rather than two allows to accommodate into each AAV vector larger and more potent regulatory elements (i.e. a full-length CMV promoter and/or WPRE) and this leads to higher levels of full-length protein expression than those obtained with two AAV intein vectors with weaker regulatory elements, despite the need to achieve co-infection of the same cell by three vectors. Pivotal to the development of triple AAV intein vectors has been the use of different inteins, i.e. DnaE and DnaB, which do not cross-react thus preventing improper *trans*-splicing between the polypeptides produced by AAV I and AAV III. Despite this extensive optimization, the levels of therapeutic large CEP290 protein achieved by intein-mediated *trans*-splicing were lower than those achieved for EGFP compared to a full-length expression cassette (**Fig. 34**), thus confirming that large therapeutic proteins are more challenging to reconstitute than the small and stable EGFP. One of the requirements for *trans*-splicing to occur is that the different polypeptide fragments reside in the same subcellular compartment. The three CEP290 polypeptides show a pattern comparable to that previously described for CEP290 products with a similar amino acid sequence (*81*).

The WB analysis of both cells and retinas administered with AAV intein vectors shows the presence of both intein excised from the mature protein and truncated protein products that derive from either non *trans*-spliced polypeptides or *trans*-splicing occurring only between two of three polypeptides. This observation questions the safety of AAV intein that will require formal long-term toxicity studies to be definitively addressed; however *in vivo* electrophysiological and morphological analysis shows no sign of toxicity up to 12 weeks post-injection in eyes injected with AAV-*CEP290* intein vectors. Finally and more importantly, the improvement in the retinal phenotype of LCA10 animal model of inherited retinal diseases following subretinal injection of the AAV intein vectors strongly suggests that the reconstituted proteins have been properly processed and targeted.

In conclusion, I have shown that AAV intein-mediated protein *trans*-splicing reconstitutes large proteins both *in vitro* and in the retina of mouse, pig and in human retinal organoids to levels that are significantly superior to other platforms used to overcome AAV limited cargo capacity, which establishes this system as the most efficient approach for large gene delivery to the retina.

CONCLUSION

During my Ph.D. thesis, I focused my efforts on the identification of AAV-based strategies for delivery of large genes to the retina and on providing proof of principle of their efficacy in animal models of inherited retinal disease (IRDs). In my study, I demonstrated that triple AAV vectors drive large gene reconstitution both *in vitro* and *in vivo,* thus extending AAV transfer capacity up to 14 kb in the retina. Importantly, although the levels of transgene expression achieved with triple AAV vectors are low, they result in mild and transient improvement of the retinal phenotype of the mouse model of Alström syndrome type I (ALMS). However, due to its low transduction efficiency, this strategy is not sufficient for significant improvement of the retinal phenotype of the ALMS mouse model, as might be for the treatment of other animal models of IRDs. This results, lead me to investigate an alternative strategy for large genes reconstitution in the retina, potentially more effective than dual or triple AAV vectors.

So, I took advantage of the intrinsic ability of split-inteins to mediate protein *trans*-splicing to reconstitute large full-length proteins following their fragmentation into either two or three split-intein-flanked polypeptides whose sequences fit into single AAV vector. To determine the efficiency of AAV intein in the retina I used the reporter EGFP protein and compared them to either single or dual AAV vectors. As result, AAV intein reconstitute EGFP at levels that are 3 times higher than that of dual AAV vectors (both in mouse and pig retina). Notably, in the pig retina, I found that the levels of the reconstituted EGFP protein were comparable to those achieved by single AAV vectors.

Additionally, I have chosen Leber congenital amaurosis (LCA) type 10 due to mutations in the large CEP290 gene, one of the most common forms LCA, to investigate the efficiency of split-inteins at reconstituting large proteins in the retina. After extensive optimization, the levels of therapeutic large proteins achieved by intein-mediated *trans*-splicing resulted in significant improvement of the retinal phenotype of *rd16* mice, the LCA type 10 mouse model available.

Importantly, I showed that AAV intein-mediated protein *trans*-splicing occurs in photoreceptors across species up to human from iPSCs-derived retinal organoids.

In conclusion, these data provide evidence of the therapeutic potential of AAV intein vectors for gene therapy of blinding diseases due to mutations in large genes.

REFERENCES

1. A. J. Smith, J. W. Bainbridge, R. R. Ali, Gene supplementation therapy for recessive forms of inherited retinal dystrophies. *Gene Ther* **19**, 154-161 (2012).
2. S. Veleri *et al.*, Biology and therapy of inherited retinal degenerative disease: insights from mouse models. *Dis Model Mech* **8**, 109-129 (2015).
3. J. L. Duncan *et al.*, Inherited Retinal Degenerations: Current Landscape and Knowledge Gaps. *Transl Vis Sci Technol* **7**, 6 (2018).
4. S. Qin, G. A. Rodrigues, Progress and perspectives on the role of RPE cell inflammatory responses in the development of age-related macular degeneration. *J Inflamm Res* **1**, 49-65 (2008).
5. B. M. Nash, D. C. Wright, J. R. Grigg, B. Bennetts, R. V. Jamieson, Retinal dystrophies, genomic applications in diagnosis and prospects for therapy. *Transl Pediatr* **4**, 139-163 (2015).
6. S. Daya, K. I. Berns, Gene therapy using adeno-associated virus vectors. *Clin Microbiol Rev* **21**, 583-593 (2008).
7. R. R. Caspi, A look at autoimmunity and inflammation in the eye. *J Clin Invest* **120**, 3073-3083 (2010).
8. S. Masli, J. L. Vega, Ocular immune privilege sites. *Methods Mol Biol* **677**, 449-458 (2011).
9. I. Trapani, A. Puppo, A. Auricchio, Vector platforms for gene therapy of inherited retinopathies. *Prog Retin Eye Res* **43**, 108-128 (2014).
10. Q. Li *et al.*, Intraocular route of AAV2 vector administration defines humoral immune response and therapeutic potential. *Mol Vis* **14**, 1760-1769 (2008).
11. N. Kumaran, M. Michaelides, A. J. Smith, R. R. Ali, J. W. B. Bainbridge, Retinal gene therapy. *Br Med Bull* **126**, 13-25 (2018).
12. F. Sonntag, K. Schmidt, J. A. Kleinschmidt, A viral assembly factor promotes AAV2 capsid formation in the nucleolus. *Proc Natl Acad Sci U S A* **107**, 10220-10225 (2010).
13. W. W. Hauswirth, K. I. Berns, Origin and termination of adeno-associated virus DNA replication. *Virology* **78**, 488-499 (1977).
14. B. Balakrishnan, G. R. Jayandharan, Basic biology of adeno-associated virus (AAV) vectors used in gene therapy. *Curr Gene Ther* **14**, 86-100 (2014).
15. B. R. Schultz, J. S. Chamberlain, Recombinant adeno-associated virus transduction and integration. *Mol Ther* **16**, 1189-1199 (2008).
16. R. J. Samulski, N. Muzyczka, AAV-Mediated Gene Therapy for Research and Therapeutic Purposes. *Annu Rev Virol* **1**, 427-451 (2014).
17. J. F. Wright, Manufacturing and characterizing AAV-based vectors for use in clinical studies. *Gene Ther* **15**, 840-848 (2008).
18. L. H. Vandenberghe, A. Auricchio, Novel adeno-associated viral vectors for retinal gene therapy. *Gene Ther* **19**, 162-168 (2012).
19. A. Srivastava, In vivo tissue-tropism of adeno-associated viral vectors. *Curr Opin Virol* **21**, 75-80 (2016).
20. A. Auricchio, Pseudotyped AAV vectors for constitutive and regulated gene expression in the eye. *Vision Res* **43**, 913-918 (2003).
21. C. Lebherz, A. Maguire, W. Tang, J. Bennett, J. M. Wilson, Novel AAV serotypes for improved ocular gene transfer. *J Gene Med* **10**, 375-382 (2008).
22. A. Auricchio *et al.*, Exchange of surface proteins impacts on viral vector cellular specificity and transduction characteristics: the retina as a model. *Hum Mol Genet* **10**, 3075-3081 (2001).

23. A. Dinculescu, L. Glushakova, S. H. Min, W. W. Hauswirth, Adeno-associated virus-vectored gene therapy for retinal disease. *Hum Gene Ther* **16**, 649-663 (2005).
24. R. R. Ali *et al.*, Gene transfer into the mouse retina mediated by an adeno-associated viral vector. *Hum Mol Genet* **5**, 591-594 (1996).
25. M. Allocca *et al.*, Novel adeno-associated virus serotypes efficiently transduce murine photoreceptors. *J Virol* **81**, 11372-11380 (2007).
26. A. J. Lotery *et al.*, Adeno-associated virus type 5: transduction efficiency and cell-type specificity in the primate retina. *Hum Gene Ther* **14**, 1663-1671 (2003).
27. C. Mussolino *et al.*, AAV-mediated photoreceptor transduction of the pig cone-enriched retina. *Gene Ther* **18**, 637-645 (2011).
28. K. Stieger *et al.*, Subretinal delivery of recombinant AAV serotype 8 vector in dogs results in gene transfer to neurons in the brain. *Mol Ther* **16**, 916-923 (2008).
29. L. H. Vandenberghe *et al.*, Dosage thresholds for AAV2 and AAV8 photoreceptor gene therapy in monkey. *Sci Transl Med* **3**, 88ra54 (2011).
30. L. P. Pellissier *et al.*, Specific tools for targeting and expression in Muller glial cells. *Mol Ther Methods Clin Dev* **1**, 14009 (2014).
31. E. M. Surace, A. Auricchio, Versatility of AAV vectors for retinal gene transfer. *Vision Res* **48**, 353-359 (2008).
32. A. Asokan, D. V. Schaffer, R. J. Samulski, The AAV vector toolkit: poised at the clinical crossroads. *Mol Ther* **20**, 699-708 (2012).
33. M. A. Kotterman, D. V. Schaffer, Engineering adeno-associated viruses for clinical gene therapy. *Nat Rev Genet* **15**, 445-451 (2014).
34. J. Weinmann, D. Grimm, Next-generation AAV vectors for clinical use: an ever-accelerating race. *Virus Genes* **53**, 707-713 (2017).
35. P. Colella, G. Ronzitti, F. Mingozzi, Emerging Issues in AAV-Mediated In Vivo Gene Therapy. *Mol Ther Methods Clin Dev* **8**, 87-104 (2018).
36. D. Dalkara *et al.*, In vivo-directed evolution of a new adeno-associated virus for therapeutic outer retinal gene delivery from the vitreous. *Sci Transl Med* **5**, 189ra176 (2013).
37. H. Petrs-Silva *et al.*, Novel properties of tyrosine-mutant AAV2 vectors in the mouse retina. *Mol Ther* **19**, 293-301 (2011).
38. R. R. Klimczak, J. T. Koerber, D. Dalkara, J. G. Flannery, D. V. Schaffer, A novel adeno-associated viral variant for efficient and selective intravitreal transduction of rat Muller cells. *PLoS One* **4**, e7467 (2009).
39. M. F. Kuranda K., AAV Vector-Based Gene Therapy, Progress and Current Challenges. *Springer, Cham*, (2017).
40. G. M. Acland *et al.*, Long-term restoration of rod and cone vision by single dose rAAV-mediated gene transfer to the retina in a canine model of childhood blindness. *Mol Ther* **12**, 1072-1082 (2005).
41. G. M. Acland *et al.*, Gene therapy restores vision in a canine model of childhood blindness. *Nat Genet* **28**, 92-95 (2001).
42. J. W. Bainbridge *et al.*, Effect of gene therapy on visual function in Leber's congenital amaurosis. *N Engl J Med* **358**, 2231-2239 (2008).
43. W. W. Hauswirth *et al.*, Treatment of leber congenital amaurosis due to RPE65 mutations by ocular subretinal injection of adeno-associated virus gene vector: short-term results of a phase I trial. *Hum Gene Ther* **19**, 979-990 (2008).
44. A. M. Maguire *et al.*, Safety and efficacy of gene transfer for Leber's congenital amaurosis. *N Engl J Med* **358**, 2240-2248 (2008).
45. J. Bennett *et al.*, Safety and durability of effect of contralateral-eye administration of AAV2 gene therapy in patients with childhood-onset blindness caused by RPE65 mutations: a follow-on phase 1 trial. *Lancet* **388**, 661-672 (2016).

46. M. D. Fischer, On Retinal Gene Therapy. *Ophthalmologica* **236**, 1-7 (2016).
47. FDA approves hereditary blindness gene therapy. *Nat Biotechnol* **36**, 6 (2018).
48. I. Trapani, A. Auricchio, Seeing the Light after 25 Years of Retinal Gene Therapy. *Trends Mol Med*, (2018).
49. J. C. Grieger, R. J. Samulski, Packaging capacity of adeno-associated virus serotypes: impact of larger genomes on infectivity and postentry steps. *J Virol* **79**, 9933-9944 (2005).
50. M. L. Hirsch, M. Agbandje-McKenna, R. J. Samulski, Little vector, big gene transduction: fragmented genome reassembly of adeno-associated virus. *Mol Ther* **18**, 6-8 (2010).
51. M. Allocca *et al.*, Serotype-dependent packaging of large genes in adeno-associated viral vectors results in effective gene delivery in mice. *J Clin Invest* **118**, 1955-1964 (2008).
52. V. S. Lopes *et al.*, Retinal gene therapy with a large MYO7A cDNA using adeno-associated virus. *Gene Ther* **20**, 824-833 (2013).
53. B. Dong, H. Nakai, W. Xiao, Characterization of genome integrity for oversized recombinant AAV vector. *Mol Ther* **18**, 87-92 (2010).
54. Y. Lai, Y. Yue, D. Duan, Evidence for the failure of adeno-associated virus serotype 5 to package a viral genome > or = 8.2 kb. *Mol Ther* **18**, 75-79 (2010).
55. D. Duan *et al.*, Circular intermediates of recombinant adeno-associated virus have defined structural characteristics responsible for long-term episomal persistence in muscle tissue. *J Virol* **72**, 8568-8577 (1998).
56. D. Duan, Y. Yue, J. F. Engelhardt, Expanding AAV packaging capacity with trans-splicing or overlapping vectors: a quantitative comparison. *Mol Ther* **4**, 383-391 (2001).
57. A. Ghosh, Y. Yue, Y. Lai, D. Duan, A hybrid vector system expands adeno-associated viral vector packaging capacity in a transgene-independent manner. *Mol Ther* **16**, 124-130 (2008).
58. Z. Yan, Y. Zhang, D. Duan, J. F. Engelhardt, Trans-splicing vectors expand the utility of adeno-associated virus for gene therapy. *Proc Natl Acad Sci U S A* **97**, 6716-6721 (2000).
59. S. J. Reich *et al.*, Efficient trans-splicing in the retina expands the utility of adeno-associated virus as a vector for gene therapy. *Hum Gene Ther* **14**, 37-44 (2003).
60. A. Ghosh, Y. Yue, D. Duan, Efficient transgene reconstitution with hybrid dual AAV vectors carrying the minimized bridging sequences. *Hum Gene Ther* **22**, 77-83 (2011).
61. I. Trapani *et al.*, Effective delivery of large genes to the retina by dual AAV vectors. *EMBO Mol Med* **6**, 194-211 (2014).
62. F. M. Dyka, S. L. Boye, V. A. Chiodo, W. W. Hauswirth, S. E. Boye, Dual adeno-associated virus vectors result in efficient in vitro and in vivo expression of an oversized gene, MYO7A. *Hum Gene Ther Methods* **25**, 166-177 (2014).
63. P. Colella *et al.*, Efficient gene delivery to the cone-enriched pig retina by dual AAV vectors. *Gene Ther* **21**, 450-456 (2014).
64. Z. Wu, H. Yang, P. Colosi, Effect of genome size on AAV vector packaging. *Mol Ther* **18**, 80-86 (2010).
65. K. Chamberlain, J. M. Riyad, T. Weber, Expressing Transgenes That Exceed the Packaging Capacity of Adeno-Associated Virus Capsids. *Hum Gene Ther Methods* **27**, 1-12 (2016).
66. D. J. Truong *et al.*, Development of an intein-mediated split-Cas9 system for gene therapy. *Nucleic Acids Res* **43**, 6450-6458 (2015).
67. K. V. Mills, M. A. Johnson, F. B. Perler, Protein splicing: how inteins escape from precursor proteins. *J Biol Chem* **289**, 14498-14505 (2014).
68. H. Wu, Z. Hu, X. Q. Liu, Protein trans-splicing by a split intein encoded in a split DnaE gene of Synechocystis sp. PCC6803. *Proc Natl Acad Sci U S A* **95**, 9226-9231 (1998).
69. Y. Li, Split-inteins and their bioapplications. *Biotechnol Lett* **37**, 2121-2137 (2015).
70. D. W. Wood, J. A. Camarero, Intein applications: from protein purification and labeling to metabolic control methods. *J Biol Chem* **289**, 14512-14519 (2014).

71. C. Schmelas, D. Grimm, Split Cas9, Not Hairs - Advancing the Therapeutic Index of CRISPR Technology. *Biotechnol J* **13**, e1700432 (2018).
72. L. Villiger *et al.*, Treatment of a metabolic liver disease by in vivo genome base editing in adult mice. *Nat Med* **24**, 1519-1525 (2018).
73. F. Zhu, Z. Liu, X. Chi, H. Qu, Protein trans-splicing based dual-vector delivery of the coagulation factor VIII gene. *Sci China Life Sci* **53**, 683-689 (2010).
74. F. Zhu *et al.*, Inter-chain disulfide bond improved protein trans-splicing increases plasma coagulation activity in C57BL/6 mice following portal vein FVIII gene delivery by dual vectors. *Sci China Life Sci* **56**, 262-267 (2013).
75. J. Li, W. Sun, B. Wang, X. Xiao, X. Q. Liu, Protein trans-splicing as a means for viral vector-mediated in vivo gene therapy. *Hum Gene Ther* **19**, 958-964 (2008).
76. A. Auricchio, M. Hildinger, E. O'Connor, G. P. Gao, J. M. Wilson, Isolation of highly infectious and pure adeno-associated virus type 2 vectors with a single-step gravity-flow column. *Hum Gene Ther* **12**, 71-76 (2001).
77. L. S. Ostedgaard *et al.*, A shortened adeno-associated virus expression cassette for CFTR gene transfer to cystic fibrosis airway epithelia. *Proc Natl Acad Sci U S A* **102**, 2952-2957 (2005).
78. E. Senis *et al.*, CRISPR/Cas9-mediated genome engineering: an adeno-associated viral (AAV) vector toolbox. *Biotechnol J* **9**, 1402-1412 (2014).
79. S. C. Khani *et al.*, AAV-mediated expression targeting of rod and cone photoreceptors with a human rhodopsin kinase promoter. *Invest Ophthalmol Vis Sci* **48**, 3954-3961 (2007).
80. T. Yokoyama, G. I. Liou, R. B. Caldwell, P. A. Overbeek, Photoreceptor-specific activity of the human interphotoreceptor retinoid-binding protein (IRBP) promoter in transgenic mice. *Exp Eye Res* **55**, 225-233 (1992).
81. T. G. Drivas, E. L. Holzbaur, J. Bennett, Disruption of CEP290 microtubule/membrane-binding domains causes retinal degeneration. *J Clin Invest* **123**, 4525-4539 (2013).
82. H. Iwai, S. Zuger, J. Jin, P. H. Tam, Highly efficient protein trans-splicing by a naturally split DnaE intein from Nostoc punctiforme. *FEBS Lett* **580**, 1853-1858 (2006).
83. J. Zettler, V. Schutz, H. D. Mootz, The naturally split Npu DnaE intein exhibits an extraordinarily high rate in the protein trans-splicing reaction. *FEBS Lett* **583**, 909-914 (2009).
84. S. W. Lockless, T. W. Muir, Traceless protein splicing utilizing evolved split inteins. *Proc Natl Acad Sci U S A* **106**, 10999-11004 (2009).
85. G. Gao *et al.*, Purification of recombinant adeno-associated virus vectors by column chromatography and its performance in vivo. *Hum Gene Ther* **11**, 2079-2091 (2000).
86. M. Doria, A. Ferrara, A. Auricchio, AAV2/8 vectors purified from culture medium with a simple and rapid protocol transduce murine liver, muscle, and retina efficiently. *Hum Gene Ther Methods* **24**, 392-398 (2013).
87. L. Drittanti, C. Rivet, P. Manceau, O. Danos, M. Vega, High throughput production, screening and analysis of adeno-associated viral vectors. *Gene Ther* **7**, 924-929 (2000).
88. X. Xiao, J. Li, R. J. Samulski, Production of high-titer recombinant adeno-associated virus vectors in the absence of helper adenovirus. *J Virol* **72**, 2224-2232 (1998).
89. K. Jennings *et al.*, Proteasome inhibition enhances AAV-mediated transgene expression in human synoviocytes in vitro and in vivo. *Mol Ther* **11**, 600-607 (2005).
90. R. Sangermano *et al.*, Photoreceptor Progenitor mRNA Analysis Reveals Exon Skipping Resulting from the ABCA4 c.5461-10T-->C Mutation in Stargardt Disease. *Ophthalmology* **123**, 1375-1385 (2016).
91. T. Nakano *et al.*, Self-formation of optic cups and storable stratified neural retina from human ESCs. *Cell Stem Cell* **10**, 771-785 (2012).

92. X. Zhong *et al.*, Generation of three-dimensional retinal tissue with functional photoreceptors from human iPSCs. *Nat Commun* **5**, 4047 (2014).
93. M. P. Krebs *et al.*, Mouse models of human ocular disease for translational research. *PLoS One* **12**, e0183837 (2017).
94. B. Chang *et al.*, In-frame deletion in a novel centrosomal/ciliary protein CEP290/NPHP6 perturbs its interaction with RPGR and results in early-onset retinal degeneration in the rd16 mouse. *Hum Mol Genet* **15**, 1847-1857 (2006).
95. F. Q. Liang, V. Anand, A. M. Maguire, J. Bennett, Intraocular delivery of recombinant virus. *Methods Mol Med* **47**, 125-139 (2001).
96. E. V. Polishchuk, R. S. Polishchuk, Analysis of Golgi complex function using correlative light-electron microscopy. *Methods Cell Biol* **118**, 243-258 (2013).
97. B. W. Bisgrove, H. J. Yost, The roles of cilia in developmental disorders and disease. *Development* **133**, 4131-4143 (2006).
98. G. Li *et al.*, A role for Alstrom syndrome protein, alms1, in kidney ciliogenesis and cellular quiescence. *PLoS Genet* **3**, e8 (2007).
99. T. Hearn *et al.*, Mutation of ALMS1, a large gene with a tandem repeat encoding 47 amino acids, causes Alstrom syndrome. *Nat Genet* **31**, 79-83 (2002).
100. S. Tang, M. Xie, N. Cao, S. Ding, Patient-Specific Induced Pluripotent Stem Cells for Disease Modeling and Phenotypic Drug Discovery. *J Med Chem* **59**, 2-15 (2016).
101. K. J. Wahlin *et al.*, Photoreceptor Outer Segment-like Structures in Long-Term 3D Retinas from Human Pluripotent Stem Cells. *Sci Rep* **7**, 766 (2017).
102. M. Cheriyan, S. H. Chan, F. Perler, Traceless splicing enabled by substrate-induced activation of the Nostoc punctiforme Npu DnaE intein after mutation of a catalytic cysteine to serine. *J Mol Biol* **426**, 4018-4029 (2014).
103. J. E. Donello, J. E. Loeb, T. J. Hope, Woodchuck hepatitis virus contains a tripartite posttranscriptional regulatory element. *J Virol* **72**, 5085-5092 (1998).
104. A. Auricchio, A. J. Smith, R. R. Ali, The Future Looks Brighter After 25 Years of Retinal Gene Therapy. *Hum Gene Ther* **28**, 982-987 (2017).
105. T. Koo, L. Popplewell, T. Athanasopoulos, G. Dickson, Triple trans-splicing adeno-associated virus vectors capable of transferring the coding sequence for full-length dystrophin protein into dystrophic mice. *Hum Gene Ther* **25**, 98-108 (2014).
106. W. Lostal, K. Kodippili, Y. Yue, D. Duan, Full-length dystrophin reconstitution with adeno-associated viral vectors. *Hum Gene Ther* **25**, 552-562 (2014).
107. P. Bovolenta, E. Cisneros, Retinitis pigmentosa: cone photoreceptors starving to death. *Nat Neurosci* **12**, 5-6 (2009).
108. H. Petrs-Silva *et al.*, High-efficiency transduction of the mouse retina by tyrosine-mutant AAV serotype vectors. *Mol Ther* **17**, 463-471 (2009).
109. A. Maddalena *et al.*, Triple Vectors Expand AAV Transfer Capacity in the Retina. *Mol Ther* **26**, 524-541 (2018).
110. P. Subramanyam *et al.*, Manipulating L-type calcium channels in cardiomyocytes using split-intein protein transsplicing. *Proc Natl Acad Sci U S A* **110**, 15461-15466 (2013).

APPENDIX

Molecular Therapy

Volume 26 Number 2 February 7, 2018 Pages 000–000

Molecular Therapy

Volume 26 Number 2
February 7, 2018

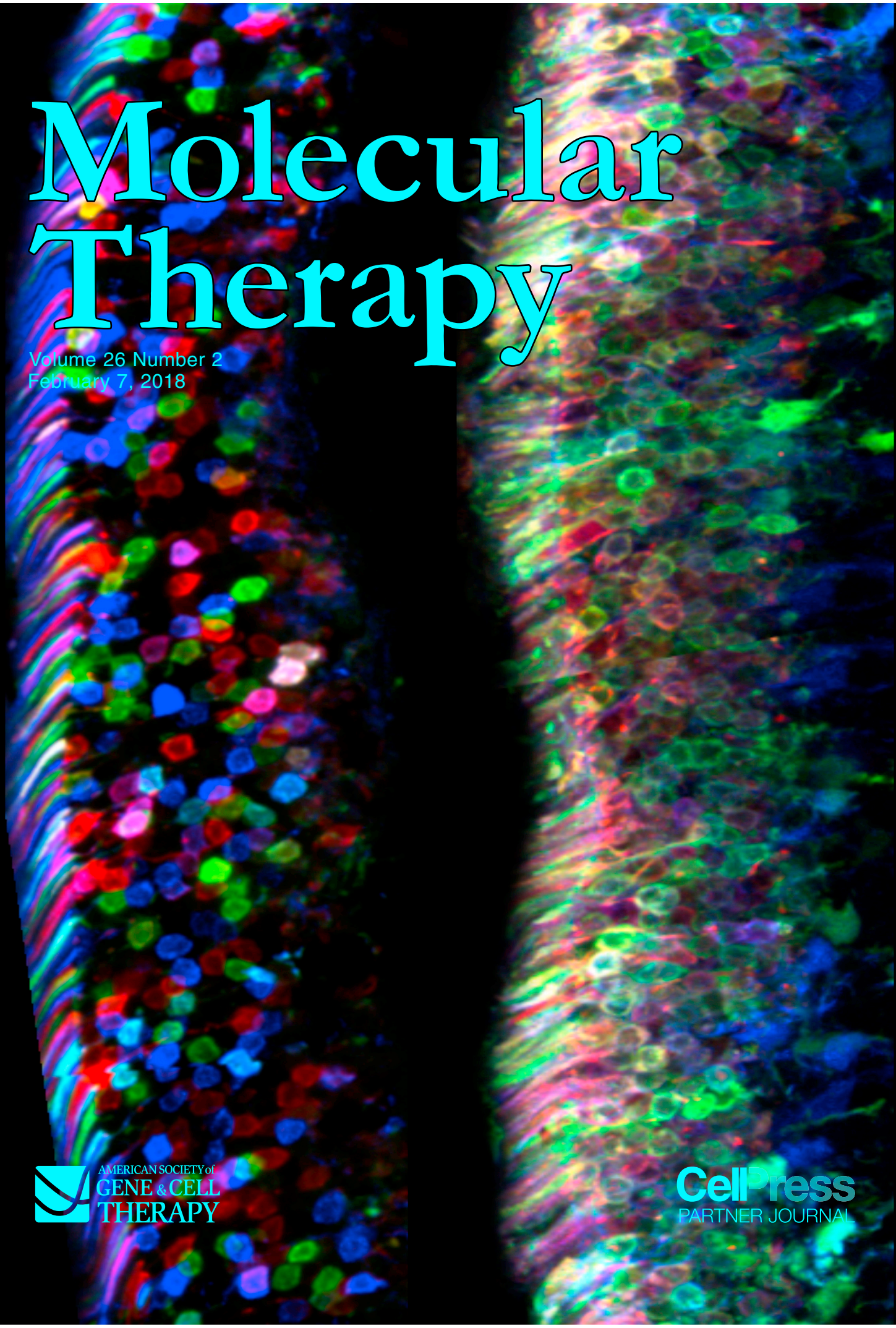

AMERICAN SOCIETY of GENE & CELL THERAPY

CellPress
PARTNER JOURNAL

Molecular Therapy
Original Article

Triple Vectors Expand AAV Transfer Capacity in the Retina

Andrea Maddalena,[1,6] Patrizia Tornabene,[1,6] Paola Tiberi,[1] Renato Minopoli,[1] Anna Manfredi,[1,2] Margherita Mutarelli,[1] Settimio Rossi,[3] Francesca Simonelli,[3] Jurgen K. Naggert,[4] Davide Cacchiarelli,[1,2] and Alberto Auricchio[1,5]

[1]Telethon Institute of Genetics and Medicine (TIGEM), Pozzuoli 80078, Italy; [2]Armenise/Harvard Laboratory of Integrative Genomics, TIGEM, Pozzuoli 80078, Italy; [3]Eye Clinic, Multidisciplinary Department of Medical, Surgical and Dental Sciences, Second University of Naples, Naples 80121, Italy; [4]The Jackson Laboratory, Bar Harbor, ME 04609, USA; [5]Medical Genetics, Department of Advanced Biomedicine, Federico II University, Naples 80131, Italy

Retinal gene transfer with adeno-associated viral (AAV) vectors holds great promise for the treatment of inherited retinal degenerations (IRDs). One limit of AAV is its transfer capacity of about 5 kb, which can be expanded to about 9 kb, using dual AAV vectors. This strategy would still not suffice for treatment of IRDs such as Usher syndrome type 1D or Alström syndrome type I (ALMS) due to mutations in *CDH23* or *ALMS1*, respectively. To overcome this limitation, we generated triple AAV vectors, with a maximal transfer capacity of about 14 kb. Transcriptomic analysis following triple AAV transduction showed the expected full-length products along a number of aberrant transcripts. However, only the full-length transcripts are efficiently translated *in vivo*. We additionally showed that approximately 4% of mouse photoreceptors are transduced by triple AAV vectors and showed correct localization of recombinant ALMS1. The low-photoreceptor transduction levels might justify the modest and transient improvement we observe in the retina of a mouse model of ALMS. However, the levels of transduction mediated by triple AAV vectors in pig retina reached 40% of those observed with single vectors, and this bodes well for further improving the efficiency of triple AAV vectors in the retina.

INTRODUCTION

Inherited retinal degenerations (IRDs), with an overall global prevalence of 1/2,000,[1] are a major cause of blindness worldwide. IRDs are mostly monogenic and are caused by mutations in genes mainly expressed in retinal photoreceptors (PRs; rods and cones) and to a lesser extent in retinal pigmented epithelium (RPE).[2] To date, gene therapy based on adeno-associated viral (AAV) vectors represents the most promising therapeutic approach for IRDs. AAVs are (1) safe and effective when delivered subretinally in patients with Leber congenital amaurosis type 2, a severe form of inherited childhood blindness[3–8] and (2) to date, the most effective gene transfer vector for PRs in addition to RPE.[9–15] However, the relatively small DNA packaging capacity of AAV, which is considered to be restricted to the size of the parental genome (4.7 kb),[16–19] prevents its application from the treatment of those IRDs caused by mutations in genes having a coding sequence (CDS) larger than 5 kb, such as Stargardt disease (STGD1; MIM_248200), Usher syndrome types IB (USH1B; MIM_276900) and 1D (USH1D; MIM_601067), or Alström syndrome (ALMS; MIM_203800), among others.

Dual AAV vectors[20–23] have been developed to overcome the limited-cargo capacity of AAV by splitting a large transgene expression cassette in two separate halves, each independently packaged in a single normal-size (<5 kb) AAV vector.[20,21,23,24] The reconstitution of the full-length expression cassette is achieved upon co-infection of the same cell by both dual AAV vectors followed by inverted terminal repeat (ITR)-mediated tail-to-head concatemerization of the 5′ and 3′ genomes and/or followed by splicing (dual AAV *trans*-splicing vectors [TS]);[20–22,25] homologous recombination between overlapping regions contained in both the 5′ and 3′ genomes (dual AAV overlapping vectors)[21] or a combination of the two (dual AAV hybrid vectors), where the directional concatemerization can be favored by the presence of highly recombinogenic sequences.[23] We have recently shown that both dual AAV TS and hybrid AK vectors (that contain the short AK recombinogenic region from the F1 phage) efficiently transduce mouse PRs and RPE, and rescue mouse models of STGD1 and USH1B[26] caused by mutations in *ABCA4* (ATP-binding cassette subfamily A member 4; CDS, 6.8 kb) and *MYO7A* (MYOSIN VII A; CDS, 6.6 kb), respectively. Robust *MYO7A* reconstitution by dual AAV vectors was confirmed in the mouse retina by Dyka et al.,[27] while several examples of dual AAV systems for minidystrophin (CDS, 6.2 kb) expression in mouse muscle are available.[23,28] The efficacy of dual AAV vectors, with a maximum transfer capacity of around 9 kb, opens the venue for further expansion to triple AAV vectors with a theoretical transfer capacity of around 14 kb.

Triple AAV vectors, in principle, would enable the development of gene therapies for IRDs due to mutations in genes whose CDS is

Received 7 May 2017; accepted 28 November 2017;
https://doi.org/10.1016/j.ymthe.2017.11.019.

[6]These authors contributed equally to this work.

Correspondence: Alberto Auricchio, MD, Telethon Institute of Genetics and Medicine (TIGEM), Via Campi Flegrei 34, Pozzuoli (Naples) 80078, Italy.
E-mail: auricchio@tigem.it

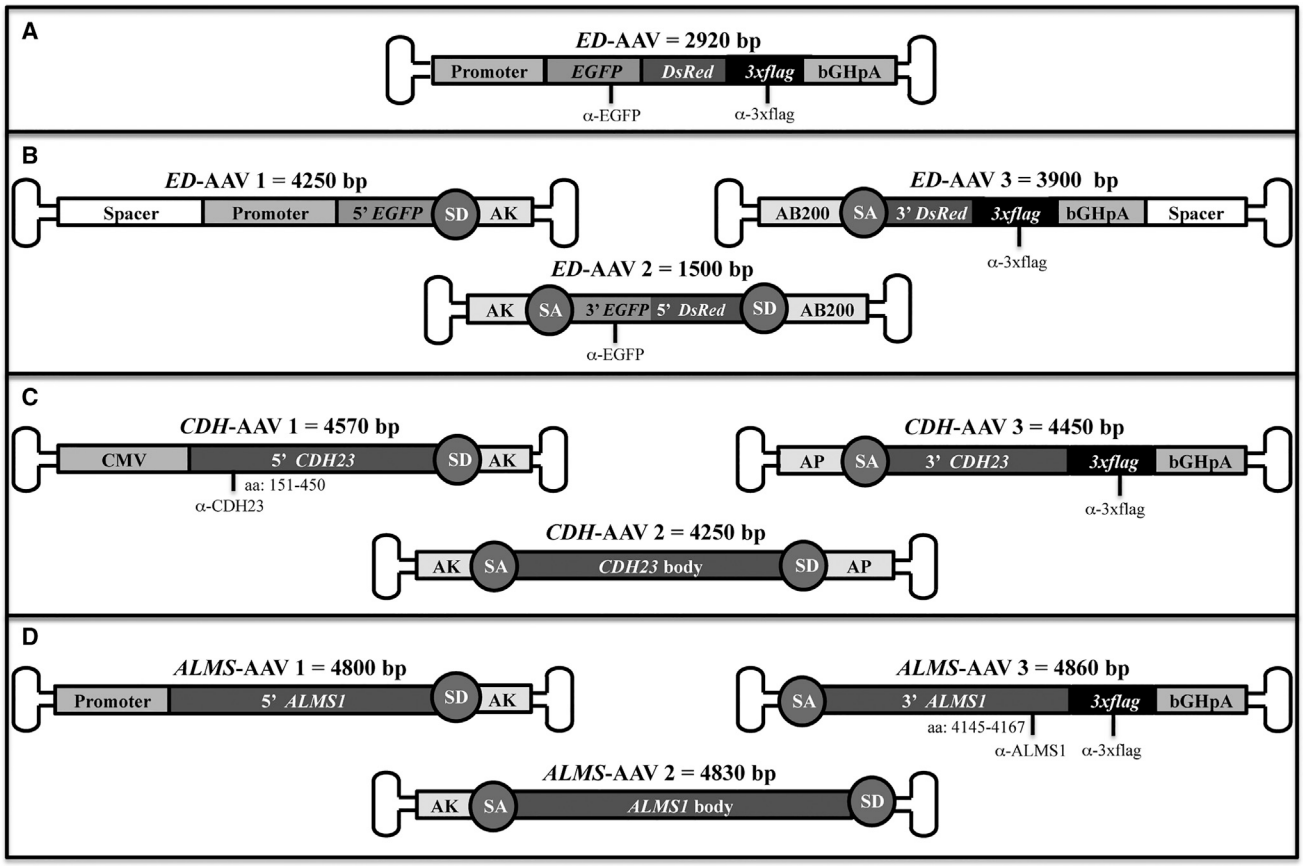

Figure 1. Schematic Representation of Single and Triple AAV Vectors

Single *ED*-AAV (A); triple *ED*-AAVs (B); triple *CDH*-AAVs (C); triple *ALMS*-AAVs (D). The position of the epitopes recognized by the antibodies used in this study is indicated. The vector genome size is depicted above each vector. bGHpA, bovine growth hormone polyadenylation signal; SD, splicing donor signal; SA, splicing acceptor signal; AP, alkaline phosphatase recombinogenic region; AK, F1 phage recombinogenic region; AB200, *ABCA4* recombinogenic region; *3xflag*, triple flag tag; CMV, cytomegalovirus; α-EGFP, anti-EGFP antibodies; α-3xflag, anti-3xflag antibodies; α-CDH23, anti-CDH23 antibodies; α-ALMS1, anti-ALMS1 antibodies.

larger than 9 kb (herein referred to as large genes). Among those IRDs are (1) USH1D, a severe form of autosomal recessive blindness-deafness which accounts for 19%–35% of cases of Usher syndrome type 1[29–31] and which is caused by mutations in *CDH23* (CDS, 10.1 kb), which encodes for the Cadherin-related family member 23[32,33] and (2) ALMS, an autosomal recessive condition, with a prevalence of less than one per million[34], and characterized by a combination of features including obesity, insulin resistance, and retinal dystrophy. ALMS is caused by mutations in *ALMS1* (CDS, 12.5 kb), which encodes for a ciliary/centrosomal protein thought to play a key role in transport along the PR axoneme.[34–38] Triple AAV vectors have previously been exploited to reconstruct full-length *dystrophin* (CDS, 11.1 kb) in the muscle of dystrophic mice.[39,40] Low levels of full-length dystrophin expression were obtained by both TS[40] and hybrid systems.[39] These results demonstrated great potential for testing triple AAV vectors in the retina to restore *CDH23* and *ALMS1* gene expression. Indeed, the enclosed and small subretinal space should favor co-infection and transduction of the same cell by three independent AAV vectors.

RESULTS

Generation of Single and Triple AAV Vectors

In order to test transduction efficiency mediated by triple AAV vectors, we generated a reporter protein by fusing the CDS of *EGFP* to that of *Discosoma red fluorescent protein* (*DsRed*) (herein referred to as *ED*) separated by a 13 amino acid spacer. A triple flag tag (*3xflag*) was added at the 3′ end of *ED* CDS (Figure 1A), which was placed under the control of (1) the ubiquitous cytomegalovirus (CMV) promoter, (2) the PR-specific human interphotoreceptor retinoid-binding protein (IRBP) promoter,[41,42] or (3) the RPE-specific vitelliform macular dystrophy 2 (VMD2) promoter.[43] The *ED* cassettes were either packed in a single AAV vector or split in three parts, each packed in a different AAV vector (Figure 1B and Materials and Methods) from here called *ED*-AAV 1, *ED*-AAV 2, *ED*-AAV 3. Upon HEK293 transfection with plasmids expressing ED, the ED spontaneous fluorescence appeared weaker than the fluorescence detected when single EGFP- or single DsRed-expressing plasmids were used (Figure S1).

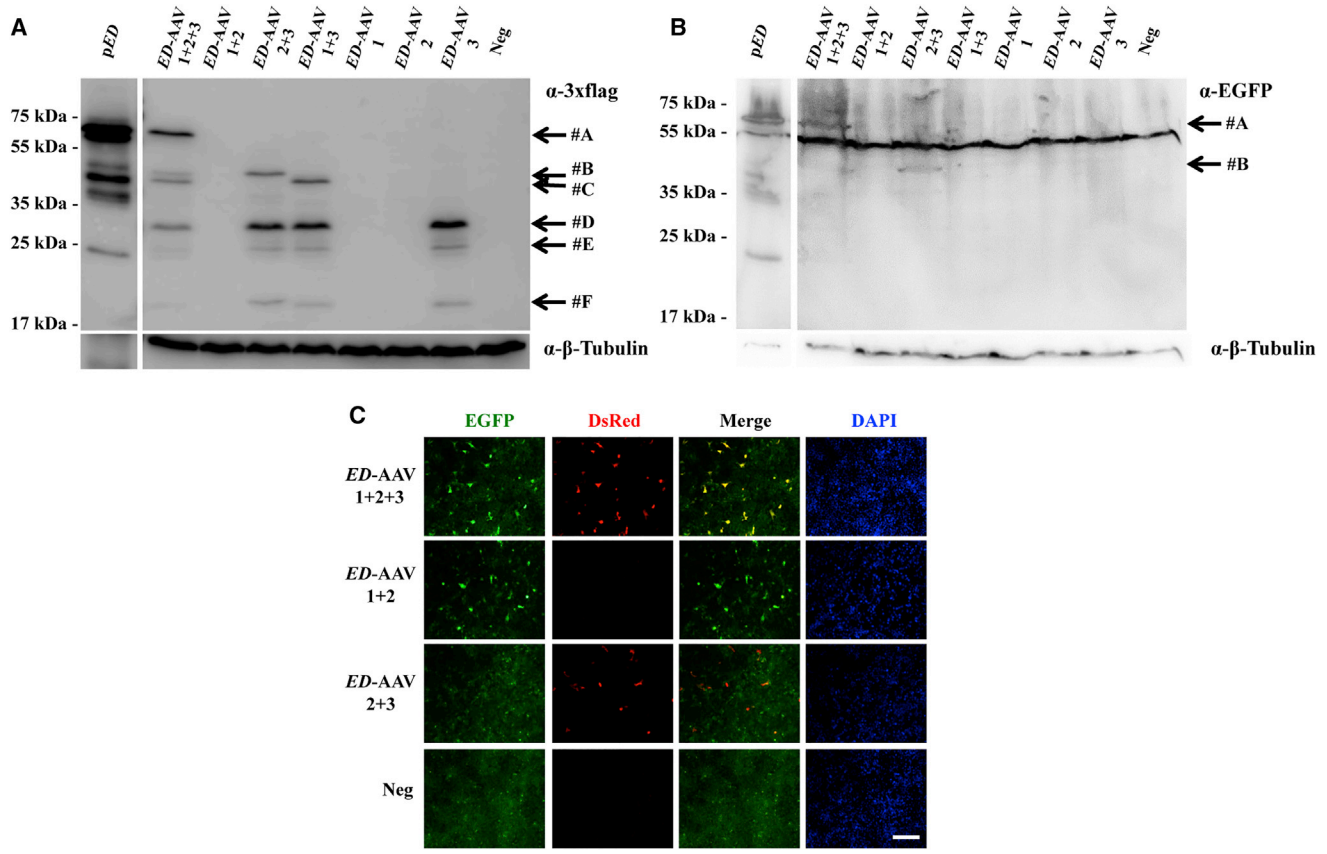

Figure 2. Triple *ED*-AAV Vectors Efficiently Transduce ED *In Vitro*

(A and B) Western blot (WB) analysis of lysates from HEK293 cells either transfected with p*ED* or infected with triple AAV2/2 vectors encoding for ED and stained with α-3xflag (A) and α-EGFP (B) antibodies. The arrows on the right indicate the following protein products: #A, ED full-length protein; #B, from AAV 2 + 3; #C, from AAV 1 + 3; #F, from AAV 3; #D and #E, aggregates of AAV 3. α-3xflag, WB with anti-3xflag antibodies; α-EGFP, WB with anti-EGFP antibodies; α-β-Tubulin, WB with anti-β-Tubulin antibodies, used as loading control. Neg, not infected cells. The molecular weight ladder is depicted on the left; 20 and 200 μg of proteins for transfected and infected samples, respectively, were loaded. The WB images are representative of n = 4 independent experiments. (C) Fluorescent analysis of HEK293 cells infected with triple AAV2/2 vectors encoding for ED. The scale bar (200 μm) is depicted in the figure. DsRed, Discosoma red fluorescent protein; Merge: overlay of EGFP and DsRed images.

Similarly, *CDH23-3xflag* and *ALMS1-3xflag* were split in three parts each cloned in a separate AAV vector (Figures 1C and 1D and Materials and Methods) from here called *CDH*-AAV 1, *CDH*-AAV 2, *CDH*-AAV 3, and *ALMS*-AAV 1, *ALMS*-AAV 2, *ALMS*-AAV 3. *CDH*-AAV 1 and *ALMS*-AAV 1 included the ubiquitous CMV and either the short CMV (shCMV) or the PR-specific human G protein-coupled receptor kinase 1 (GRK1) promoters, respectively. For the *in vitro* experiments, we generated AAV2/2 vectors, which efficiently transduce HEK293 cells.[44] In the experiments performed in the mouse and pig retinas, we used AAV2/8 vectors, which efficiently transduce RPE and PRs[9–11] but poorly infect HEK293 cells.

Triple *ED*-AAV Vectors Efficiently Transduce HEK293 Cells

First, we evaluated the efficiency of triple *ED*-AAV-mediated large gene transduction *in vitro* by infecting HEK293 cells with AAV2/2 vectors at an MOI of 5×10^4 genome copies (GC)/cell of each vector. Seventy-two hours after infection, cell lysates were analyzed and the ED expression was evaluated by western blot (WB) using anti-3xflag (Figure 2A) or anti-EGFP (Figure 2B) antibodies (please see their specific epitope localization in Figure 1), by direct microscope imaging (Figure 2C) and by cytofluorimetry. As shown in Figures 2A and 2B, full-length proteins (#A) of the expected size (≈60 kDa) were detected only following co-infection with the three *ED*-AAV vectors. Various shorter products were detected by the anti-3xflag antibodies when *ED*-AAV 3, which includes the 3xflag tag, was added to the infection mix (Figure 2A). These include (1) a product that derives from *ED*-AAV 2 + 3 (#B); (2) a product that might derive from the concatemerization of *ED*-AAV 1 + 3 and the use of an alternative ATG in frame with the 3xflag (#C); (3) a product from *ED*-AAV 3 alone (#F); and (4) products that might represent aggregates of #F (#D and #E). WB with anti-EGFP antibodies (Figure 2B) confirmed the presence of both full-length ED (#A) when the 3 *ED*-AAV vectors were used and the shorter #B product in the *ED*-AAV 2 + 3 sample. Interestingly, the relative amount of the truncated products decreases when the 3 *ED*-AAV vectors are used.

ED expression was also evaluated by direct imaging of native fluorescence (Figure 2C). Double EGFP and DsRed-positive cells could be detected only when the 3 *ED*-AAVs were used. Cells that are positive for either EGFP or DsRed alone were detected when *ED*-AAV 1 + 2 or *ED*-AAV 2 + 3 were respectively used, but they were almost absent in the *ED*-AAV 1 + 2 + 3 samples.

The efficiency of triple *ED*-AAVs transduction was then quantified by cytofluorimetry, which showed that double EGFP and DsRed-positive cells were present above background only in single *ED*-AAV (46.69% ± 5.66%; n = 4) and in *ED*-AAV 1 + 2 + 3 (2.78% ± 0.84%; n = 3) samples. Therefore, the efficiency of triple *ED*-AAVs transduction is 5.96% ± 1.95% of that of the corresponding single vector.

Triple *CDH*- and *ALMS*-AAV Vectors Efficiently Transduce HEK293 Cells

HEK293 cells were infected with the various combinations of *CDH*- and *ALMS*-AAV2/2 vectors at an MOI of 5×10^4 GC/cell and analyzed 72 hr post-infection. The expression of full-length and truncated products of CDH23 and ALMS1 was evaluated at both transcriptional and translational levels.

cDNAs from HEK293 infected cells were analyzed by real-time qPCR. For each transgene, six primers (A→F) were used, each annealing to one extremity of the three CDSs separately included in each of the triple vectors (Figure 3A). First, we observed that the real-time qPCR amplification using primers D (located at the 3′ end of vector 2) and E (located at the 5′ of vector 3) following infection with AAV 2 + 3 is significantly lower than the one obtained when AAV 1 + 2 + 3 are used (2% for *CDH23* and 20% for *ALMS1*). This means that amplification with this set of primers can be used as a close estimate of full-length transcript following concatemerization of the three vectors. For simplicity, from now on, such measurement will be set to 1 as reference, and the abundance of the other products will be presented as fold change relative to the reference. To detect the transcripts from all possible triple AAV concatemers, the A→F primers were tested in all possible combinations. The sets of primers that generated a PCR product with a relative abundance >0.1 compared to full-length are reported in Figure 3B, along with a schematic representation of the corresponding predicted AAV concatemer. For both *CDH23* and *ALMS1* transgenes, amplification of products with a relative abundance higher than full-length was obtained with the following primer couples: B + C, A + B, B + E, and, only in the case of *ALMS1*, C + D (shown in bold in Figure 3B, "*in vitro*" column). Direct sequencing of real-time qPCR products revealed that, upon correct assembly of the triple *CDH*- or *ALMS*-AAV, correct splicing occurs (data not shown).

As the real-time qPCR analysis cannot reveal the generation of alternative splicing within the three CDSs, we additionally performed a targeted RNA-seq analysis with *de novo* annotation of the two transgenes. The analysis annotated the presence of the full-length transcript in both CDH23 (Figure S2A) and ALMS1 (Figure S2B) samples. Similar to what we observed in the real-time qPCR analysis, the most represented products derive from the concatemerization of AAV 1 + 3. It is interesting to note that the CDS of *CDH*-AAV 3 seems to generate several isoforms as a consequence of alternative splicing.

Following detailed transcriptional characterization of HEK293 cells infected with triple AAV vectors, we tested the presence of full-length and truncated CDH23 and ALMS1 protein products. WB analysis of lysates from infected cells was performed using antibodies (please see their specific epitope localization in Figure 1) directed to either the 3xflag tag (Figures 4A and 4C) or CDH23 and ALMS1 (Figures 4B and 4D). In all cases, full-length protein (#A) was detected with both anti-3xflag and anti-CDH23 or anti-ALMS1 antibodies only when the three *CDH*- (Figures 4A and 4B; ≈360 kDa) or *ALMS*-AAVs (Figures 4C and 4D; ≈461 kDa) were used. Please note that the shape of the ALMS1 bands in the lanes *ALMS*-AAV 1 + 2 + 3 may be due to the challenging migration of such high molecular weight proteins in the SDS-PAGE. In addition to the full-length proteins, several shorter products were observed: (1) a truncated product (#B) which corresponds to CDH23 C terminus was detected with anti-3xflag antibodies when *CDH*-AAV 3 was included in the infection mix (Figure 4A); (2) only in the sample infected with *CDH*-AAV 1 + 3, a smear of bands was observed that was greatly reduced when the three *CDH*-AAV vectors were included in the infection mix (Figure 4A); (3) a truncated product of ≈270 kDa (#B) was detected with anti-3xflag antibodies when *ALMS*-AAV 1 + 3 was included in the infection mix (Figure 4C). The two bands of ≈171 and ≈117 kDa present in all lanes of the WB shown in Figure 4D are presumably due to aspecific antibody binding.

Subretinal Administration of Triple *ED*-AAVs Results in Full-Length Transgene Expression in Mouse and Pig Retina

We hypothesized that the enclosed and small subretinal space should favor co-infection and transduction of the same cell by three independent AAV vectors. To evaluate this, we injected subretinally triple CMV-*ED*-AAV2/8 vectors (dose of each vector/eye, 4.2×10^9 GC) in 4-week-old C57BL/6J mice (n = 7 eyes). Eyes were harvested 2 months later, and we analyzed, on retinal cryosections, the number of PR cells expressing ED (Figure 5A). We found, in the transduced area of 5 out of 7 eyes, that 2.9% ± 0.5% were positive for EGFP alone (which derives from concatemerization of only *ED*-AAV 1 + 2) and 3.6% ± 0.3% were positive for both EGFP and DsRed (which derives from concatemerization of *ED*-AAV 1 + 2 + 3). As no PRs were positive for DsRed alone (which derives from *ED*-AAV 2 + 3), we conclude that the co-expression of EGFP-DsRed indicates full-length protein expression deriving from proper directional concatemerization of *ED*-AAV 1 + 2 + 3.

To confirm by WB analysis the retinal expression of full-length ED protein as well as to detect potential byproducts from *ED*-AAV 1 + 3 that could not be viewed on retinal histological sections, the following combinations of triple *ED*-AAVs (dose of each vector/eye, 4.2×10^9 GC) were injected subretinally in 4-week-old C57BL/6J mice: *ED*-AAV 1 + 2 + 3 (n = 8 eyes); *ED*-AAV 2 + 3

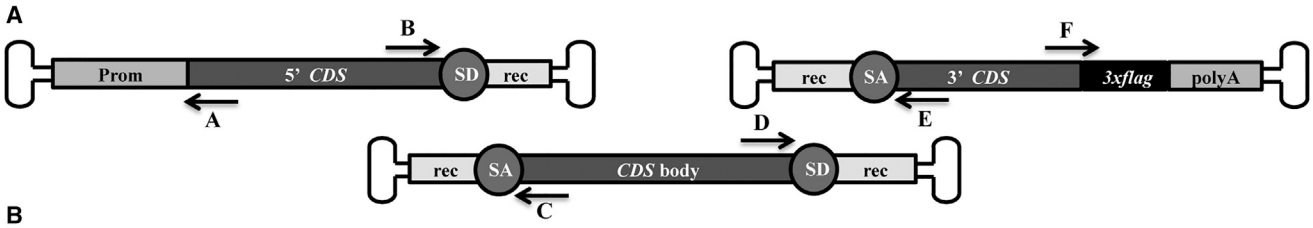

B

Vector assembly	Gene	*In vitro (fold change vs full-length ± SE)*	*Mouse retina (fold change vs full-length ± SE)*
D AK SA CDS body SD (AP) / (AP) SA 3' CDS 3xflag bGHpA E	*CDH23*	*1*	*1*
	ALMS1	*1*	*1*
B Prom 5' CDS SD AK / AK SA CDS body SD (AP) C	*CDH23*	***1.44±0.45***	***3.34±0.65***
	ALMS1	***5.58±1.51***	***2.11±0.19***
B Prom 5' CDS SD AK / Prom 5' CDS SD AK A; A 5'CDS B	CDH23	**3.73±2.04**	**125.18±31.81**
	ALMS1	**5.50±2.61**	**19.40±1.46**
D AK SA CDS body SD (AP) / Prom 5' CDS SD AK A	CDH23	0.21±0.05	**4.80±1.07**
	ALMS1	0.17±0.06	**1.78±0.57**
B Prom 5' CDS SD AK / (AP) SD CDS body VS AK C	CDH23	0.37±0.16	0.82±0.15
	ALMS1	0.22±0.05	**1.05±0.17**
B Prom 5' CDS SD AK / (AP) SA 3' CDS 3xflag bGHpA E	CDH23	**4.25±1.32**	**1.65±0.12**
	ALMS1	**5.55±1.75**	**4.01±0.77**
D AK SA CDS body SD (AP) / AK SA CDS body SD (AP) C; C CDS body D	CDH23	0.19±0.05	**2.98±0.61**
	ALMS1	**1.90±0.60**	**6.26±0.23**
F (AP) SA 3' CDS 3xflag bGHpA / AK SA CDS body SD (AP) C	CDH23	<0.1	N.D.
	ALMS1	0.15±0.02	0.28±0.09
D AK SA CDS body SD (AP) / (AP) SD CDS body VS AK C	CDH23	0.34±0.16	0.40±0.09
	ALMS1	<0.1	N.D.
F (AP) SA 3' CDS 3xflag bGHpA / (AP) SA 3' CDS 3xflag bGHpA E; E 3'CDS 3xflag F	CDH23	<0.1	N.D.
	ALMS1	0.25±0.02	**1.56±0.24**

Figure 3. Transcriptomic Analysis following Transduction with Triple AAV Vectors

(A) Schematic representation of triple *CDH* and *ALMS*-AAV vectors with primers used for real-time qPCR (A→F). Prom, promoter; CDS, coding sequence; polyA, polyadenylation signal; *3xflag*, triple flag tag; SD, splicing donor signal; SA, splicing acceptor signal; rec, recombinogenic region. (B) Results of the real-time qPCR analysis performed on cDNAs from HEK293 cells or mouse eyecups treated with either *CDH*- or *ALMS*-AAV 1 + 2 + 3 vectors. The left column shows the vector assembly predicted on the basis of the set of primers used. The two columns on the right show the abundance of the PCR products relative to full-length detected by the D + E primers. Only products with a relative abundance >0.1 are shown. Highlighted in italic is the relative abundance of PCR products resulting from the desired AAV directional concatemerization. Highlighted in bold are the PCR products with a relative abundance >1.

(n = 8 eyes); *ED*-AAV 1 + 3 (n = 6 eyes); *ED*-AAV 3 (n = 6 eyes); single *ED*-AAV (n = 6 eyes). Eyecups were harvested 2 months later, and WB analysis was performed using anti-3xflag antibodies. As shown in Figure 5B, apart from the full-length protein (#A), when the 3 *ED*-AAV vectors were included in the mix, an additional faint band of lower molecular weight was detected (#C), which has a molecular weight similar to that detected *in vitro* in the *ED*-AAV 1 + 3 sample (#C) (Figure 2A). However, this product was present only in one out of six eyes injected with *ED*-AAV 1 + 3, confirming that this is a rare event which was not detected in retinal histological sections (Figure 5A). The other bands present in *ED*-AAV 1 + 2 + 3 sample, which are also present in the samples injected with single *ED*-AAV, might represent degradation products of the full-length ED protein.

We then investigated whether triple AAV transduction occurs in different retinal cell types. Toward this end, 4-week-old C57BL/6J mice were injected subretinally with three sets of triple *ED*-AAV vectors, each with a different promoter: CMV, IRBP, and VMD2 at the doses of 4.2×10^9, 3.7×10^9, and 2.4×10^9 GC/each vector/eye, respectively. Animals were sacrificed 2 months post-injection, and protein lysates from eyecups were analyzed by WB, which showed that full-length ED reconstitution and expression can be driven by all three promoters, although with different efficiencies. Subretinal

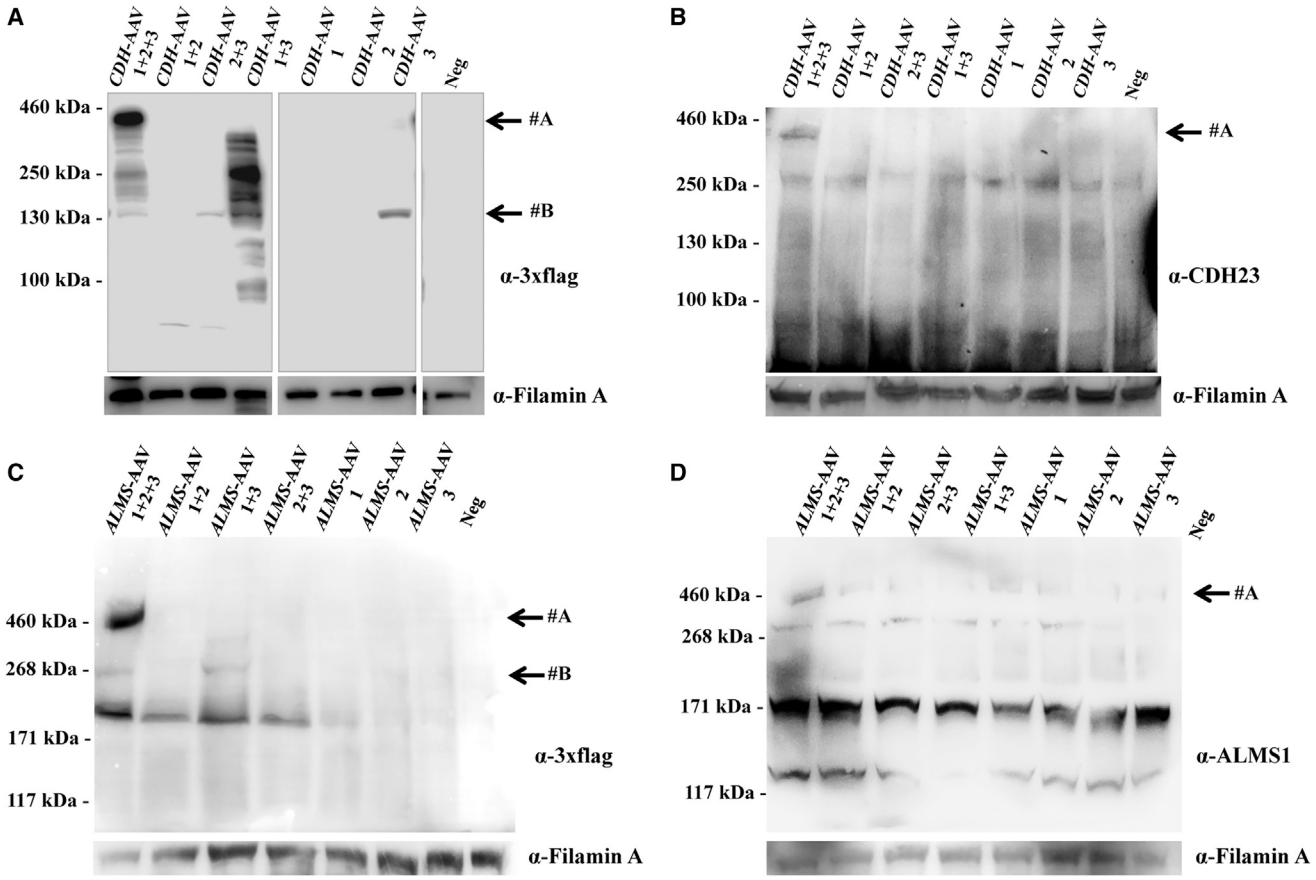

Figure 4. Triple *CDH*- and *ALMS*-AAV Vectors Efficiently Transduce CDH23 and ALMS1 *In Vitro*

(A and B) WB analysis of lysates from HEK293 cells infected with triple AAV2/2 vectors encoding for CDH23 and incubated with either anti-3xflag (A) or anti-CDH23 (B) antibodies. The arrows on the right indicate the following protein products: #A, full-length CDH23 protein; #B, from AAV 3. (C and D) WB analysis of lysates from HEK293 cells infected with triple AAV2/2 vectors encoding for ALMS1 and incubated with either anti-3xflag (C) or anti-ALMS1 (D) antibodies. The arrows on the right indicate the following protein products: #A, full-length ALMS1 protein; #B, from AAV 1 + 3. α-3xflag, WB with anti-3xflag antibodies; α-CDH23, WB with anti-CDH23 antibodies; α-ALMS1, WB with anti-ALMS1 antibodies; α-Filamin A, WB with anti-Filamin A antibodies, used as loading control. Neg, cells infected with control AAV2/2-CMV-*EGFP* vectors. The molecular weight ladder is depicted on the left, 100 (A), 250 (B), or 200 μg (C and D) of proteins were loaded.

injection of triple VMD2-*ED*-AAV vectors, which includes the RPE-specific VMD2 promoter, displayed strong protein expression in 10/10 analyzed eyes. The ubiquitous CMV promoter resulted in slightly higher levels of ED expression compared to VMD2 in 13/18 (72%) analyzed eyes. The IRBP promoter, specific for PR expression, resulted in faint ED expression in 14/19 (74%) analyzed eyes (Figure 5C).

To assess if the weak PR transduction observed with the IRBP promoter was due to poor transcriptional activity of the promoter in the PRs or limited recombination upon co-infection of the three vectors, we compared the expression of the ED protein encoded by the triple AAV vectors to the expression by a single AAV vector containing the same expression cassette (Figures 5D and 5E; Figures S3 and S4). The experiment was performed with both the CMV (Figures 5D and S3) and IRBP (Figures 5E and S4) promoters, and ED protein expression was evaluated by WB analysis with anti-3xflag antibodies. WB band intensity showed that, in the case of the CMV promoter, the level of ED expression obtained with the triple AAV vectors was 27% ± 6% of the one obtained with the single AAV vector (n of eyes injected with single AAV = 12; n of eyes injected with triple AAVs = 14), while this decreased to 2% ± 1% when IRBP promoter was used (n of eyes injected with single AAV = 6; n of eyes injected with triple AAVs = 8), thus suggesting that multiple AAV transduction, rather than the promoter strength, impacts on mouse PR transduction, as also previously observed with dual AAV vectors.[45]

We then evaluated the efficacy of the triple *ED*-AAV vectors at transducing PRs in the pig retina. The pig retina is an excellent model to evaluate viral vector transduction characteristics because of its size, which is similar to the human retina, and because it is enriched with cones that are concentrated in a streak-like region similar to what happens in the primate macula.[10] We injected subretinally Large

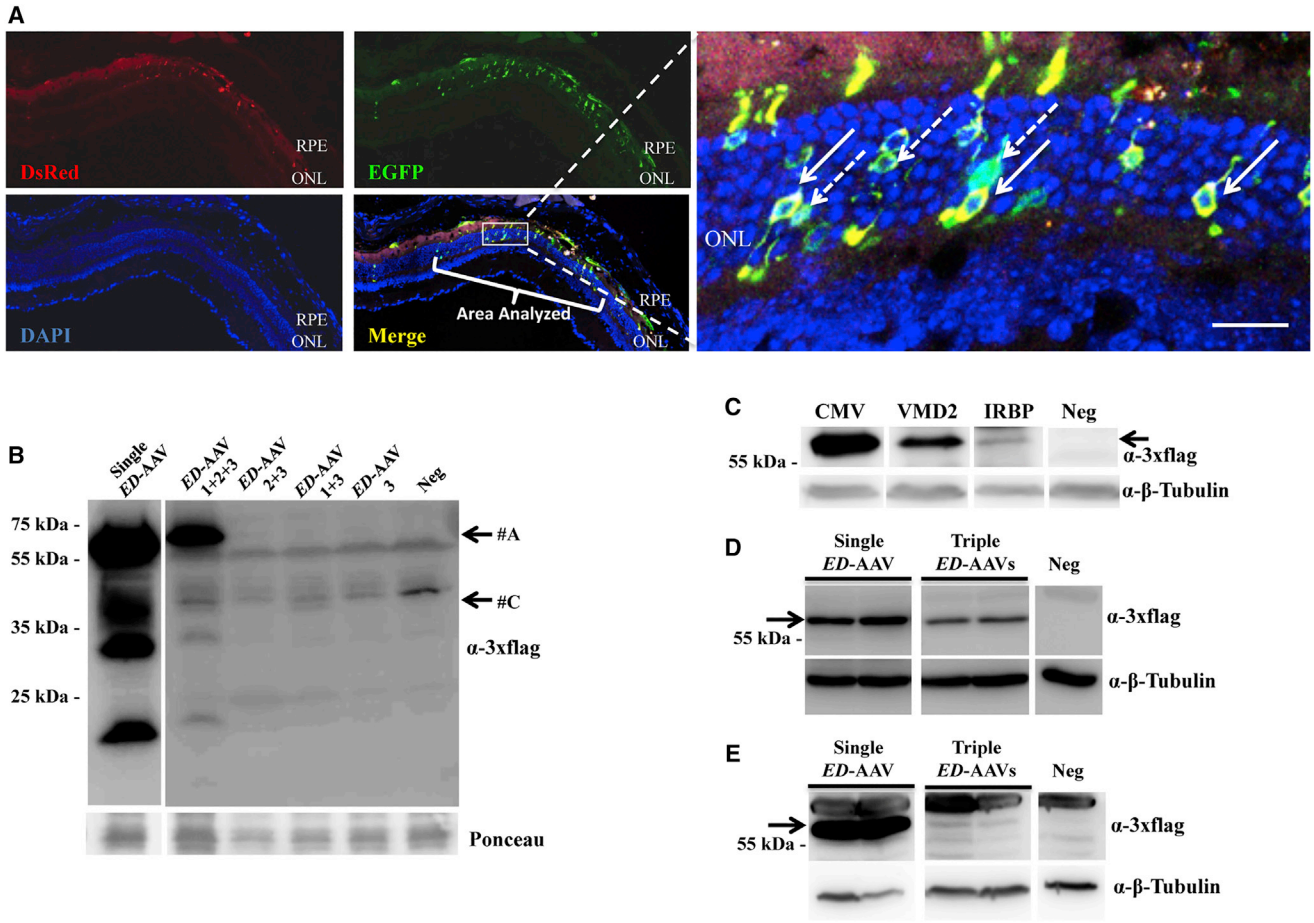

Figure 5. Triple AAV Vectors Drive Full-Length Protein Expression in the Mouse Retina

(A) Fluorescence analysis of retinal cryosections from C57BL/6J mice 2 months following subretinal injection of triple *ED*-AAV2/8 vectors under the control of the ubiquitous CMV promoter. The pictures with insets at higher magnification are representative of n = 5 injected eyes. Full arrows indicate EGFP and DsRed double-positive PRs. Dashed arrows indicate EGFP-only positive PRs. The scale bar (20 μm) is depicted in the figure. DsRed, Discosoma red fluorescent protein; Merge, overlay of EGFP, DsRed, and DAPI images; RPE, retinal pigmented epithelium; ONL, outer nuclear layer. (B) Western blot (WB) analysis of truncated products in eyecup lysates from C57BL/6J mice 2 months following subretinal injection of the combinations of *ED*-AAVs. The arrows indicate the following products: #A, ED full-length protein; #C, from AAV 1 + 3. (C) WB analysis of lysates from C57BL/6J eyecup 2 months following subretinal injection of triple AAV2/8 vectors encoding for ED under the control of the ubiquitous CMV, the RPE-specific VMD2, and the PR-specific IRBP promoters. The arrow indicates the full-length protein. (D) WB analysis of eyecup lysates from C57BL/6J mice 2 months following subretinal injection of single and triple AAV2/8 vectors encoding for ED under the control of the ubiquitous promoter CMV. (E) WB analysis of eyecup lysates from C57BL/6J mice 2 months following subretinal injection of single and triple AAV2/8 vectors encoding for ED under the control of the PR-specific promoter IRBP. CMV, cytomegalovirus; VMD2, vitelliform macular dystrophy 2; IRBP, human interphotoreceptors retinoid binding proteins. α-3xflag, WB with anti-3xflag antibodies; Ponceau, staining with Ponceau, used as loading control; α-β-Tubulin, WB with anti-β-Tubulin antibodies, used as loading control. Neg, lysates of eyecups following injection with PBS. The molecular weight ladder is depicted on the left; 100 (D), 150 (B and C), and 200 (E) μg of proteins were loaded.

White pigs with single and triple AAV2/8 vectors encoding ED protein under the transcriptional control of the PR-specific promoter IRBP (dose of each vector/eye, 1×10^{11} GC), and found two out of three positive eyes in both groups. WB band intensity quantification showed that ED protein expression with triple AAV vectors was 39% ± 17% (n = 2) of that observed with a single AAV vector (Figure 6A). Moreover, no truncated products were detected by WB analysis with anti 3xflag antibodies of neural retina lysates following subretinal injection of *ED*-AAV 1 + 2 + 3 (Figure 6B). A shorter product was observed in the *ED*-AAV 1 + 3 sample (#E), which is similar to the one observed in infected cells (#E) (Figure 2A). Overall, these data suggest that triple AAV vectors transduce pig PRs more efficiently than mouse, as previously observed with dual AAV vectors.[26]

Expression of Therapeutic Transgenes Mediated by Triple AAV Vectors in the Mouse Retina

We then tested whether subretinal administration of triple AAV2/8 vectors results in expression of *CDH23* and *ALMS1*, which are both mutated in syndromic forms of retinitis pigmentosa.[32–37]

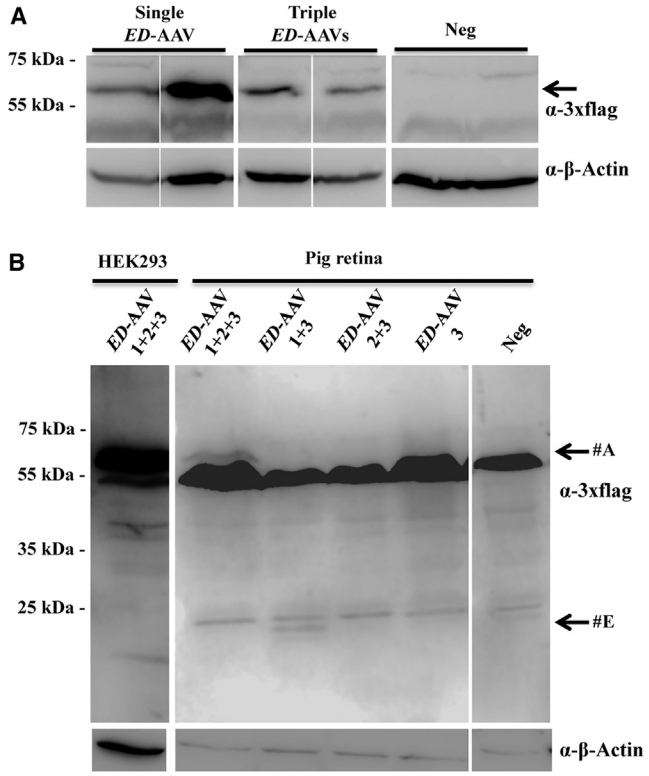

Figure 6. Triple AAV Vectors Drive Full-Length Protein Expression in the Pig Retina

(A) Western blot (WB) analysis of lysates from Large White pig retina 2 months following subretinal injection of either single or triple AAV2/8 vectors encoding for ED under the control of the PR-specific promoter IRBP. The arrow indicates the full-length protein. (B) WB analysis of truncated products in lysates from Large White pig retina 2 months following subretinal injection of the combinations of triple *ED*-AAVs. Lysates of HEK293 cells infected with an *ED*-AAV 1 + 2 + 3 are shown on the left as positive control. The arrows indicate the following products: #A, ED full-length protein; #E, probably from AAV 3. α-3xflag, WB with anti-3xflag antibodies; α-β-Actin, WB with anti-β-Actin antibodies, used as loading control. Neg, lysates of retinas following injection with PBS. The molecular weight ladder is depicted on the left; 200 μg of proteins were loaded.

We injected subretinally 4-week-old C57BL/6J mice with either triple CMV-*CDH*-AAV (dose of each vector/eye, 2×10^9 GC) or triple shCMV-*ALMS*-AAV vectors (dose of each vector/eye, 2×10^9 GC). Animals were sacrificed 2 to 3 months post-injection, and transgene expression was evaluated by both real-time qPCR and WB. Under the assumption that the PCR product amplified with the D + E primer couple derives mostly from full-length transcripts, we compared the levels of triple AAV-mediated transgene expression to endogenous. We found that transgenic *CDH23* and *ALMS1* were 102% ± 55% and 7% ± 2% of endogenous, respectively (n = 3 eyes/each group). The apparently different levels of CDH23 and ALMS1 transgene expression result from different levels of their corresponding endogenous transcripts: indeed, endogenous CDH23 is less expressed (0.005% ± 0.002% of glyceraldehyde 3-phosphate dehydrogenase [GAPDH]) than endogenous ALMS1 (0.22% ± 0.02% of GAPDH).

Then, the RNA population emerging following triple AAVs subretinal administration was analyzed by real-time qPCR using primer sets which were previously shown to amplify *in vitro* transcripts with a relative abundance >0.1 of full-length (Figure 3B, "*in vitro*" column). Among them, the following primer resulted in amplification of transcripts with a relative abundance higher than full-length: A + B, A + D, B + C, B + E, C + D, and, only for ALMS1, B + D and E + F (shown in bold in Figure 3B, "mouse retina" column).

To understand which of these transcripts were translated to detectable levels, WB analysis of injected retinas was performed using anti-3xflag antibodies: a faint but consistent band corresponding to full-length protein was detected in 11 out of 15 eyes and in 5 out of 8 eyes injected with either *CDH*- (Figure 7A) or *ALMS*-AAVs, respectively (Figure 7B). A shorter product was observed in the CDH23 sample (#C), which is similar to the most intense band present in the *CDH*-AAV 1 + 3 sample *in vitro* (Figure 4A). No truncated products were observed by WB in retinas injected with triple *ALMS*-AAVs. Immunohistochemistry (IHC) analysis of retinal cryosections following subretinal injections with triple *CDH*-AAVs confirmed expression in PRs (data not shown). A similar analysis was performed with the set of triple *ALMS*-AAV vectors used to rescue the retina of ALMS mice (see next paragraph and Figure 8A).

Subretinal Administration of Triple AAV Vectors in ALMS Mice

Retinal thickness and electrophysiological responses of *Alms1*$^{-/-}$ were both reduced compared to littermate control (*Alms1*$^{-/+}$ or wild-type) mice starting around 4–6 months (data not shown), similar to what observed in other *Alms1*$^{-/-}$ models.[46,47]

To test whether the levels of PR transduction obtained with triple AAV vectors are therapeutically relevant, we have generated triple *ALMS*-AAV vectors that include the GRK1 promoter, which restricts transgene expression to PRs, where ALMS1 is known to localize.[48,49] Subretinal injection of these vectors (dose of each vector/eye, 2×10^9 GC) in 4-week-old C57BL/6J mice results in ALMS1 proper PR localization 2 months after injection (Figure 8A). We can infer that transgenic ALMS1 staining derives from full-length protein, as ALMS1 potential localization signal is predicted to be at the N terminus of the protein[50] while the 3xflag tag at the C terminus, and transcripts from *ALMS*-AAV 1 + 3 would be out of frame. Triple GRK1-*ALMS*-AAV vectors were then injected subretinally in 4-week-old *Alms1*$^{-/-}$ mice,[51] which received PBS in the contralateral eye. Four months post-injection, we evaluated by real-time qPCR the expression of transgenic *ALMS1* transcript and found that this was 8.1% ± 6.6% of endogenous. Based on this, we then moved to evaluate their impact on *Alms1*$^{-/-}$ retinal morphology and function: in the *Alms1*$^{-/-}$ eyes injected with triple vectors we observed a modest, not significant improvement in the outer nuclear layer (ONL) thickness (Figure 8B), and in the electroretinogram a- (Figure 8C) and b-wave (Figure 8D) amplitudes between 5 and 7 months of age (i.e., 4–6 months after gene delivery), which was lost at 9–11 months of age (Figures 8B–8D).

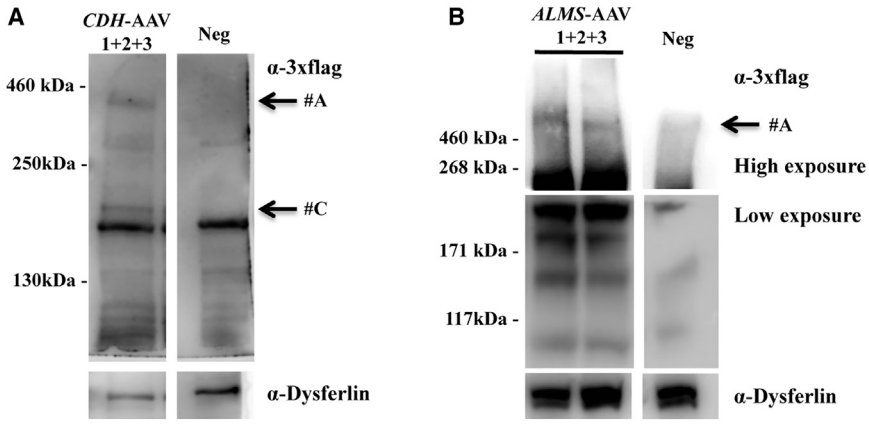

Figure 7. Subretinal Administration of Triple AAV Vectors Results in Full-Length CDH23 and ALMS1 Protein Expression in the Mouse Retina

(A) Western blot (WB) analysis of eyecup lysates from C57BL/6J mice 3 months following subretinal injection of triple AAV2/8 encoding for CDH23 under the control of the ubiquitous CMV promoter. The arrows on the right indicate the following products: #A, full-length proteins; #C, probably from AAV 1 + 3. (B) WB analysis of eyecup lysates from C57BL/6J mice 3 months following subretinal injection of triple AAV2/8 encoding for ALMS1 under the control of the ubiquitous short CMV promoter. The arrow on the right indicates full-length ALMS1. α-3xflag, WB with anti-3xflag antibodies; α-Dysferlin, WB with anti-Dysferlin antibodies, used as loading control. Neg, lysates of eyecups following injection with PBS. The molecular weight ladder is depicted on the left; 200 μg of proteins (A) or the whole-eyecup lysates (B) were loaded.

DISCUSSION

While AAV-mediated gene therapy is effective in animal models and in patients with inherited blinding conditions,[3–7,52] its application to diseases affecting the retina and requiring transfer of sequences larger than 5 kb is limited by the small cargo capacity of AAV. To overcome this, dual AAV vectors, which exploit AAV genome tendency to concatemerize upon infection,[25,53,54] have been developed in order to expand AAV DNA transfer capacity to around 9 kb. Here, we demonstrate both *in vitro* and in the mouse and pig retina that similar strategies can be further implemented by including a third vector in the system, thus expanding AAV transfer capacity to approximately 14 kb.

Using the ubiquitous CMV as well as the PR- and RPE-specific IRBP and VMD2 promoters, we showed that full-length gene reconstitution and expression is more efficient in mouse RPE than in PRs. This difference is probably due to a combination of the well-known preferential ability of AAV to transduce RPE than PRs,[9] as well as of poor triple AAV genome recombination in PRs. Weak promoter activity appears as a less likely explanation, as we observed robust ED expression from the IRBP promoter using a single AAV vector (Figure 5E). This low efficiency in PR transduction with triple AAVs is similar to what we have previously observed with dual AAV vectors,[26] and is consistent with the low levels of homologous recombination reported in post-mitotic neurons.[45] It is important to note that the spontaneous fluorescence of the fusion protein ED is weaker than the fluorescence of the single native reporters (Figure S1). Thus, the actual number of PRs transduced by triple AAV vectors may be higher than 3.6% observed in Figure 5A.

The percentage of mouse PR transduction is similar to the percentage of HEK293 cells transduced by triple AAV vectors (2.78% of total cells or 5.96% of transduced cells) despite the 25–50 times lower MOI predicted in the retina than used in *in vitro* infections. Indeed, Ortín-Martínez et al.[55] estimated that the total number of PRs in a mouse retina is 6.4×10^6. Considering that we transduce, on average, one-third of the retina (which corresponds to about 2×10^6 PRs) we can infer that the MOI in the retina is between 1,000 and 2,000, as opposed to 5×10^4 GC/cell used *in vitro*. The imaging data only apparently differ from what we observe in the WB, where the levels of transgene expression appear weaker *in vivo* than *in vitro* (CDH23, Figure 4A versus Figure 7A; ALMS1, Figure 4C versus Figure 7B). Indeed, the *in vivo* WB analyses are performed on material extracted from whole eyes as opposed to the imaging analysis, which is conducted on the transduced area: thus, in WB, the transgenic protein from the transduced area is diluted within untransduced tissue.

Interestingly, while in mouse retina, ED expression observed with triple IRBP-*ED*-AAV vectors represented only 2% of that obtained with single IRBP-*ED*-AAV, in pig retina this increased to 39%. This is consistent with our previous results that the relative PR-EGFP expression obtained upon subretinal delivery of dual AAV vectors is 6% in mice[26] and 40% in pigs of that obtained with single AAV, which was explained by the higher PR co-transduction rate of two independent AAVs observed in pigs (74%) than in mice (24%).[56] This could be due to thicker physical barriers in the pig than in the mouse retina that might limit vector diffusion, thus concentrating the vector in a smaller area and maximizing co-infection of the same cells by multiple vectors. Also, species-specific differences in the efficiency of both AAV2/8 transduction and/or vector intermolecular recombination cannot be excluded. This result is particularly important, considering that the pig retina is an excellent pre-clinical model with a size and architecture more similar to the human than the mouse retina.[10,57–61]

An important concern for clinical use of multiple AAVs is the possible generation of truncated proteins, which might affect both safety and functionality of the treatment. We addressed this important issue by characterizing both transcripts and translated products from triple AAV vectors *in vitro* and in the mouse retina. The *in vitro* real-time qPCR and RNA-seq analyses showed that most of the products expressed at high levels are predicted to be generated by similar AAV genome concatemers between triple *CDH*- and *ALMS*-AAVs (Figure 3). Interestingly, in addition to the products from concatemers containing either simultaneously the promoter

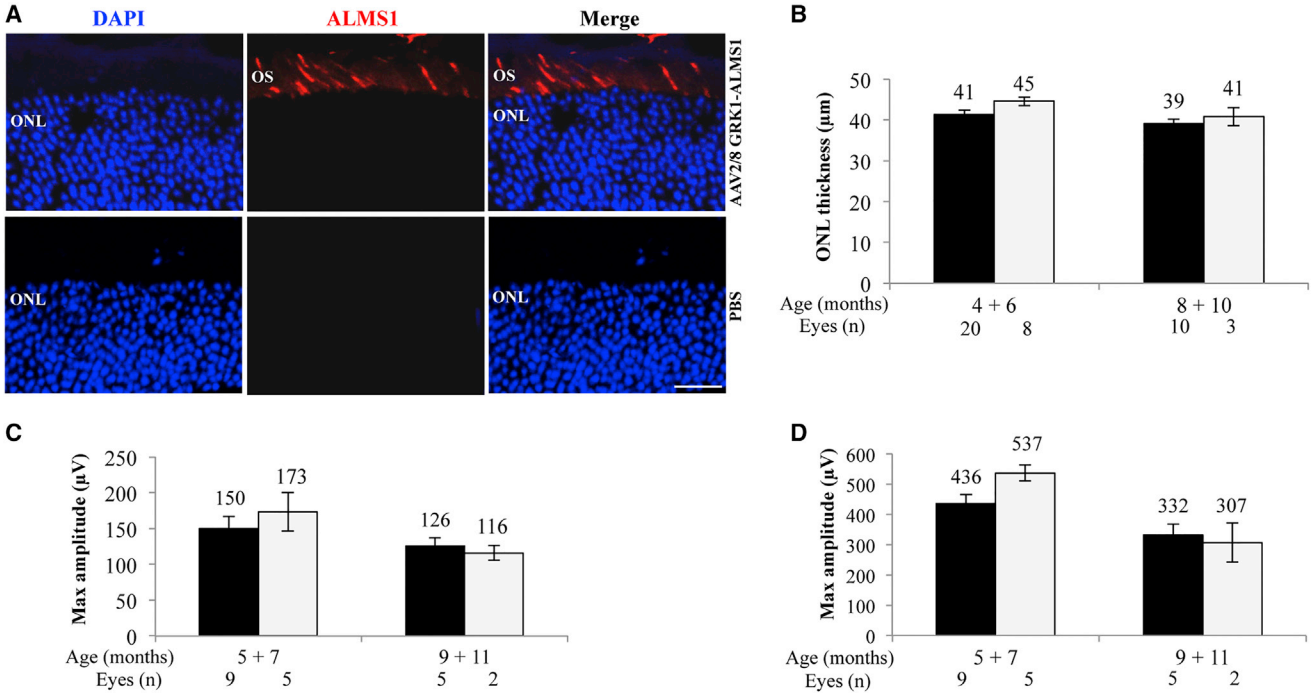

Figure 8. *Alms1*$^{-/-}$ Retinal Structure and Function following Subretinal Delivery of Triple AAV Vectors

(A) Immunohistochemical (IHC) analysis with anti-3xflag antibodies of retinal cryosections from C57BL/6J mice 2 months following subretinal injections of either triple AAV2/8 encoding for ALMS1 under the control of the PR-specific GRK1 promoter (top panels) or PBS (bottom panels). The pictures are representative of n = 4 injected eyes. The scale bar (20 µm) is depicted in the figure. Merge, overlay of DAPI and ALMS1. ONL, outer nuclear layer; OS, outer segment. (B) Spectral domain optical coherence tomograms (SD-OCT) analysis of *Alms1*$^{-/-}$ mice injected subretinally with either triple GRK1-*ALMS*-AAV vectors (white bars) in one eye or PBS in the contralateral eye (black bars). Results are reported as means ± SE. (C and D) Electroretinographic analysis of a-wave (C) and b-wave (D) light responses of *Alms1*$^{-/-}$ mice injected subretinally with either triple GRK1-*ALMS*-AAV vectors (white bars) or PBS in the contralateral eye (black bars). Results are reported as means ± SE. Light intensity of 20 cd s/m^2 (a-wave); background white light of 50 cd s/m^2 and light intensity of 20 cd s/m^2 (b-wave).

and the polyadenilation signal (i.e., AAV 1 + 3 and AAV 1 + 2 + 3) or the promoter alone (AAV 1 with or without AAV 2), we found high levels of expression from AAV 2 in the case of *ALMS1*. It is possible that, in this case, the ITR-mediated promotorial activity[62] combined with stability of the transcript results in high levels of aberrant transcript. However, the absence of a Kozak consensus sequence with a close-by ATG suggests that this transcript should not be efficiently translated.

Importantly, the translation of the various aberrant transcripts detected appears to be inefficient, as only few truncated products, mostly predicted from AAV 1 + 3 concatemerization, were observed in the WB analysis of cells infected with triple AAVs. One exception appears to be a protein product that is predicted to derive from *CDH*-AAV 3 that was detected, despite its low level of transcription, suggesting a high stability of this product. Interestingly, the various alternative CDH23 isoforms shown by RNA-seq (Figure S2A) may be responsible for the great number of protein products present in *CDH*-AAV 1 + 3 sample. One important phenomenon that we have observed is that most of the truncated products present when only 1 or 2 vectors were used for the infection decreased when the third vector was added (Figures 2A–2C and 4A). This suggests that when evaluating the potential toxicity of triple AAV vectors, this should be done in the context of all vector components and not be extrapolated from combinations of single AAV.

The levels of aberrant proteins observed *in vivo* was even lower than that observed *in vitro* (Figures 5B and 7). This is interesting, as some of the transcripts detected by real-time qPCR in the mouse retinas transduced with triple AAVs were more abundant than in cells (primer sets A + B, A + D, B + C, B + D, C + D, and E + F) and suggests a more stringent protein quality control in live animals than in HEK293 cells. The only exception seems the detection of EGFP-only positive cells in retinal sections of animals injected with *ED*-AAV 1 + 2 + 3 (Figure 5A). This could be the result of products from *ED*-AAV 1 + 2 that are particularly stable and might accumulate over the 2-month time of the *in vivo* but not of the shorter *in vitro* experiments (Figure 2C). The low sensitivity of the WB with anti-EGFP antibodies may explain why the product from *ED*-AAV 1 + 2 is only detected by direct fluorescence analysis of retinal cryosections. In addition, the presence of protein products deriving from alternative open reading frames (ORFs), which would not be detected with the set of antibodies used in this study, cannot be excluded at this point.

In agreement with the low levels of unexpected protein products in the mouse retinas, no evident signs of toxicity were observed by optical coherence tomography analysis (data not shown) in animals injected 2 months before with either *CDH*- or *ALMS*-AAV 1 + 3, the combination of viruses that produced the highest levels of truncated products *in vitro*. Nevertheless, before considering the system for a therapeutic use in humans, more efforts should be focused to evaluate potential toxicity of truncated products, as well as strategies to eliminate them, such as the inclusion of degradation signals strategically placed in the vectors, which we have recently demonstrated to be effective at abolishing selectively truncated proteins from dual AAV vectors.[63]

The possibility to further expand the dual AAV vectors to triple in order to express larger genes has been recently evaluated in mouse muscle[39,40] for dystrophin transduction, but with poor efficiency. Although a direct comparison between the triple AAV vectors used in that study and our triple AAV vectors is difficult, the levels of full-length transgene expression we achieve in the retina with triple AAV vectors appear to be higher, as we are able to detect full-length protein reconstitution by WB, in addition to fluorescence analysis on histological sections that were used for dystrophin detection in Lostal et al.[39] and Koo et al.[40]

The expression levels achieved in mice with triple *ED*-AAV compared to single *ED*-AAV vectors are similar to those that we previously observed with dual AAV vectors, both in the mouse and in the pig retina,[26] suggesting that, in the subretinal space, co-infection by multiple AAV vectors is favored.

If we consider that 3.6% of PRs are transduced by triple AAV vectors following subretinal administration in mice (Figure 5A) and we calculate the transgene expression levels per cell, we find that the 102% of endogenous CDH23 achieved with triple *CDH*-AAVs corresponds to around 3,000% per cell. This is, however, due to the low levels of endogenous CDH23 expression in mice (where it reaches only 0.005% of GAPDH levels) but not in humans[64] (http://retina.tigem.it). If we, instead, consider ALMS1, whose endogenous levels are higher than CDH23 and reach 0.22% of GAPDH, the levels of recombinant *ALMS1*, which are 7%–8% of endogenous, correspond to approximately 200% per cell. In essence, the levels of *CDH23* and *ALMS1* transgene expression from triple AAV vectors relative to GAPDH are similar, while endogenous ALMS1 is expressed at higher levels than CDH23 in mice.

Mice with ALMS1[46] but not CDH23[65] deficiency present with PR degeneration. To understand whether the transduction levels from triple AAV vectors may be therapeutically relevant, we have treated *Alms1*$^{-/-}$ mice with subretinal injections of triple GRK1-*ALMS*-AAV vectors, but, besides a transient improvement, we did not observe any significant amelioration of the phenotype. After confirming that transgenic *ALMS1* is properly expressed in PRs at levels around 8% of endogenous, there could be several reasons that justify this lack of therapeutic efficacy: (1) as we have transferred the human *ALMS1* transgene in *Alms1*$^{-/-}$ mice, we cannot exclude that interspecies differences might be responsible for low therapeutic efficacy; (2) the non-cell-autonomous PR degeneration described in retinitis pigmentosa[66] may as well account for the lack of therapeutic effect; and (3) as observed with triple *ED*-AAVs, only 3.6% of PRs are transduced (Figure 5A), and such fraction might not be sufficient to detect a significant rescue. It is possible that higher levels of transduction may improve the efficacy of triple AAV vector. This could be obtained (1) with higher vectors doses, (2) with more efficient AAV serotypes than those used here (i.e., AAV Y444, 500, 730F with mutated tyrosine residues),[67,68] (3) by enlarging the transduced area with a different injection technique (i.e., double injection) or by intravitreal injection of highly penetrating serotypes such as AAV7m8,[69] (4) by using a more potent expression cassette than the one used in this work, or (5) by co-injection of AAV transduction enhancers (i.e., proteasome inhibitors).[70–72] Although these levels of rescue appear insufficient in *Alms1*$^{-/-}$ mice, it is important to note that, similar to what is observed with dual AAV vectors, the level of pig PR ED transduction by triple versus single AAV2/8 vectors is higher than in mice, which is promising in view of future therapeutic applications, given the closer similarity between human and pig than mouse retina.

Overall, our data demonstrate that triple AAV vectors drive large gene reconstitution both *in vitro* and *in vivo* and that this approach leads to the reconstitution of expression of large genes mutated in IRDs like USHID or ALMS, thus extending AAV transfer capacity up to 14 kb in the retina. This bodes well for the development of triple AAV vectors for other retinal and non-retinal conditions, which require transfer of such large sequences.

MATERIALS AND METHODS

Generation of AAV Vector Plasmids

The plasmids used for AAV vector production derived from the pAAV2.1[73] plasmids that contain the ITRs of AAV serotype 2.

The *EGFP-DsRed*-AAV (*ED*-AAV) vectors were generated by cloning Discosoma red fluorescent protein (DsRed) CDS (675 bp), from the p*DsRed*-Express2 plasmid (#632535; Clontech, Saint-Germain-en-Laye, France) after the EGFP CDS (717 bp) of pAAV2.1-CMV-*EGFP* plasmid[73] separated by a 39-bp spacer and followed by a 3xflag sequence and the bovine growth hormone polyadenylation signal (bGHpA).

To generate triple *ED*-AAV vector plasmids, the *ED* CDS was split into three constructs: the first one (*ED*-AAV 1) containing the promoter and the N-terminal *EGFP* CDS[74] (bp 1–393), the second one (*ED*-AAV 2) containing the C-terminal *EGFP* CDS[74] (bp 394–717) plus the N-terminal *DsRed* CDS (FJ226077, bp 1–307), and the last one (*ED*-AAV 3) containing the C-terminal *DsRed* CDS (FJ226077, bp 308–675) plus the *3xflag*.

As recombinogenic regions at the 3′ end of *ED*-AAV 1 and 5′ end of *ED*-AAV 2, we used the AK sequence, derived from the phage F1 genome (J02448.1, bp 5,850–5,926), which we previously

demonstrated to be effective in the context of dual AAV vectors.[26] As a second recombinogenic region (at the 3′ end of *ED*-AAV 2 and 5′ end of *ED*-AAV 3), we used a 200-bp sequence (NM_000350.2, bp 3,103–3,302) derived from the human ATP-binding cassette, sub-family A 4 gene (*ABCA4*), which we found to be recombinogenic in dual overlapping AAV vectors (AB200; data not shown).

To generate plasmids for triple *CDH*- and *ALMS*-AAV vectors, the three fragments for each *CHD23* (AF312024.1) and *ALMS1* isoform 1 (NM_015120.4) were obtained by gene synthesis (MWG, now Eurofins Genomics, Ebersberg, Germany). *CDH*- and *ALMS*-AAV 1 contain the N-terminal CDS (*CDH23*, AF312024.1, bp 1–3,369; *ALMS1*, NM_015120.4, bp 112–4,188); *CDH*- and *ALMS*-AAV 2 contain the body of the CDS (*CDH23*, AF312024.1, bp 3,370–6,712; *ALMS1*, NM_015120.4, bp 4,189–8,452); and *CDH*- and *ALMS*-AAV 3 contain the C-terminal CDS (*CDH23*, AF312024.1, bp 6,713–10,065; *ALMS1*, NM_015120.4, bp 8,453–12,618) followed by a 3xflag tag and the bGHpA.

Note that the *CDH23* CDS was split at a natural exon-exon junction, while this was not possible for *ALMS1*, due to the exon length. Moreover, in both systems, fragment 1 and fragment 3 were designed in order to generate out-of-frame transcripts in case of undesired concatemerization.

The AK recombinogenic sequence was placed at the 3′ of both *CDH*- and *ALMS*-AAV 1 and at the 5′ of *CDH*- and *ALMS*-AAV 2. In the *CDH23* expression system, we placed the AP sequence (NM_001632.4, bp 1,802–1,516) derived from the human placental alkaline phosphatase gene[75] at the 3′ of *CDH*-AAV 2 and at the 5′ of *CDH*-AAV 3, which results in levels of *CDH23* expression higher than with AB200 (data not shown). Due to size constraint, no recombination signals were placed at the 3′ of *ALMS*-AAV 2 nor at the 5′ of the *ALMS*-AAV 3; full-length gene reconstitution, in this case, relies exclusively on ITR-mediated joining followed by splicing.

The splice donor (SD) and splice acceptor (SA) signals contained in triple AAV vector plasmids are as follows: 5′-GTAAGTATCAAGGTTACAAGACAGGTTTAAGGAGACCAATAGAAACTGGGCTTGTCGAGACAGAGAAGACTCTTGCGTTTCT-3′ (SD); 5′-GATAGGCACCTATTGGTCTTACTGACATCCACTTTGCCTTTCTCTCCACAG-3′ (SA).

The ubiquitous CMV promoter is the one contained in pAAV2.1-CMV-*EGFP*;[73] the ubiquitous shCMV promoter is the one described in Pellissier et al.[76]; the PR-specific human IRBP (X53044.1, bp 2,603–2,837) and the human GRK1 promoter (AY327580.1, bp 1,793–2,087) have been both described to drive high levels of combined rod and cone PR transduction in various species;[14,41,42] the RPE-specific VMD2 promoter (NG_009033.1, bp 4,870–5,516) corresponds to the previously described EcoRI-XcmI promoter fragment[43] and was amplified from human genomic DNA. The details of the cloning strategies as well as plasmid sequences are available upon request.

AAV Vector Production and Characterization

AAV vectors were produced by the TIGEM AAV Vector Core by triple transfection of HEK293 cells followed by two rounds of $CsCl_2$ purification.[77] For each viral preparation, physical titers (GC/mL) were determined by averaging the titer achieved by dot-blot analysis[78] and by PCR quantification using TaqMan (Applied Biosystems, Carlsbad, CA, USA).[77] The probes used for dot-blot and PCR analyses were designed to anneal with the promoter for the 5′ vector, the bGHpA region for the 3′ vectors, and within the gene for the body vectors. The length of probes varied between 200 and 700 bp.

Transfection and AAV Infection of HEK293 Cells

HEK293 cells were maintained in DMEM containing 10% fetal bovine serum (FBS) and 2 mM L-glutamine (Gibco, Thermo Fisher Scientific, Waltham, MA, USA). Depending on the experiment, cells were plated in 6-well plates (1×10^6 cells/well), 24-well plate (2.5×10^5 cells/well), or 8-chamber (1×10^5 cells/well) and transfected 16 hr later with the plasmids encoding for the desired transgene using the calcium phosphate method (1 to 2 μg/1×10^6 cells); medium was replaced 4 hr later.

For AAV infection, plated cells were first transfected with 1.5 μg/1×10^6 cells of pDeltaF6 helper plasmid, which contains the Ad helper genes.[79] After 4 hr, cells were washed once with serum-free DMEM and incubated with AAV2/2 vectors (MOI 5×10^4 GC/cell of each vector) in a final volume of 700 μL of serum-free DMEM. Two hours later, 1.3 mL of complete DMEM was added to the cells.

To increase transgene expression, 7.5 μM Calpain inhibitor I ([PI] A6185; Sigma-Aldrich, St. Louis, MO, USA), which is known to increase AAV-mediated transduction,[80] was added either once after infection with triple *ED*- and *CDH*-AAVs or daily after infection with triple *ALMS*-AAVs.

Animal Models

Mice were housed at the Institute of Genetics and Biophysics animal house (Naples, Italy) and maintained under a 12-hr light/dark cycle. C57BL/6J mice were purchased from Harlan Italy SRL (Udine, Italy).

ALMS (referred as *Alms1*$^{-/-}$) mice were imported from The Jackson Laboratory. The mice were maintained by crossing heterozygous females with heterozygous males. The *Alms1*$^{-/-}$ mouse harbors the chemically-induced *Alms1* c.1080 + 2T > C splice mutation (exon 6-intron 6 splice junction) predicted to result in a frameshift and truncation of ALMS1.[51] The genotype of mice was confirmed by PCR analysis on genomic DNA (extracted from the mouse tail tip) followed by DNA sequencing. The primers used for the PCR amplification are as follows:

Fw: 5′-GGTGCACAGAGTGAAAGAATTGC-3′

Rev: 5′-ACTTACCAGTTAAGCCTTGTAGG-3′,

which generate a product of 147 bp that was subsequently sequenced using the Fw primer.

The Large White female pigs (Azienda Agricola Pasotti, Imola, Italy) used in this study were registered as purebred in the LWHerd Book of the Italian National Pig Breeders' Association and were housed at the Centro di Biotecnologie A.O.R.N. Antonio Cardarelli (Naples, Italy) and maintained under a 12-hr light/dark cycle.

Subretinal Injection of AAV Vectors in Mice and Pigs

This study was carried out in accordance with the Association for Research in Vision and Ophthalmology Statement for the Use of Animals in Ophthalmic and Vision Research and with the Italian Ministry of Health regulation for animal procedures (Ministry of Health authorization number 147/2015-PR). Surgery was performed under general anesthesia, and all efforts were made to minimize animal suffering. Mice (4 to 5 weeks old) were anesthetized with an intraperitoneal injection of 2 mL/100 g body weight of ketamine/xylazine, then AAV2/8 vectors were delivered subretinally via a trans-scleral trans-choroidal approach, as described by Liang et al.[81] Eyes were injected with 1 μL of vector solution. The AAV2/8 doses (GC/eye) varied across different mouse experiments, as described in the Results section. PI, at a final concentration of 30 μM, was added to the vector mix in mouse eyes intended for histology, real-time qPCR, and in 3 out of 15 eyes injected with triple *CDH*-AAV vectors and destined for WB analysis.

Subretinal delivery of AAV2/8 vectors to the pig retina was performed as previously described.[10] Eyes (n = 3) were injected with 100 μL of AAV2/8 vector solution. The AAV2/8 dose was 1×10^{11} GC of each vector/eye; thus, co-injection of triple AAV vectors resulted in a total of 3×10^{11} GC/eye.

WB Analysis

Samples (HEK293 cells plated in 6-well plates or eyecups [cups + retinas]) for WB analysis were lysed in radio-immunoprecipitation assay (RIPA) buffer (50 mM Tris-HCl [pH 8.0], 150 mM NaCl, 1% NP40, 0.5% Na-deoxycholate, 1 mM EDTA, 0.1% SDS [pH 8.0]) to extract ED, CDH23, and ALMS1 proteins from HEK293 cells and eyecups. Lysis buffers were supplemented with protease inhibitors (Complete Protease inhibitor cocktail tablets; Roche, Basel, Switzerland) and 1 mM phenylmethylsulfonyl. After lysis, ED, CDH23, and ALMS1 samples were denatured at 99°C for 5 min in 1× Laemmli sample buffer. For ALMS1, 1× Laemmli sample buffer was supplemented with 4 M urea. Lysates were separated by 12% (ED samples), 6% (CDH23 samples), or gradient (#4561086; Bio-Rad, Hercules, CA, USA) 4%–15% (ALMS1 samples) SDS-PAGE.

The antibodies and dilutions used for immunoblotting are as follows: anti-EGFP (1:1,000, ab1218; Abcam, Cambridge, UK); anti-3xflag (1:1,000, A8592; Sigma-Aldrich, St. Louis, MO, USA); anti-CDH23 (1:500, sc-166005, Santa Cruz Biotechnology, Dallas, TX, USA); anti-ALMS1 (1:1,000, polyclonal; ab4306, Abcam, Cambridge, UK); anti-β Tubulin (1:3,000, T5201; Sigma Aldrich, St. Louis, MO, USA); anti-Filamin A (1:1,000, #4762; Cell Signaling Technology, Danvers, MA, USA); anti-Dysferlin (1:500, Dysferlin, clone Ham1/7B6, MONX10795; Tebu-bio, Le Perray-en-Yveline, France); anti-β-Actin (1:1,000, NB600-501; Novus Biological, Littleton, CO, USA).

Notably, the epitope to which the monoclonal anti-EGFP antibodies were raised has not been disclosed by the company; however, we deduced that it maps to the C terminus of EGFP based on the pattern observed in the WB analysis in Figure 2B.

The quantification of ED bands detected by WB was performed using ImageJ software (http://rsbweb.nih.gov/ij/); to compare data across different experiments, in each WB, the average intensity of the bands deriving from single AAV-transduced eye was set as 1, and the intensity of triple AAV transduced eye was divided by that of single AAV-transduced eye and calculated accordingly.

Histology and Light and Fluorescence Microscopy

To evaluate ED expression *in vitro*, HEK293 cells, plated in 8-chambers at a density of 1×10^5, were infected as previously described. Seventy-two hours post-infection, cells were washed once with PBS, fixed for 7 min with 4% paraformaldehyde (PFA) in PBS, washed three times with PBS, and mounted with Vectashield with DAPI (Vector Lab, Peterborough, UK). Cells were analyzed under the Axio Observer Z1 (Carl Zeiss, Oberkochen, Germany) equipped with ZEN software (Carl Zeiss) and using appropriate excitation and detection settings for EGFP, DsRed, and DAPI.

To evaluate transgene expression in histological sections, C57BL/6J mice were injected subretinally with triple AAV vectors (supplemented with PI at a final concentration of 30 μM). Two months later, mice were sacrificed and eyes were fixed in 4% paraformaldehyde overnight and infiltrated with 30% sucrose overnight; the cornea and the lens were then dissected, and the eyecups were embedded in optimal cutting temperature compound (O.C.T. matrix; Kaltek, Padua, Italy). Ten-micrometer-thick serial retinal cryosections were cut along the horizontal meridian, progressively distributed on slides, and mounted with Vectashield with DAPI (Vector Lab, Peterborough, UK). Then, the cryosections were analyzed under the confocal LSM-700 microscope (Carl Zeiss, Oberkochen, Germany) using appropriate excitation and detection settings.

For assessment of PR transduction in mouse retinal cryosections following triple *ED*-AAV administration, a single section/eye within the transduced area was selected; the whole slice was acquired at 40× magnification and then analyzed using ImageJ software (http://rsbweb.nih.gov/ij/). A minimum of 600 PRs, identified by DAPI staining, were counted for each eye. PRs with signal compatible with EGFP and DsRed co-expression were unequivocally identified based on their identical shape on picture micrographs of the same field.

In the case of fluorescent IHC staining of ALMS1, sections were washed in PBS for 10 min and were permeabilized and blocked with 0.3% Triton X-100, 5% next-generation sequencing (NGS), 3% BSA in PBS for 3 hr, then the sections were pre-treated with

Avidin/Biotin (SP-2001, Vector Lab, Peterborough, UK) according to manufacturer's instructions. Sections were incubated overnight with anti-3xflag antibodies (1:200 F1804 Sigma-Aldrich, St. Louis, MO, USA). Endogenous peroxidase were blocked with 0.3% hydrogen peroxide (H1009, Sigma-Aldrich, St. Louis, MO, USA). Signal was developed using the Vectastain ABC kit (PK-6200 Vector Laboratories, CA, USA) followed by the SuperBoost Tyramide signal amplification (B40942, Thermo Fisher Scientific, Waltham, MA, USA) according to the manufacturer's instructions. Stained sections were mounted with Vectashield with DAPI (Vector Laboratories, CA, USA). Cryosections were analyzed under the confocal LSM-700 microscope (Carl Zeiss, Oberkochen, Germany) and acquired at 63× magnification.

Cytofluorimetric Analysis

HEK293 cells, plated in 6- or 24-well plates, were washed once with PBS, detached with trypsin 0.05% EDTA (Thermo Fisher Scientific, Waltham, MA USA), washed twice with PBS, and resuspended in PBS 5% FBS, 2.5 mM EDTA. Cells were analyzed on a BD FACS ARIA III (BD Biosciences, San Jose, CA, USA) equipped with BD FACSDiva software (BD Biosciences) using appropriate excitation and detection settings for EGFP and DsRed. Thresholds for fluorescence detection were set on not infected cells, and a minimum of 10,000 cells/sample were analyzed.

RNA Extraction, cDNA Production, and Reverse Transcription Analysis

Total RNA was extracted using the RT-PCR RNeasy MiniKit (QIAGEN, Milan, Italy) from either HEK293 cells plated in 6- or 24-well plates and infected or not with triple AAV vectors or mouse eyecups or retina. RNA (500 ng from cells or eyecups and 360 ng from retina) was submitted to DNase I digestion (RNase Free DNase set; QIAGEN) and 20 μL cDNA was generated using the SuperScript III Reverse Transcriptase kit (Thermo Fisher Scientific, Waltham, MA, USA) using oligo dT primers. For each sample, the same amount of RNA did not receive the retrotranscriptase enzyme and was used as a control for genomic DNA contamination. Primers for real-time qPCR were designed using the bioinformatic program "Primer Blast" (https://www.ncbi.nlm.nih.gov/tools/primer-blast/) and purchased from Eurofins Genomics (Eurofins Genomics, Ebersberg, Germany; Table S1). Serial dilutions of the cDNAs obtained from cells infected with either triple *CDH*- or *ALMS*-AAV 1 + 2 + 3 were used to measure the primer efficiency, which was between 1.75 and 2.25 for all primer sets shown in Figure 3B. SybrGreen real-time qPCR kit was purchased from Roche (Roche, Monza, Italy) and used following the manufacturer's protocol on the LyghtCycler 96 system (Roche). Five microliters of diluted cDNA (1:25 to 1:50 for *in vitro* experiments and 1:5 for the *in vivo* experiments) and 10 pmol of primers were used for PCR in a total volume of 20 μL. Thermal cycling for all genes initiated with an initial denaturation step at 95°C for 5 min, followed by 45 cycles with denaturation at 95°C for 10 s, annealing at 60°C for 20 s, and extension at 72°C for 20 s. Expression data were then normalized versus the corresponding housekeeping genes (h-β-ACTIN for HEK293 cells and mouse GAPDH (mGAPDH) for eyecups and retinas).

RNA-Seq Libraries Preparation and Sequencing

A total of 47.5 ng of RNA was used as input for the synthesis of cDNA with the SMART-Seq v4 Ultra Low Input RNA Kit for Sequencing (Takara Bio USA, Mountain View, CA, USA). Manufacturer suggested protocol was followed, with minor modifications. The second strand synthesis of cDNA was performed by replacing the SMART-Seq v4 Oligo with custom primers specific for the transgenes of interest (CDH23 oligo, 5′-AAGCAGTGGTATCAACGCAGAGTacttgtt gatctccgaagataccc-3′; ALMS1 oligo, 5′-AAGCAGTGGTATCAACG CAGAGTtagtggtggaggaagtagaggag-3′ [bp in capital letters belong to the RNA-seq adaptor]).

Seventy-five pg of cDNA generated with SMART-Seq v4 Kit were used for library preparation using the NEXTERA XT DNA Library Preparation kit (Illumina, San Diego, CA, USA), following the suggested protocol.

Samples were sequenced using NextSeq 500/550 Mid Output v2 kit in a 150 + 150 paired-end run. The data were deposited in GEO: GSE107173.

RNA-Seq Analysis

Sequence reads were trimmed using Trim Galore! software (https://www.bioinformatics.babraham.ac.uk/projects/trim_galore/) to remove adaptor sequences and low-quality end bases and then analyzed using the "new tuxedo" software suite.[82] The idea was to generate a custom reference with a "genomic" sequence of the three vector inserts where to align the reads. The expected full-length transcript was used as known reference, but the aligner software was allowed to introduce new splicing junctions and generate also alternative transcripts if supported by reads (Figure S2).

First, the custom reference sequence was built to perform the viral vector library sequences alignment. For each transgene, the sequence of the three vector inserts were pasted sequentially side by side, separated by a stretch of N bases as spacers to simulate a "genomic" sequence and then added to the human genome (build hg19) as separate contigs. The ITR ends were not included to reduce the possibility of aberrant splicing junctions due to mis-aligned repeated reads. The relative coordinates of the actual CDSs of each transgene were used as reference of a single transcript composed of three exons. The first exon start and the last exon end bases were defined to coincide respectively with the beginning of the specific PCR primer and the expected transcription stop signal, in order to reproduce the expected drop in coverage of the aligned reads due to library construction, to minimize the generation of alternative predicted transcripts only differing from the reference by the start or end coordinates.

Then the analysis was performed following the protocol described in Pertea et al.[82] Reference-guided alignment was performed with

HISAT2[83] followed by transcript assembly with Stringtie.[84] The assembly generated for each sample can be slightly different due to the actual coverage of exons and reads spanning exon-exon junctions, so the individual assemblies of each sample were merged into a common consensus with the Stringtie merge function to make them comparable. The expression levels of each transcript of the assembled consensus were then estimated with a final run of Stringtie used to count reads supporting each transcript without allowing the annotation of any further isoform. The R/Biocondictor package Ballgown[85] was then used to visualize results and extract the raw counts and normalization was performed with DESeq.[86]

To estimate the relative abundance of each annotated alternative isoform, their normalized counts were divided by the corresponding full-length one and the ratios were averaged among three replicate samples.

Spectral Domain Optical Coherence Tomography

Spectral domain optical coherence tomography (SD-OCT) images were obtained using the Bioptigen Spectral Domain Ophthalmic Imaging System (SDOIS; Envisu R2200, Bioptigen, Morrisville, NC, USA). *ALMS* mice were anesthetized and pupils were dilated by applying 1–2 drops of topical 0.5% tropicamide (Visufarma, Rome, Italy). To prevent corneal desiccation during the procedure, topical lubricant eye drops (Recugel; Bausch & Lomb, Rochester, NY, USA) were applied bilaterally with a small brush. Mice were positioned into the animal imaging mount and rodent alignment stage (AIM-RAS; Bioptigen, Morrisville, NC, USA); the laser source was placed in front of the mouse, and images were acquired by the InVivoVue Clinic software (Bioptigen, Morrisville, NC, USA). Three images, one central, one superior, and one inferior to the optic nerve, were taken from each eye. ONL thickness was manually measured three times from each OCT scan image and averaged.

Electrophysiological Recordings

For electroretinographic analyses, *ALMS* mice were dark-adapted for 3 hr. Mice were anesthetized and positioned in a stereotaxic apparatus, under dim red light. Their pupils were dilated with a drop of 0.5% tropicamide (Visufarma, Rome, Italy), and body temperature was maintained at 37.5°C. Light flashes were generated by a Ganzfeld stimulator (CSO, Costruzione Strumenti Oftalmici, Florence, Italy). The electrophysiological signals were recorded through gold-plate electrodes inserted under the lower eyelids in contact with the cornea. The electrodes in each eye were referred to a needle electrode inserted subcutaneously at the level of the corresponding frontal region. The different electrodes were connected to a two-channel amplifier. After completion of responses obtained in dark-adapted conditions (scotopic), the recording session continued with the purpose of dissecting the cone pathway mediating the light response (photopic). To minimize the noise, different responses evoked by light were averaged for each luminance step. The maximal scotopic response of rods and cones was measured in dark conditions (scotopic) with two flashes of 0.7 Hz and a light intensity of 20 cd s/m^2, photopic cone responses were isolated in light conditions with a continuous background white light of 50 cd s/m^2, with 10 flashes of 0.7 Hz and a light intensity of 20 cd s/m^2.

SUPPLEMENTAL INFORMATION

Supplemental Information includes four figures and one table and can be found with this article online at https://doi.org/10.1016/j.ymthe.2017.11.019.

AUTHOR CONTRIBUTIONS

The study was conceived, designed, and written by A.A., A. Maddalena, and P. Tornabene. All data were generated by A. Maddalena, P. Tornabene, and R.M. except the *Alms1* mouse phenotyping, which was performed by P. Tiberi, and the RNAseq experiments, which were performed by D.C., A. Manfredi, and M.M. S.R. and F.S. performed subretinal injections in pigs. J.K.N. provided the *Alms1*$^{-/-}$ mice.

CONFLICTS OF INTEREST

The authors declare no conflict of interest.

ACKNOWLEDGMENTS

We thank the following people from TIGEM, Naples, Italy: Annamaria Carissimo (Bioinformatics Core) for the statistical analyses; Linda Colecchi for helping with mouse electrophysiological analysis; Fabio Dell' Aquila for technical help; Carolina Iodice for subretinal injections in mice; Manel Llado for cytofluorimetric analysis; the AAV Vector Core for AAV vector production; the Microscopy Core for assistance in microscope imaging; Graciana Diez-Roux and Raffaele Castello (Scientific Office) for the critical reading of this manuscript. We thank Gayle B. Collin (The Jackson Laboratory, Bar Harbor, ME, USA) for helping with *Alms1*$^{-/-}$ mice and Annalaura Torella for the RNA sequencing (Next Generation Sequencing Facility, Department of Biochemistry, Biophysics and General Pathology, "Luigi Vanvitelli" University, Naples, Italy). This work was supported by the European Research Council (ERC) (grant numbers, 282085 "RetGeneTx" and 694323 "EYEGET" to A.A.), the European Union (grant number FP7 291778 "DTI-IMPORT" to A. Maddalena), and the Italian Telethon Foundation (grant number TGM16MT1 to A.A.).

REFERENCES

1. Sohocki, M.M., Daiger, S.P., Bowne, S.J., Rodriquez, J.A., Northrup, H., Heckenlively, J.R., Birch, D.G., Mintz-Hittner, H., Ruiz, R.S., Lewis, R.A., et al. (2001). Prevalence of mutations causing retinitis pigmentosa and other inherited retinopathies. Hum. Mutat. *17*, 42–51.

2. Berger, W., Kloeckener-Gruissem, B., and Neidhardt, J. (2010). The molecular basis of human retinal and vitreoretinal diseases. Prog. Retin. Eye Res. *29*, 335–375.

3. Bainbridge, J.W., Smith, A.J., Barker, S.S., Robbie, S., Henderson, R., Balaggan, K., Viswanathan, A., Holder, G.E., Stockman, A., Tyler, N., et al. (2008). Effect of gene therapy on visual function in Leber's congenital amaurosis. N. Engl. J. Med. *358*, 2231–2239.

4. Cideciyan, A.V., Hauswirth, W.W., Aleman, T.S., Kaushal, S., Schwartz, S.B., Boye, S.L., Windsor, E.A., Conlon, T.J., Sumaroka, A., Roman, A.J., et al. (2009). Vision 1 year after gene therapy for Leber's congenital amaurosis. N. Engl. J. Med. *361*, 725–727.

5. Maguire, A.M., Simonelli, F., Pierce, E.A., Pugh, E.N., Jr., Mingozzi, F., Bennicelli, J., Banfi, S., Marshall, K.A., Testa, F., Surace, E.M., et al. (2008). Safety and efficacy of gene transfer for Leber's congenital amaurosis. N. Engl. J. Med. *358*, 2240–2248.
6. Maguire, A.M., High, K.A., Auricchio, A., Wright, J.F., Pierce, E.A., Testa, F., Mingozzi, F., Bennicelli, J.L., Ying, G.S., Rossi, S., et al. (2009). Age-dependent effects of RPE65 gene therapy for Leber's congenital amaurosis: a phase 1 dose-escalation trial. Lancet *374*, 1597–1605.
7. Simonelli, F., Maguire, A.M., Testa, F., Pierce, E.A., Mingozzi, F., Bennicelli, J.L., Rossi, S., Marshall, K., Banfi, S., Surace, E.M., et al. (2010). Gene therapy for Leber's congenital amaurosis is safe and effective through 1.5 years after vector administration. Mol. Ther *18*, 643–650.
8. Testa, F., Maguire, A.M., Rossi, S., Pierce, E.A., Melillo, P., Marshall, K., Banfi, S., Surace, E.M., Sun, J., Acerra, C., et al. (2013). Three-year follow-up after unilateral subretinal delivery of adeno-associated virus in patients with Leber congenital Amaurosis type 2. Ophthalmology *120*, 1283–1291.
9. Allocca, M., Mussolino, C., Garcia-Hoyos, M., Sanges, D., Iodice, C., Petrillo, M., Vandenberghe, L.H., Wilson, J.M., Marigo, V., Surace, E.M., and Auricchio, A. (2007). Novel adeno-associated virus serotypes efficiently transduce murine photoreceptors. J. Virol. *81*, 11372–11380.
10. Mussolino, C., della Corte, M., Rossi, S., Viola, F., Di Vicino, U., Marrocco, E., Neglia, S., Doria, M., Testa, F., Giovannoni, R., et al. (2011). AAV-mediated photoreceptor transduction of the pig cone-enriched retina. Gene Ther. *18*, 637–645.
11. Vandenberghe, L.H., Bell, P., Maguire, A.M., Cearley, C.N., Xiao, R., Calcedo, R., Wang, L., Castle, M.J., Maguire, A.C., Grant, R., et al. (2011). Dosage thresholds for AAV2 and AAV8 photoreceptor gene therapy in monkey. Sci. Transl. Med. *3*, 88ra54.
12. Auricchio, A. (2011). Fighting blindness with adeno-associated virus serotype 8. Hum. Gene Ther. *22*, 1169–1170.
13. Natkunarajah, M., Trittibach, P., McIntosh, J., Duran, Y., Barker, S.E., Smith, A.J., Nathwani, A.C., and Ali, R.R. (2008). Assessment of ocular transduction using single-stranded and self-complementary recombinant adeno-associated virus serotype 2/8. Gene Ther. *15*, 463–467.
14. Boye, S.E., Alexander, J.J., Boye, S.L., Witherspoon, C.D., Sandefer, K.J., Conlon, T.J., Erger, K., Sun, J., Ryals, R., Chiodo, V.A., et al. (2012). The human rhodopsin kinase promoter in an AAV5 vector confers rod- and cone-specific expression in the primate retina. Hum. Gene Ther. *23*, 1101–1115.
15. Vandenberghe, L.H., Bell, P., Maguire, A.M., Xiao, R., Hopkins, T.B., Grant, R., Bennett, J., and Wilson, J.M. (2013). AAV9 targets cone photoreceptors in the nonhuman primate retina. PLoS ONE *8*, e53463.
16. Lai, Y., Yue, Y., and Duan, D. (2010). Evidence for the failure of adeno-associated virus serotype 5 to package a viral genome ≥8.2 kb. Mol. Ther *18*, 75–79.
17. Hermonat, P.L., Quirk, J.G., Bishop, B.M., and Han, L. (1997). The packaging capacity of adeno-associated virus (AAV) and the potential for wild-type-plus AAV gene therapy vectors. FEBS Lett. *407*, 78–84.
18. Dong, B., Nakai, H., and Xiao, W. (2010). Characterization of genome integrity for oversized recombinant AAV vector. Mol. Ther *18*, 87–92.
19. Wu, Z., Yang, H., and Colosi, P. (2010). Effect of genome size on AAV vector packaging. Mol. Ther *18*, 80–86.
20. Yan, Z., Zhang, Y., Duan, D., and Engelhardt, J.F. (2000). Trans-splicing vectors expand the utility of adeno-associated virus for gene therapy. Proc. Natl. Acad. Sci. USA *97*, 6716–6721.
21. Duan, D., Yue, Y., and Engelhardt, J.F. (2001). Expanding AAV packaging capacity with trans-splicing or overlapping vectors: a quantitative comparison. Mol. Ther *4*, 383–391.
22. Ghosh, A., and Duan, D. (2007). Expanding adeno-associated viral vector capacity: a tale of two vectors. Biotechnol. Genet. Eng. Rev. *24*, 165–177.
23. Ghosh, A., Yue, Y., Lai, Y., and Duan, D. (2008). A hybrid vector system expands adeno-associated viral vector packaging capacity in a transgene-independent manner. Mol. Ther *16*, 124–130.
24. Reich, S.J., Auricchio, A., Hildinger, M., Glover, E., Maguire, A.M., Wilson, J.M., and Bennett, J. (2003). Efficient trans-splicing in the retina expands the utility of adeno-associated virus as a vector for gene therapy. Hum. Gene Ther. *14*, 37–44.
25. Duan, D., Sharma, P., Yang, J., Yue, Y., Dudus, L., Zhang, Y., Fisher, K.J., and Engelhardt, J.F. (1998). Circular intermediates of recombinant adeno-associated virus have defined structural characteristics responsible for long-term episomal persistence in muscle tissue. J. Virol. *72*, 8568–8577.
26. Trapani, I., Colella, P., Sommella, A., Iodice, C., Cesi, G., de Simone, S., Marrocco, E., Rossi, S., Giunti, M., Palfi, A., et al. (2014). Effective delivery of large genes to the retina by dual AAV vectors. EMBO Mol. Med. *6*, 194–211.
27. Dyka, F.M., Boye, S.L., Chiodo, V.A., Hauswirth, W.W., and Boye, S.E. (2014). Dual adeno-associated virus vectors result in efficient in vitro and in vivo expression of an oversized gene, MYO7A. Hum. Gene Ther. Methods *25*, 166–177.
28. Pryadkina, M., Lostal, W., Bourg, N., Charton, K., Roudaut, C., Hirsch, M.L., and Richard, I. (2015). A comparison of AAV strategies distinguishes overlapping vectors for efficient systemic delivery of the 6.2 kb Dysferlin coding sequence. Mol. Ther. Methods Clin. Dev. *2*, 15009.
29. Ouyang, X.M., Yan, D., Du, L.L., Hejtmancik, J.F., Jacobson, S.G., Nance, W.E., Li, A.R., Angeli, S., Kaiser, M., Newton, V., et al. (2005). Characterization of Usher syndrome type I gene mutations in an Usher syndrome patient population. Hum. Genet. *116*, 292–299.
30. Roux, A.F., Faugère, V., Le Guédard, S., Pallares-Ruiz, N., Vielle, A., Chambert, S., Marlin, S., Hamel, C., Gilbert, B., Malcolm, S., and Claustres, M.; French Usher Syndrome Collaboration (2006). Survey of the frequency of USH1 gene mutations in a cohort of Usher patients shows the importance of cadherin 23 and protocadherin 15 genes and establishes a detection rate of above 90%. J. Med. Genet. *43*, 763–768.
31. Oshima, A., Jaijo, T., Aller, E., Millan, J.M., Carney, C., Usami, S., Moller, C., and Kimberling, W.J. (2008). Mutation profile of the CDH23 gene in 56 probands with Usher syndrome type I. Hum. Mutat. *29*, E37–E46.
32. Bolz, H., von Brederlow, B., Ramírez, A., Bryda, E.C., Kutsche, K., Nothwang, H.G., Seeliger, M., del C-Salcedó Cabrera, M., Vila, M.C., Molina, O.P., et al. (2001). Mutation of CDH23, encoding a new member of the cadherin gene family, causes Usher syndrome type 1D. Nat. Genet. *27*, 108–112.
33. Bork, J.M., Peters, L.M., Riazuddin, S., Bernstein, S.L., Ahmed, Z.M., Ness, S.L., Polomeno, R., Ramesh, A., Schloss, M., Srisailpathy, C.R., et al. (2001). Usher syndrome 1D and nonsyndromic autosomal recessive deafness DFNB12 are caused by allelic mutations of the novel cadherin-like gene CDH23. Am. J. Hum. Genet. *68*, 26–37.
34. Marshall, J.D., Maffei, P., Collin, G.B., and Naggert, J.K. (2011). Alström syndrome: genetics and clinical overview. Curr. Genomics *12*, 225–235.
35. Collin, G.B., Marshall, J.D., Ikeda, A., So, W.V., Russell-Eggitt, I., Maffei, P., Beck, S., Boerkoel, C.F., Sicolo, N., Martin, M., et al. (2002). Mutations in ALMS1 cause obesity, type 2 diabetes and neurosensory degeneration in Alström syndrome. Nat. Genet. *31*, 74–78.
36. Alstrom, C.H., Hallgren, B., Nilsson, L.B., and Asander, H. (1959). Retinal degeneration combined with obesity, diabetes mellitus and neurogenous deafness: a specific syndrome (not hitherto described) distinct from the Laurence-Moon-Bardet-Biedl syndrome: a clinical, endocrinological and genetic examination based on a large pedigree. Acta Psychiatr. Neurol. Scand., Suppl. *129*, 1–35.
37. Marshall, J.D., Beck, S., Maffei, P., and Naggert, J.K. (2007). Alström syndrome. Eur. J. Hum. Genet. *15*, 1193–1202.
38. Wheway, G., Parry, D.A., and Johnson, C.A. (2014). The role of primary cilia in the development and disease of the retina. Organogenesis *10*, 69–85.
39. Lostal, W., Kodippili, K., Yue, Y., and Duan, D. (2014). Full-length dystrophin reconstitution with adeno-associated viral vectors. Hum. Gene Ther. *25*, 552–562.
40. Koo, T., Popplewell, L., Athanasopoulos, T., and Dickson, G. (2014). Triple trans-splicing adeno-associated virus vectors capable of transferring the coding sequence for full-length dystrophin protein into dystrophic mice. Hum. Gene Ther. *25*, 98–108.
41. Yokoyama, T., Liou, G.I., Caldwell, R.B., and Overbeek, P.A. (1992). Photoreceptor-specific activity of the human interphotoreceptor retinoid-binding protein (IRBP) promoter in transgenic mice. Exp. Eye Res. *55*, 225–233.

42. Liou, G.I., Matragoon, S., Yang, J., Geng, L., Overbeek, P.A., and Ma, D.P. (1991). Retina-specific expression from the IRBP promoter in transgenic mice is conferred by 212 bp of the 5′-flanking region. Biochem. Biophys. Res. Commun. *181*, 159–165.

43. Esumi, N., Oshima, Y., Li, Y., Campochiaro, P.A., and Zack, D.J. (2004). Analysis of the VMD2 promoter and implication of E-box binding factors in its regulation. J. Biol. Chem. *279*, 19064–19073.

44. Dong, X., Tian, W., Wang, G., Dong, Z., Shen, W., Zheng, G., Wu, X., Xue, J., Wang, Y., and Chen, J. (2010). Establishment of an AAV reverse infection-based array. PLoS ONE *5*, e13479.

45. Fishel, M.L., Vasko, M.R., and Kelley, M.R. (2007). DNA repair in neurons: so if they don't divide what's to repair? Mutat. Res. *614*, 24–36.

46. Norris, D.P., and Grimes, D.T. (2012). Mouse models of ciliopathies: the state of the art. Dis. Model. Mech. *5*, 299–312.

47. Collin, G.B., Cyr, E., Bronson, R., Marshall, J.D., Gifford, E.J., Hicks, W., Murray, S.A., Zheng, Q.Y., Smith, R.S., Nishina, P.M., and Naggert, J.K. (2005). Alms1-disrupted mice recapitulate human Alström syndrome. Hum. Mol. Genet. *14*, 2323–2333.

48. Bisgrove, B.W., and Yost, H.J. (2006). The roles of cilia in developmental disorders and disease. Development *133*, 4131–4143.

49. Li, G., Vega, R., Nelms, K., Gekakis, N., Goodnow, C., McNamara, P., Wu, H., Hong, N.A., and Glynne, R. (2007). A role for Alström syndrome protein, alms1, in kidney ciliogenesis and cellular quiescence. PLoS Genet. *3*, e8.

50. Hearn, T., Renforth, G.L., Spalluto, C., Hanley, N.A., Piper, K., Brickwood, S., White, C., Connolly, V., Taylor, J.F., Russell-Eggitt, I., et al. (2002). Mutation of ALMS1, a large gene with a tandem repeat encoding 47 amino acids, causes Alström syndrome. Nat. Genet. *31*, 79–83.

51. Krebs, M.P., Collin, G.B., Hicks, W.L., Yu, M., Charette, J.R., Shi, L.Y., Wang, J., Naggert, J.K., Peachey, N.S., and Nishina, P.M. (2017). Mouse models of human ocular disease for translational research. PLoS ONE *12*, e0183837.

52. Jacobson, S.G., Acland, G.M., Aguirre, G.D., Aleman, T.S., Schwartz, S.B., Cideciyan, A.V., Zeiss, C.J., Komaromy, A.M., Kaushal, S., Roman, A.J., et al. (2006). Safety of recombinant adeno-associated virus type 2-RPE65 vector delivered by ocular subretinal injection. Mol. Ther *13*, 1074–1084.

53. Duan, D., Yan, Z., Yue, Y., and Engelhardt, J.F. (1999). Structural analysis of adeno-associated virus transduction circular intermediates. Virology *261*, 8–14.

54. Straus, S.E., Sebring, E.D., and Rose, J.A. (1976). Concatemers of alternating plus and minus strands are intermediates in adenovirus-associated virus DNA synthesis. Proc. Natl. Acad. Sci. USA *73*, 742–746.

55. Ortín-Martínez, A., Nadal-Nicolás, F.M., Jiménez-López, M., Alburquerque-Béjar, J.J., Nieto-López, L., García-Ayuso, D., Villegas-Pérez, M.P., Vidal-Sanz, M., and Agudo-Barriuso, M. (2014). Number and distribution of mouse retinal cone photoreceptors: differences between an albino (Swiss) and a pigmented (C57/BL6) strain. PLoS ONE *9*, e102392.

56. Colella, P., Sommella, A., Marrocco, E., Di Vicino, U., Polishchuk, E., Garcia Garrido, M., Seeliger, M.W., Polishchuk, R., and Auricchio, A. (2013). Myosin7a deficiency results in reduced retinal activity which is improved by gene therapy. PLoS ONE *8*, e72027.

57. Hendrickson, A., and Hicks, D. (2002). Distribution and density of medium- and short-wavelength selective cones in the domestic pig retina. Exp. Eye Res. *74*, 435–444.

58. Karali, M., Manfredi, A., Puppo, A., Marrocco, E., Gargiulo, A., Allocca, M., Corte, M.D., Rossi, S., Giunti, M., Bacci, M.L., et al. (2011). MicroRNA-restricted transgene expression in the retina. PLoS ONE *6*, e22166.

59. Manfredi, A., Marrocco, E., Puppo, A., Cesi, G., Sommella, A., Della Corte, M., Rossi, S., Giunti, M., Craft, C.M., Bacci, M.L., et al. (2013). Combined rod and cone transduction by adeno-associated virus 2/8. Hum. Gene Ther. *24*, 982–992.

60. Puppo, A., Bello, A., Manfredi, A., Cesi, G., Marrocco, E., Della Corte, M., Rossi, S., Giunti, M., Bacci, M.L., Simonelli, F., et al. (2013). Recombinant vectors based on porcine adeno-associated viral serotypes transduce the murine and pig retina. PLoS ONE *8*, e59025.

61. Testa, F., Surace, E.M., Rossi, S., Marrocco, E., Gargiulo, A., Di Iorio, V., Ziviello, C., Nesti, A., Fecarotta, S., Bacci, M.L., et al. (2011). Evaluation of Italian patients with leber congenital amaurosis due to AIPL1 mutations highlights the potential applicability of gene therapy. Invest. Ophthalmol. Vis. Sci. *52*, 5618–5624.

62. Flotte, T.R., Afione, S.A., Solow, R., Drumm, M.L., Markakis, D., Guggino, W.B., Zeitlin, P.L., and Carter, B.J. (1993). Expression of the cystic fibrosis transmembrane conductance regulator from a novel adeno-associated virus promoter. J. Biol. Chem. *268*, 3781–3790.

63. Trapani, I., Toriello, E., de Simone, S., Colella, P., Iodice, C., Polishchuk, E.V., Sommella, A., Colecchi, L., Rossi, S., Simonelli, F., et al. (2015). Improved dual AAV vectors with reduced expression of truncated proteins are safe and effective in the retina of a mouse model of Stargardt disease. Hum. Mol. Genet. *24*, 6811–6825.

64. Lagziel, A., Overlack, N., Bernstein, S.L., Morell, R.J., Wolfrum, U., and Friedman, T.B. (2009). Expression of cadherin 23 isoforms is not conserved: implications for a mouse model of Usher syndrome type 1D. Mol. Vis. *15*, 1843–1857.

65. Libby, R.T., Kitamoto, J., Holme, R.H., Williams, D.S., and Steel, K.P. (2003). Cdh23 mutations in the mouse are associated with retinal dysfunction but not retinal degeneration. Exp. Eye Res. *77*, 731–739.

66. Bovolenta, P., and Cisneros, E. (2009). Retinitis pigmentosa: cone photoreceptors starving to death. Nat. Neurosci. *12*, 5–6.

67. Petrs-Silva, H., Dinculescu, A., Li, Q., Deng, W.T., Pang, J.J., Min, S.H., Chiodo, V., Neeley, A.W., Govindasamy, L., Bennett, A., et al. (2011). Novel properties of tyrosine-mutant AAV2 vectors in the mouse retina. Mol. Ther *19*, 293–301.

68. Petrs-Silva, H., Dinculescu, A., Li, Q., Min, S.H., Chiodo, V., Pang, J.J., Zhong, L., Zolotukhin, S., Srivastava, A., Lewin, A.S., and Hauswirth, W.W. (2009). High-efficiency transduction of the mouse retina by tyrosine-mutant AAV serotype vectors. Mol. Ther *17*, 463–471.

69. Dalkara, D., Byrne, L.C., Klimczak, R.R., Visel, M., Yin, L., Merigan, W.H., Flannery, J.G., and Schaffer, D.V. (2013). In vivo-directed evolution of a new adeno-associated virus for therapeutic outer retinal gene delivery from the vitreous. Sci. Transl. Med. *5*, 189ra76.

70. Duan, D., Yue, Y., Yan, Z., Yang, J., and Engelhardt, J.F. (2000). Endosomal processing limits gene transfer to polarized airway epithelia by adeno-associated virus. J. Clin. Invest. *105*, 1573–1587.

71. Jennings, K., Miyamae, T., Traister, R., Marinov, A., Katakura, S., Sowders, D., Trapnell, B., Wilson, J.M., Gao, G., and Hirsch, R. (2005). Proteasome inhibition enhances AAV-mediated transgene expression in human synoviocytes in vitro and in vivo. Mol. Ther *11*, 600–607.

72. Lopes, V.S., Boye, S.E., Louie, C.M., Boye, S., Dyka, F., Chiodo, V., Fofo, H., Hauswirth, W.W., and Williams, D.S. (2013). Retinal gene therapy with a large MYO7A cDNA using adeno-associated virus. Gene Ther. *20*, 824–833.

73. Auricchio, A., Hildinger, M., O'Connor, E., Gao, G.P., and Wilson, J.M. (2001). Isolation of highly infectious and pure adeno-associated virus type 2 vectors with a single-step gravity-flow column. Hum. Gene Ther. *12*, 71–76.

74. Tsien, R.Y. (1998). The green fluorescent protein. Annu. Rev. Biochem. *67*, 509–544.

75. Ghosh, A., Yue, Y., and Duan, D. (2011). Efficient transgene reconstitution with hybrid dual AAV vectors carrying the minimized bridging sequences. Hum. Gene Ther. *22*, 77–83.

76. Pellissier, L.P., Hoek, R.M., Vos, R.M., Aartsen, W.M., Klimczak, R.R., Hoyng, S.A., Flannery, J.G., and Wijnholds, J. (2014). Specific tools for targeting and expression in Müller glial cells. Mol. Ther. Methods Clin. Dev. *1*, 14009.

77. Doria, M., Ferrara, A., and Auricchio, A. (2013). AAV2/8 vectors purified from culture medium with a simple and rapid protocol transduce murine liver, muscle, and retina efficiently. Hum. Gene Ther. Methods *24*, 392–398.

78. Drittanti, L., Rivet, C., Manceau, P., Danos, O., and Vega, M. (2000). High throughput production, screening and analysis of adeno-associated viral vectors. Gene Ther. *7*, 924–929.

79. Xiao, X., and Samulski, R.J. (1998). Production of High-Titer Recombinant Adeno-Associated Virus Vectors in the Absence of Helper Adenovirus. J. Virol. *72*, 2224–2232.

80. Grieger, J.C., and Samulski, R.J. (2005). Packaging capacity of adeno-associated virus serotypes: impact of larger genomes on infectivity and postentry steps. J. Virol. *79*, 9933–9944.

81. Liang, F.Q., Anand, V., Maguire, A.M., and Bennett, J. (2001). Intraocular delivery of recombinant virus. Methods Mol. Med. *47*, 125–139.

82. Pertea, M., Kim, D., Pertea, G.M., Leek, J.T., and Salzberg, S.L. (2016). Transcript-level expression analysis of RNA-seq experiments with HISAT, StringTie and Ballgown. Nat. Protoc. *11*, 1650–1667.

83. Kim, D., Langmead, B., and Salzberg, S.L. (2015). HISAT: a fast spliced aligner with low memory requirements. Nat. Methods *12*, 357–360.

84. Pertea, M., Pertea, G.M., Antonescu, C.M., Chang, T.C., Mendell, J.T., and Salzberg, S.L. (2015). StringTie enables improved reconstruction of a transcriptome from RNA-seq reads. Nat. Biotechnol. *33*, 290–295.

85. Frazee, A.C., Pertea, G., Jaffe, A.E., Langmead, B., Salzberg, S.L., and Leek, J.T. (2015). Ballgown bridges the gap between transcriptome assembly and expression analysis. Nat. Biotechnol. *33*, 243–246.

86. Anders, S., and Huber, W. (2010). Differential expression analysis for sequence count data. Genome Biol. *11*, R106.